The role of *KANL1KE1* and *KANLIKE2* genes in leaf development

Kurukulasuriya Hiruni Nimasha Fernando

A thesis submitted to fulfil requirements for the degree of

Doctor of Philosophy

School of Life and Environmental Sciences

Faculty of Science

The University of Sydney

November 2025

Statement of originality

This is to certify that the intellectual content of this thesis is the product of my own work and that all the assistance received in preparing this thesis and sources have been acknowledged. Also, this thesis has not been submitted for any degree or other purposes.

Kurukulasuriya Hiruni Nimasha Fernando

Gen AI attribution statement

No content produced by generative AI tools has been used in the preparation of this thesis.

Kurukulasuriya Hiruni Nimasha Fernando

Table of contents

List of figures

List of tables

Acknowledgement

I am grateful to the University of Sydney and the Australian government for awarding me the International Strategic Tuition Fee Scholarship and the living stipend scholarship to study for a PhD. The university administration is very much appreciated for securing my scholarship during the difficult times of the COVID pandemic in 2020-2021 when it was challenging for me to travel to Australia and start my PhD studies. I also hold dear my experiences at Wayamba University in Sri Lanka, where I earned my BSc (Hons), and Jeju National University, where I completed my MSc. These institutions helped me to get this scholarship to pursue a PhD at the University of Sydney.

I am thankful to my PhD supervisor, Associate Professor Marcus Heisler, for the opportunity to work on this interesting project and in his lab. Additionally, thank you, Marcus; this has been a great PhD project that allowed me to learn about fascinating plant development, different microscopy and molecular biology techniques.

Dr. Carolyn Ohno developed all the transgenic lines I analysed for this project; her patience during the cloning and transformation processes was incredible. She taught me many molecular techniques and helped me to maintain my plants. Thank you, Carolyn; I could not have completed my PhD without your support. You were always there, encouraging and supporting me and my project at every turn.

I'm so grateful to my parents, my brother, sister, and my little niece Shenaya. During the difficult times of this journey, I kept all of you in my mind, which gave me the strength to move on. A big applause goes to my mother, Mum; you were my first teacher in research. I remember you working as a Technical Officer at the Coconut Research Institute in Sri Lanka, taking me to the molecular and pathology lab during my school holidays. You taught me how to do DNA extraction and PCR, which left me with my first impression of wanting to become a researcher one day. Thank you very much for the daily phone calls; you and Dad never forgot about me for

a single day. I always returned home happily, knowing that you two were calling me, no matter what happened during the day.

I'm truly grateful to my relatives in Melbourne. You all made me feel so at home in Australia, especially during the Christmas and easter breaks. I am deeply thankful to my aunt, uncle, Ashen and Shenali for the care and support they have given me. Finally, I would like to express my sincere gratitude to my beloved husband, Yasas. Your constant love, trust and confidence in me have been my biggest source of strength in this journey. I look forward to the day I can return home to celebrate this achievement with you.

Publications and the presentations during the candidature

Publication:

Hiruni Fernando and Marcus G. Heisler, Wounding and the establishment of leaf polarity: From historical perspectives to present controversies; Trends in Developmental Biology, 16, 2023 ***(Appendix)***

Conference abstracts:

1. Hiruni Fernando, Hasthi Ram, Yuzhou Wu, Carolyn Ohno, Marcus G. Heisler, *KANLIKE1* and *KANLIKE2* genes in leaf development presented at XXIIIrd International Congress of Genetics, Melbourne, Australia

2. Hiruni Fernando, Carolyn Ohno, Marcus Heisler, The role of *KANLIKE1* and *KANLIKE2* genes in leaf development, presented at Science HDR Student Conference 2023, University of Sydney, Sydney, Australia

3. Hiruni Fernando, Hasthi Ram, Yuzhou Wu, Carolyn Ohno, Marcus G. Heisler, The Role of *KANLIKE1* and *KANLIKE2* Genes in Leaf Development, presented at ANZSCDB meeting 2023, University of Sydney, Sydney, Australia

4. Hiruni Fernando, Hasthi Ram, Yuzhou Wu, Carolyn Ohno, Marcus G. Heisler, The Role of *KANLIKE1* and *KANLIKE2* Genes in Leaf Development, presented at International Plant Molecular Biology Conference 2024, Cairns, Australia (awarded as best poster presentation)

5. Hiruni Fernando, Hasthi Ram, Yuzhou Wu, Carolyn Ohno, Marcus G. Heisler, The Role of *KANLIKE1* and *KANLIKE2* Genes in Leaf Development, presented at Hunter Meeting 2025, Hunter Valley, Australia

Abstract

In *Arabidopsis thaliana,* the *Class III HOMEODOMAIN LEUCINE ZIPPER (HD-ZIP III)* genes play a crucial role in regulating leaf flatness. Recently, two closely related genes were identified by the Heisler lab to be regulated by the HD-ZIP III transcription factors and co-expressed adaxially with them in the *Arabidopsis* shoot and leaves. These genes encode transcription factors that share a similar MYB DNA binding domain to that of the KANADI transcription factors and were named *KANLIKE1 (KANL1)* and *KANLIKE2 (KANL2*). In this thesis, I investigate the role of *KANL1* and *KANL2* in the leaves of the Arabidopsis L*er* ecotype in detail. I find that the loss-of-function mutant *kanl1 kanl2* exhibits a downward-curved leaf phenotype. Analyses of plants multiply mutant for members of the *HD-ZIP III* and *KANL* genes along with ChIP (Chromatin Extraction and Immunoprecipitation)-PCR results, further support the proposal that *KANL1* and *KANL2* are direct downstream targets of the HD-ZIP III transcription factors. Similar to findings previously reported for orthologs of the *KANL* genes in tomato and strawberry, I find that CUP-SHAPED COTYLEDON2 (CUC2) and KNOTTED class 1 transcription factor KNAT1 are upregulated in *Arabidopsis kanl1 kanl2* mutants. However, in *kanl1 kanl2* leaves, I also find that the middle-domain-specific gene *WUSCHEL-RELATED HOMEOBOX (WOX1)* is expressed ectopically and that *PRESSED FLOWER (PRS)* is upregulated. By analysing the *wox1 prs kanl1 kanl2* quadruple mutant, I find that the upwardly curving leaf phenotype of *wox1 prs* mutants is epistatic to the downward curving phenotype of *kanl1 kanl2* mutants, indicating that *KANL1* and *KANL2* regulate leaf curvature in part by repressing both *WOX1* and *PRS* expression. Lastly, by combining mutations in the *KANL* genes with mutations in *ASYMMETRIC LEAVES 2* (*AS2)*, another gene known to regulate leaf curvature and *PRS*/*WOX* expression, I infer that *AS2* and the *KANL* genes act in parallel pathways.

Chapter 1 - Introduction

1.1. Plant development

Plants and animals evolved independently from a unicellular eukaryote roughly 1.6 billion years ago (Meyerowitz, 2002). Throughout evolutionary history, plants have undergone significant changes in form, including transitions in the dominance of sporophyte vs gametophyte, changes in branching structure, the repeated evolution of flat tissues optimised for photosynthesis and the generation of flowers to regulate reproduction (Friedman, Moore and Purugganan, 2004). In particular, the evolution of megaphyll leaves with photosynthetic efficiency marked a major milestone that had a remarkable environmental impact (Beerling and Fleming, 2007). Today, the leaves we observe in nature exhibit different shapes and sizes, which have fascinated plant developmental biologists for many years. These diverse leaf forms result from both genetic variation and environmental influences (Fritz, Rosa and Sicard, 2018). With advancements in science and technology, our understanding of how leaves are shaped has progressed significantly. However, there are still many questions yet to be answered. One of these questions is how flat lamina structures are established when they grow. This can be answered by studying the downstream targets of adaxial and abaxial regulators that have been discovered so far.

1.2 The shoot apical meristem

Plants possess three types of meristems, each containing undifferentiated stem cells. The primary meristems responsible for longitudinal growth are the shoot and root apical meristems (SAM and RAM), which give rise to all above-ground and below-ground parts of the plant. These meristems are established during embryogenesis but remain mostly inactive until germination (Steeves and Sussex, 1989; Greb and Lohmann, 2016). A secondary meristem, called the vascular cambium, promotes plant growth along the radial direction (Zhang et al., 2014). The shoot apical meristem

(SAM) is located at the tip of the shoot in plants (Figure 1.1) and provides cells that contribute to all the above-ground structures, including stems, leaves, flowers, and branches. The outer surface layer of the SAM, called the tunica, is composed of L1 and L2 sublayers. It encloses the internal cells of the meristem, which are named the corpus or L3. The L1 and L2 layers are characterised by anticlinal division and L3 divides in many planes. Besides the layered structure, the SAM is divided into three zones based on cytological differences and functions. At the apex of the meristem, a small group of cells that are slowly dividing, known as the central zone (CZ), maintains the meristem. The peripheral zone (PZ) is where new lateral organs are initiated with a high frequency of cell division, while the Rib Zone (RZ) produces the internal stem of the plant (Meyerowitz, 1997; Vernoux, Besnard and Traas, 2010).

The CLAVATA3 (CLV3)-WUSCHEL (WUS) signalling pathway has emerged as the key regulatory mechanism that balances stem cell proliferation and differentiation. This balance is maintained through an autoregulatory negative feedback loop (Somssich et al., 2016). KNOTTED1-like homeobox (KNOX) proteins also maintain the pluripotent stem cell population in the SAM by hormone homeostasis (Hay and Tsiantis, 2010). After germination, the shoot apical meristem transitions from a vegetative phase, producing leaves, to a reproductive phase where flowers are produced.

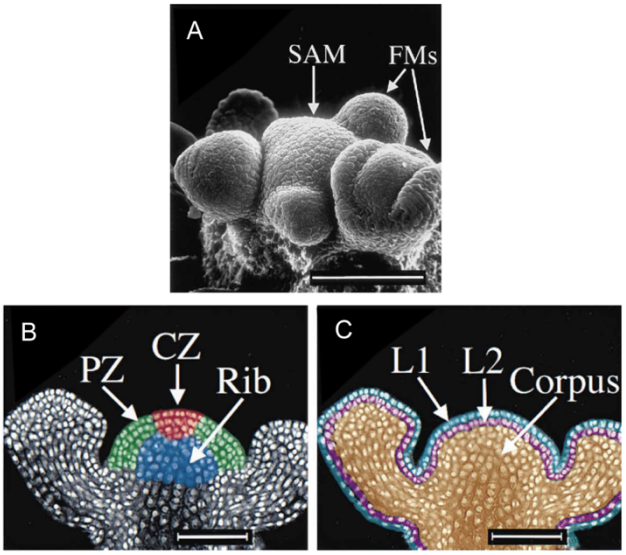

Figure 1.1 Shoot Apical Meristem (SAM) of *Arabidopsis thaliana*

(A) Scanning electron micrograph of a Shoot Apical Meristem (SAM) of *Arabidopsis thaliana* along with five visible floral meristems (FMs). (B) Three different zones of the shoot apical meristem marked in a longitudinal optical section showing cell nuclei; Central Zone (CZ), Periphery Zone (PZ) and Rib Zone (RIB). (C) Three different layers of the shoot apical meristem marked in a longitudinal optical section showing cell nuclei; Epidermal layer (L1), Subepidermal Layer (L2) and Corpus or L3. Scale Bar = 50 µm. Adapted from (Meyerowitz, 1997).

1.3. The *KNOX1* and *CUC2* genes regulate differentiation and organ boundaries, respectively

The KNOTTED class of homeodomain proteins are known to play an essential role in shoot meristem regulation (Long et al., 1996). The *KNOXI* subclass of genes is recognised for maintaining the SAM in an undifferentiated state (Scofield and Murray, 2006). The KNOX I subclass comprises SHOOT MERISTEMLESS (STM), KNAT1, also referred to as BREVIPEDICELLUS (BP), KNAT2, and KNAT6 (Scofield and Murray, 2006). Conversely, *KNOX2* subclass genes, along with their heterodimeric BELL TALE homeobox partner, promote differentiation and therefore suppress SAM activity. Organ separation in the SAM is regulated by CUC transcription factors (CUC1, CUC2, and CUC3), which belong to the NAC domain transcription family. These genes act by suppressing cell division (Aida et al., 1997; Vroemen et al., 2003).

1.4. Leaf development

Plant leaves are the primary photosynthetic organs of the plant. Their laminae enhance photosynthetic efficiency by facilitating light capture and gas exchange through adaptations in leaf size, shape, and complexity (Chitwood et al., 2012). Leaves originate as small outgrowths called leaf primordia, which develop from the SAM periphery (Huang et al., 2014). In simple leaves, such as those of *Arabidopsis thaliana (Arabidopsis)*, *KNOX1* genes are expressed in the SAM but are absent in leaf primordia; however, in compound leaf species, KNOX1 expression reemerges later in leaf primordia and is involved in the formation of compound leaves (Bharathan et al., 2002; Hay and Tsiantis, 2006). In addition to this, CUC plays a role in forming leaf margin protrusions and serrations by interacting with auxin (Bilsborough et al., 2011; Runions, Tsiantis and Prusinkiewicz, 2017).

Leaves are patterned along three primary patterning axes, thereby determining the structure and function of the leaf: the adaxial-abaxial axis, the proximal-distal axis, and the medial-lateral axis (Figure 1.2). Each axis contributes distinctively to the shaping and functionality of the leaf.

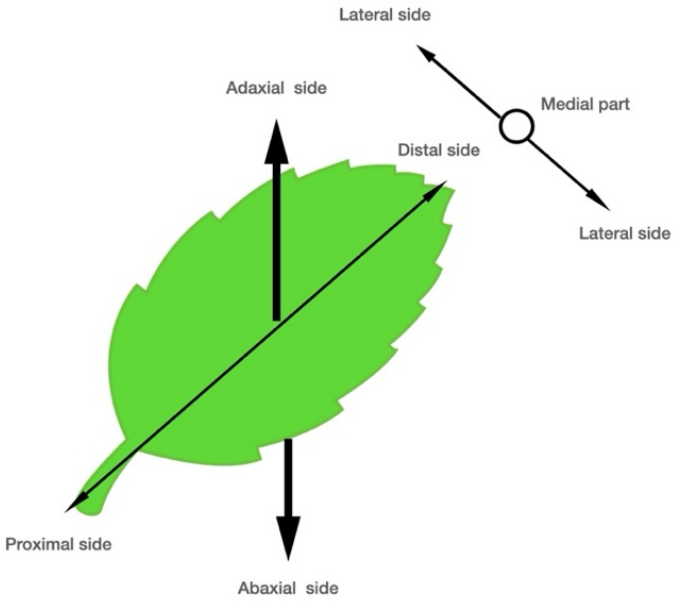

Figure 1.2 The three spatial axes of a leaf; adaxial–abaxial, proximal-distal, and medial-lateral

The adaxial-abaxial axis establishes top (adaxial) and bottom (abaxial) sides of the leaf. The adaxial surface is the closest to the SAM, and the abaxial side is the furthest from SAM. In *Arabidopsis,* functional and anatomical differences exist between the adaxial and abaxial sides. Trichomes, which are small hair-like structures on the surface of leaves, are more abundant on the adaxial side than on the abaxial side. The presence of trichomes is critical to reduce water loss, and it reflects excess sunlight and protects the leaf from herbivores and environmental stressors. The adaxial side of the leaf typically appears darker due to its higher chlorophyll concentration, which enhances its photosynthetic efficiency. The adaxial subepidermal mesophyll layer, located just beneath the upper epidermis of the leaf, comprises tightly packed, columnar-shaped palisade mesophyll cells. These cells are arranged in an orderly fashion to maximise light capture for photosynthesis, as this layer is directly exposed to sunlight. The high density and

regular shape of palisade cells allow efficient light absorption and their optimal chloroplast alignment, which enhances the photosynthetic process.

In contrast, the abaxial side is lighter and smoother. The abaxial mesophyll layer is found beneath the palisade layer and closer to the lower epidermis. It comprises loosely arranged, irregularly shaped spongy mesophyll cells and is involved in gas exchange and transpiration through stomata. The xylem, a specialised tissue responsible for transporting water and dissolved minerals, is situated closer to the adaxial side of the vascular bundle. This is oriented towards the upper surface of the leaf. The phloem, a tissue specialised in transporting sugars and other organic nutrients synthesised during photosynthesis, is positioned towards the abaxial side of the vascular bundle, which faces the lower surface of the leaf (Byrne, 2006; Kittiwongwattana, 2012; Nakata and Okada, 2013). The proximal-distal axis determines the orientation of the leaf from its base (proximal) to its tip (distal). The leaves attach to the stem or branch at the base and extend outward, maximising light capture and gas exchange. The medial-lateral axis determines the expansion of the leaf from the midline (medial) to the edges (lateral). It is responsible for the broad, flat shape of the leaf lamina, which increases the surface area for photosynthesis.

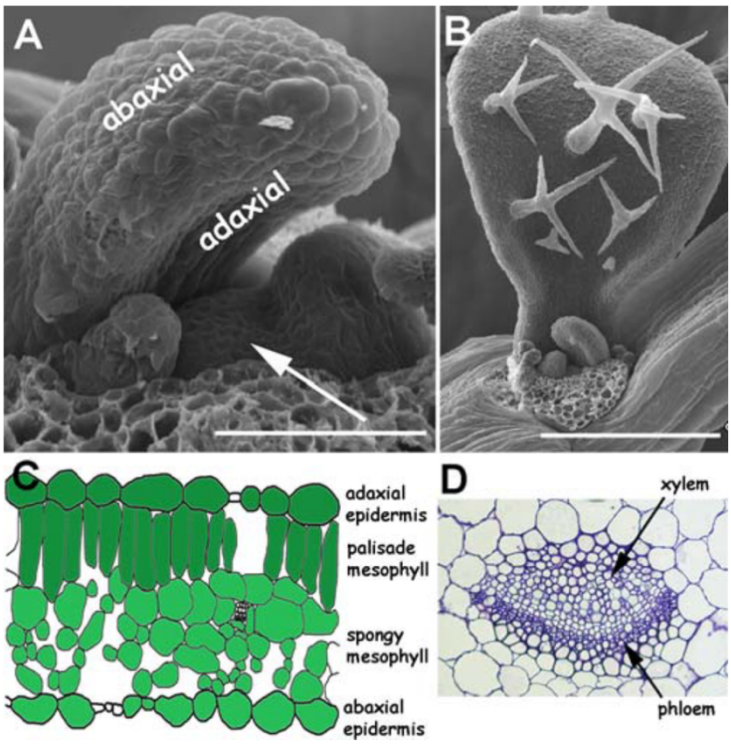

Figure 1.3 The adaxial abaxial axis of the leaf

(A) Scanning electron micrograph of leaf primordia at the vegetative SAM in *Arabidopsis.* Scale Bar = 50 μm. (B) Scanning electron micrograph showing a high density of trichomes on the adaxial side of a juvenile leaf. Scale Bar = 50 μm. (C) A schematic illustration of a leaf cross-section, indicating the adaxial and abaxial outer epidermal layers and the inner mesophyll. (D) Cross-sectional view of the leaf midvein, showing the adaxial xylem and abaxial phloem cells labelled. Adopted from (Byrne, 2006).

1.5. Patterning along the leaf adaxial-abaxial axis

In 1955, Sussex noted that in *Solanus tuberosum* (potato), making incisions to separate the shoot apical meristem from young leaf primordia led to the development of needle-like leaves that lacked a blade. Further histological analysis of these radially symmetric lateral organs revealed they were composed entirely of abaxial cell types (Sussex, 1955). Based on these findings, Sussex proposed that an inductive signal, sensitive to wounding and originating from the shoot apical meristem, was crucial for establishing adaxial identity. Without this signal, the primordium exhibited a radial pattern and became entirely abaxialised. Fifty years after Sussex's initial experiments, similar studies were conducted using infrared laser ablation on tomato shoot tips to separate young leaf primordia from the shoot apical meristem. The results mirrored Sussex's earlier findings in potatoes: the treated leaf primordia underwent abaxialisation and radialisation, forming needle-like structures composed entirely of abaxial cell types, with no differentiation into adaxial tissues (Reinhardt et al., 2005). While these data appear to support Sussex’s proposal, more recent work from the Heisler lab supports an alternative proposal that leaves largely inherit their adaxial-abaxial patterning from the radial patterning of the shoot, and that wounds disrupt the maintenance of this patterning (Caggiano et al., 2017). This controversy was described (Fernando and Heisler, 2024) and attached here in the appendix.

1.6. Adaxial Regulators

1.6.1. The *class III HOMEODOMAIN LEUCINE ZIPPER (HD-ZIP III)* family genes

Arabidopsis has five *HD-ZIP III* genes: *PHABULOSA (PHB)*, *PHAVOLUTA (PHV)*, *REVOLUTA (REV), ATHB8,* and *ATHB15/CORONA (CNA)* (Baima et al., 1995; Talbert et al., 1995; McConnell et al., 2001; Prigge et al., 2005; Byrne, 2006). During *Arabidopsis* development, HD-ZIP III transcription factors regulate embryo, shoot, and root patterning. They determine polarity establishment in leaves and the vascular system during vegetative growth (McConnell et al., 2001; Emery et al., 2003; Brandt et al., 2012). These proteins have three distinct structural domains, including the HD-ZIP domain, which is essential for DNA binding and protein dimerisation. A START domain involved in lipid or steroid binding, and also, a conserved MEKHLA domain at the C-terminal end (Schrick et al., 2004; Prigge et al., 2005). The start domain plays a critical role in enhancing the transcriptional activity of HD-ZIP III proteins by promoting dimerisation and facilitating the binding of the specific phospholipid ligands (Husbands et al., 2023).

REV is expressed in lateral organs adaxially in the shoot and within vascular tissues. *REV* and *PHB* expression determine organ initiation sites and are initially expressed during embryogenesis at the 16-cell embryo, with later expression localised to the SAM and provasculature. *PHV* and *ATHB15* have a similar expression pattern, though their activation occurs later and is more confined than *REV* and *PHB*. *ATHB15* has a strong expression in the vascular tissues and also in axillary and floral meristems. Unlike other group members, *ATHB8* expression is more confined to vascular tissues and meristematic regions, indicating a potentially different function in plant development (Byrne, 2006).

Loss-of-function *rev* plants fail to develop axillary meristems in the vegetative rosette and cauline leaves and exhibit defects in floral organs. *phb phv* double mutant plants or either single mutant, on the other hand, are indistinguishable from the wild type. However, the *phb phv* double mutant enhances *rev* single mutant defects. This indicates redundancy of the *PHB, PHV* genes with each

other and with *REV* alone. Plants that are homozygous for all three genes *(phb phv rev*) display a striking phenotype, lacking the shoot apical meristem, and with a partially or fully abaxialised cotyledon/s (Emery et al., 2003). The expression of *HD-ZIP III* genes is regulated post-translationally by microRNAs 165/166 and by little Zipper (ZPR) proteins (Brandt et al., 2012). During polarity establishment of the leaves, *KANADI (1-4)* genes and *HD-ZIP III* genes act antagonistically (Merelo et al., 2013).

1.6.2. *ASYMMETRIC LEAVES 1* and *2 (AS1* and *AS2)*

ASYMMETRIC LEAVES 1 (AS1) in *Arabidopsis* encodes a MYB domain protein closely related to *PHANTASTICA (PHAN)* in *Antirrhinum* and *ROUGH SHEATH2 (RS2)* in maize. *as1* mutants display bilaterally asymmetric leaf lobes and leaflet-like structures on their petioles (Byrne et al., 2000). A similar phenotype occurs in plants mutant for the *ASYMMETRIC LEAVES2 (AS2)* gene, which encodes a Lob domain-containing, plant-specific protein (Semiarti et al., 2001). AS1 expression is found in developing leaf primordia but is absent in the shoot apical meristem (Byrne et al., 2000). AS2 is found in adaxial leaf primordia as well as the shoot (Byrne et al., 2000; Iwakawa et al., 2007).

1.7. Abaxial Regulators

1.7.1. The *KANADI* (*KAN*) genes

KANADI 1-4 (*KAN1-4*) belong to a plant-specific GARP (Golden2, ARR-B and Psr1) gene family. KAN1 and KAN2 are expressed at the SAM periphery and in the abaxial domain of lateral organs. KAN4 is also expressed in floral organs (Eshed et al., 2001; Izhaki and Bowman, 2007). A single mutation in the *KANADI* gene leads to only mild abnormalities in leaf development; however, mutation of several genes leads to dramatic phenotypes (Huang et al., 2014). Mutations in both *KAN1* and *KAN2* result in significantly reduced leaf blade expansion

and the development of ectopic outgrowths on the abaxial leaf surface, indicating disruptions in proper adaxial-abaxial patterning and growth regulation (Eshed et al., 2001). The *kan1 kan2 kan4* triple mutant shows a severe reduction in leaf blade expansion with predominant adaxialisation. Additionally, the vascular tissue in the stem of triple mutants exhibits radialised organisation (Eshed et al., 2004). The triple mutants *kan1 kan2 kan4* display a significant phenotype characterised by the formation of ectopic leaf-like structures emerging from the hypocotyl region, and abnormal outgrowths on the abaxial side of the cotyledons (Izhaki and Bowman, 2007).

HD-ZIP III and KANADI transcription factors have opposing roles in defining polarity along the adaxial and abaxial axes of *Arabidopsis* leaves. HD-ZIP III factors promote adaxial traits, while KAN1 factors promote abaxial traits by mutual suppression (Reinhart et al., 2013). Also, KAN1 and AS2 function as mutual repressors, playing a crucial role in establishing adaxial-abaxial polarity in leaves (Merelo et al., 2013).

1.7.2. The *YABBY (YAB)* genes

Six *YABBY* genes are encoded in the *Arabidopsis* genome, including *FILAMENTOUS FLOWER* (*FIL*), *CRABS CLAW* (*CRC*), *INNER NO OUTER* (*INO*), *YABBY2* (*YAB2*), *YABBY3* (*YAB3*), and *YABBY5* (*YAB5*) (Kayani et al., 2019). Five out of the six *YABBY* genes contribute to determining organ polarity; *FIL*, *YAB2*, and *YAB3* are expressed in the abaxial domains of lateral organ primordia, establishing the abaxial cell fate. *CRC* is expressed in carpels and nectaries, while *INO* functions in the outer integument of the ovules to specify abaxial identity (Siegfried et al., 1999).

1.7.3. AUXIN RESPONSIVE FACTOR 2 (ARF2), ARF3/ ETTIN (ETT) and ARF4

Auxin Response Factors (ARFs) are pivotal transcriptional regulators in the auxin signalling pathway, functioning as effectors that mediate the plant's response to auxin and are involved in organogenesis and development (Liu et al., 2024). The middle domain genes *WOX1* and *PRS* are

repressed by *KAN1* and *KAN2*, acting together with *ARF2*, *ARF3* and *ARF4* (Pekker, Alvarez and Eshed, 2005; Alvarez et al., 2016; Yu et al., 2017; Heisler, 2021) .

1.7.4. microRNAs (miR) 165/166

The expression of *HD ZIP III* genes is restricted to the adaxial tissues by the action of two microRNAs, miR165 and miR166 (Merelo et al., 2016). The abaxial-determining *YABBY* genes function as trans-acting factors essential for establishing the miR165 activity pattern, and they are restricted to the abaxial tissue (Tatematsu et al., 2015).

1.8. Middle domain regulators

1.8.1. *WUSCHEL-RELATED HOMEOBOX (WOX1)* and *PRESSED FLOWER (PRS) /(WOX3)*

PRS and *WOX1* are expressed in the middle domain of the leaf, essential for the high rate of cell division in the lateral region, driving blade outgrowth in *Arabidopsis* (Nakata et al., 2012a). The *wox1 prs* double mutant develops narrow leaves with disrupted polarity while maintaining normal leaf length (Wang et al., 2020). *PRS* and *WOX1* directly or indirectly suppress *AS2*, and *KANADI* genes suppress *PRS* and *WOX1* in the abaxial domain (Nakata et al., 2012b). *AS2* is also known to repress *WOX1* and *PRS* in the adaxial domain (Satterlee and Scanlon, 2019).

Grass species lack the *WOX1* paralog; orthologs of *WOX1* are found in *Arabidopsis*, tobacco (*LAM1*), petunia (*MAW*), and Medicago (*STF*), and play a conserved role in promoting lateral expansion of the leaf blade (McHale and Marcotrigiano, 1998; Vandenbussche et al., 2009; Tadege et al., 2011). In maize, the *PRS* orthologs *NARROW SHEATH1 (NS1)* and *NARROW SHEATH2 (NS2)* are involved in regulating leaf outgrowth from the margins (Scanlon, Schneeberger and Freeling, 1996; Nardmann et al., 2004).

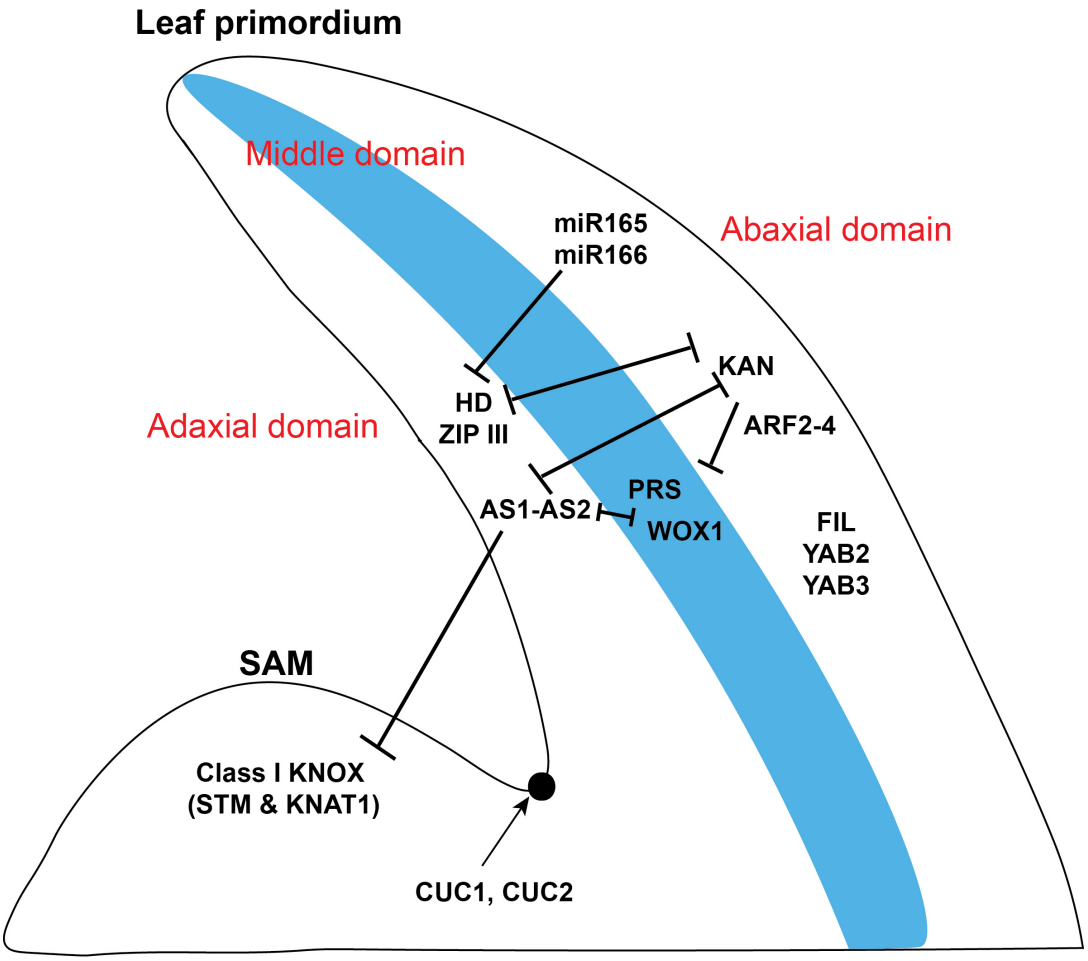

Figure 1.4 Molecular pathways involved in leaf polarity

AS1/AS2 and HD-ZIP III are expressed in the adaxial domain of the leaf. The abaxial domain is specified by ARF2-4, KAN, miR165/166 and YABBY (FIL, YAB2 YAB3). WOX1 and PRS define the middle domain of the leaf. *HD-ZIP III* genes are post-translationally regulated by miR165 and miR166. *KAN* and *HD-ZIP III* genes act antagonistically. KAN and AS2 function as mutual repressors. ARF2-4 work in conjunction with KAN in determining abaxial identity. PRS and WOX1 directly or indirectly suppress AS2, and AS2 suppress WOX1 and PRS. KNOX1 subclass transcription factors (STM and KNAT1) maintain the SAM in an undifferentiated state. CUC transcription factors (CUC1 and CUC2) are involved in the organ separation of the SAM.

1.9. *HD-ZIP III* genes and *KANADI* are expressed in non-overlapping concentric patterns in the SAM

The genes involved in adaxial-abaxial patterning also regulate organ formation in the SAM, as shown in (Izhaki and Bowman, 2007; Caggiano et al., 2017) and Figure 1.4. The HD-ZIP III transcription factor REV (*pREV::REV-2XYPET*) is expressed in the centre of the SAM and on the adaxial domain of the leaf (Figure 1.4, A, white arrowhead). KAN1 (*pKAN::KAN1-2XGFP*) is expressed in the periphery of the SAM and on the abaxial side of the leaf (Figure 1.4, A, white arrow). Before leaf formation, REV and KAN1 are expressed in non-overlapping concentric patterns in the vegetative meristem (Caggiano et al., 2017). A similar expression pattern can be observed in the inflorescence meristem, where floral bracts are initiated. The REV-2XYPET (Figure 1.4, B, white arrowhead) is expressed in the centre of the SAM while KAN1-2XGFP is expressed in the periphery (Figure 1.4, B, white arrow).

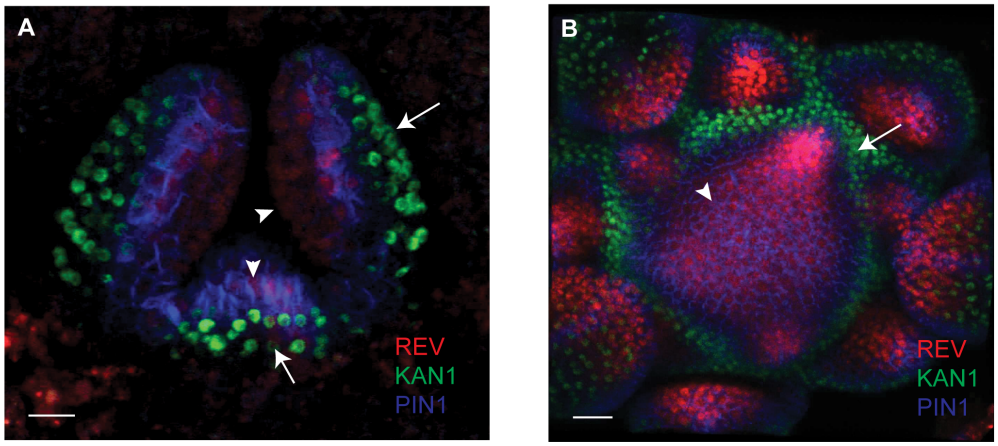

Figure 1.5 *HD-ZIP III* and *KANADI* genes are expressed in the centre and periphery of SAM

Confocal projections exhibit the expression of REV-2XYPET (red), KAN1-2XGFP, and PIN1-CFP (blue) in a vegetative meristem at 4 days after stratification (4 DAS) (A) and in an inflorescence meristem (B). White arrowheads in A indicate the expression of REV-2XYPET in the centre of the SAM and the adaxial side of the leaf. The white arrowhead in B highlights the expression of REV-2XYPET in the centre of the SAM within an inflorescence meristem. White arrows in A indicate the expression of KAN1-2XGFP in the periphery of the SAM and the abaxial side of the leaf. The white arrow in B denotes the expression of KAN1-2XGFP in the periphery of the SAM in an inflorescence meristem. Scale bars, 15 µm (A) and 20 µm (B). Modified from (Caggiano et al., 2017).

1.10. The expression of *REV* and *KAN1* genes in leaves

The radial pattern of *HD-ZIP III* and *KAN* gene expression in the shoot regulates organogenesis such that organs arise on the boundary of KAN expression and thus inherit the adaxial-abaxial pattern of *HD-ZIP III* and *KAN* gene expression respectively (Caggiano et al., 2017). Figure 1.5 illustrates the adaxial expression of *pREV::REV-2XYPET* in the leaves. REV-2XYPET is found in the adaxial epidermis, mesophyll cells, and vasculature of the developing leaf primordia. The arrowhead in Figure 1.5, B indicates the expansion of REV from the epidermis towards the inner cell layers and its presence in the vasculature. Overall, REV is present in adaxial epidermis, mesophyll, and vascular cells. The white arrow in (Figure 1.5, B) points out that *pKAN1::KAN1-2XGFP* is expressed in the epidermis of the leaves. KAN1-2XGFP is not present in the leaf vasculature but is found in the developing phloem of the root (Emery et al., 2003).

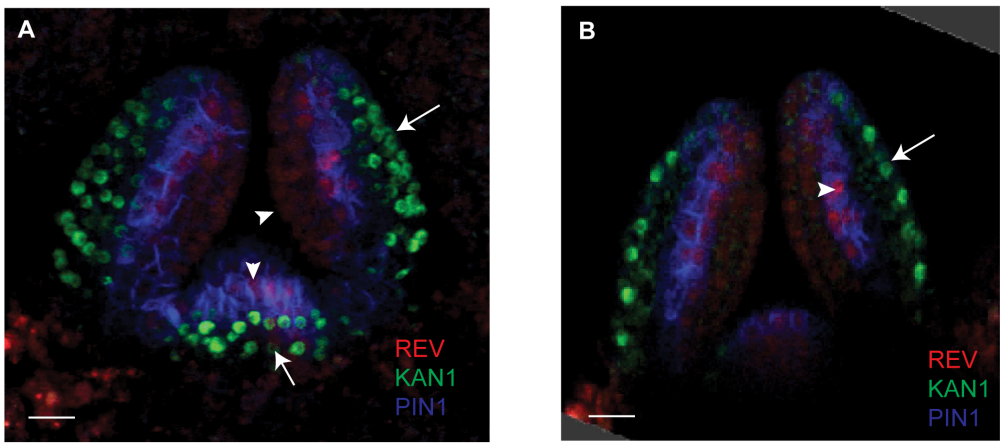

Figure 1.6 REV and KAN1 expression in the leaves

Confocal projections exhibit the expression of REV-2XYFP (red), KAN1-2XGFP, and PIN1-CFP (blue) in a vegetative meristem 4 DAS (A) and a transverse optical section to visualise the inner cell layers (B). White arrowheads in A indicate the expression of REV-2XYFP in the centre of the SAM and the adaxial side of the leaf. The white arrowhead in B denotes the expression of REV-2XYFP in the vasculature. White arrows in A indicate the expression of KAN1-2XGFP in the periphery of the SAM and the abaxial side of the leaf. The white arrow in B highlights the expression of KAN1-2XGFP in the epidermis of the leaf. Scale bar is 15 µm. Modified from (Caggiano et al., 2017).

1.11. Discovery of *KANLIKE* genes

A recent transcriptomics study (Ram et al., 2020) utilised a FACS/RNA-seq approach to identify genes that are both differentially expressed in REV and KAN1 cell types and responsive to REV and KAN1 expression in the *Arabidopsis* shoot. Among the many genes identified, a subset was particularly intriguing due to their similarity to the MYB transcription factor to *KANADI.* This subset were named *KANL1*, *KANL2*, *KANL3,* and *KANL4* because the initial BLAST (Basic Local Alignment Search Tool) indicated they were most similar to the KANADI family in *Arabidopsis*. Among these genes, *KANL3* and *KANL4* have now been studied by another research group, and were named by this group *MYS1* and *MYS2,* respectively (Liu et al., 2022). It was reported that MYS1 and MYS2 are similarly expressed in leaves, hypocotyl, flowers and roots and including in the guard cells of both leaves and sepals. From various experiments, these authors concluded that both genes are involved in wax biosynthesis and drought tolerance (Liu et al., 2022).

For this study, the genes *KANL1* and *KANL2* were selected for further investigation. Both genes were found by Ram et al., 2020 to be upregulated by REV and downregulated by KAN1, with expression detected primarily in the REV domain (Figure1.7). Further, studies have been conducted in the Heisler lab to investigate the regulation of *KANL1* and *KANL2* by REV. For instance, the plant line *35S::REVr-GR* in an *ap1 cal1* mutant background was generated to measure changes in *KANL* gene expression in response to the induction of REV expression after Dexamethasone treatment (William et al., 2004; Yamaguchi et al., 2014). Induction of both *KANL1* and *KANL2* expression was detected in both the absence and presence of cycloheximide, indicating that *KANL1* and *KANL2* are immediate targets of REV (unpublished data from the Heisler lab).

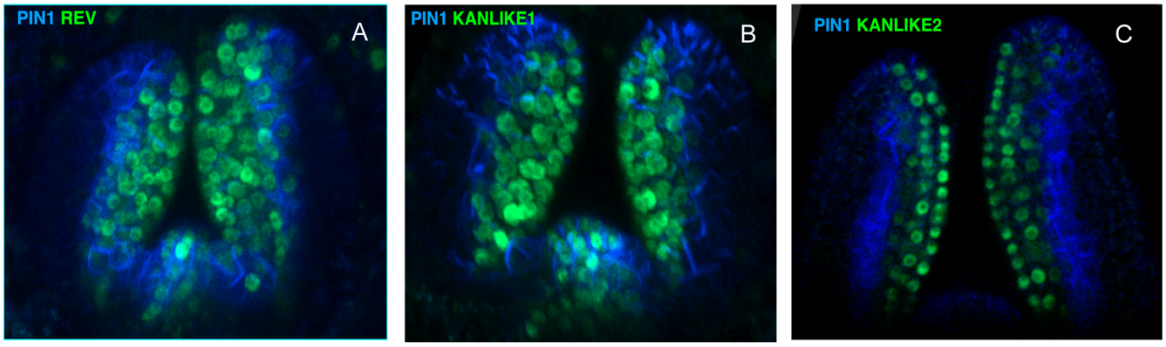

Figure 1.7 KANL1 and KANL2 are expressed in the REV domain of the leaves

Confocal projections showing the expression of REV-2YFP (A) KANL1-2XYFP (B) KANL2-2XYFP (C) with PIN1-GFP at 4 DAS in a vegetative shoot apical meristem. These data were generated by Dr. Neha Bhatia.

1.12. The *KANLIKE* gene and their orthologs

The genes called *KANLIKEs* (*Arabidopsis*) in this thesis belong to the ENOPTRON (ENO) group within the GARP transcription family while the other two groups within the GARP family are KANADI and PHOSPHOROUS STARVATION RESPONSE1/PHOSPHATE STARVATION RESPONSE/ (PSR/PHR) (Bowman et al., 2017; Briginshaw, 2020).

The *KANLIKE* genes (*KANL1-4*) encode SH[AL]QKY[RF]-class MYB (GARP DNA-binding domain) transcription factors similar to the KANADI transcription factors (Figure 1.8). In addition to the MYB domain, KANADI and the KANLIKEs /ENOs share an ethylene-responsive element binding factor (ERF)-associated amphiphilic repression (EAR) domain. Both groups of transcription factors are exclusive to land plants and are deduced to be present in the common ancestor of liverworts and angiosperms (Briginshaw, 2020). In KANADI both N-terminal and C-terminal regions that resemble EAR domain are referred to as PDLSL and LEFTL, respectively. The KANLs/ ENOs feature a LxLxL EAR domain alongside the MYB domain.

Previous studies have identified two orthologs of *Arabidopsis KANL1* and *KANL2,* in other species. A similar SH[AL]QKY[RF]-class MYB transcription factor is present in tomato (*Solanum lycopersicum*) named CLAUSA (Bar et al., 2016) while the second, SALAD, was

discovered in wild diploid strawberry (*Fragaria vesca subsp. vesca*) (Luo et al., 2024). Like the KANLs, CLAUSA and SALAD contain the MYB DNA binding domain and an EAR motif. This EAR motif, characterised by the conserved sequence "LxLxL," is a key feature shared by the three types of proteins as can be seen in a multiple protein sequence alignment (Figure 1.9), suggesting functional importance.

KANL1 and KANL2 form a clade that is closely related to CALUSA from tomato and SALAD from diploid strawberry, suggesting they share a recent common ancestor (Figure 1.10). In contrast, MYS1 (KANL3) and MYS2 (KANL4) are more distantly related to this group but are more closely associated with the KANL homolog of *Marchantia polymorpha* (ENO).

They also show an early divergence from KAN in *Marchantia polymorpha*, *Arabidopsis*, and PSR in *Chlamydomonas reinhardtii.*

Both *SALAD* and *CLAUSA* play a role in compound leaf morphogenesis. Phenotypic characteristics of *clau*, such as highly divided leaves with acute serrations, were first described in tomatoes in 1967 (Khush and Rick, 1967). In addition to the phenotypic characters in leaves, *clau* shows striking phenotypes in flowers, inflorescences, and fruits (Avivi et al., 2000). Unlike the adaxial expression of *KANL1* and *KANL2*, *CLAUSA* is expressed at the tomato leaf margin during leaflet morphogenesis. *CLAUSA* is also expressed at low levels in the shoot apical meristem (Figure 2 in Bar et al.,2016). *CLAUSA* has been reported to suppress expression of GOBLET (GOB), a member of the CUC transcription factor subfamily, as well as the KNOX1 transcription factor LeT6/Tkn2 and cytokinin responses during leaf morphogenesis (Bar et al., 2015; 2016). Similar to *CLAUSA*, *SALAD* is also expressed at the leaf margin and suppresses the NAM/CUC class transcription factor CUC2a in strawberries. However, unlike *CLAUSA*, it does not regulate KNOX1 levels (Luo et al., 2024). To investigate the function of *SALAD* orthologs in *Arabidopsis*, this study used CRISPR to generate *kanl1 kanl2* mutants in the *Arabidopsis* Col ecotype. Their analysis reported that the double mutant exhibited deeper serrations along the leaf margin

compared to the wild type (Luo et al., 2024). No further analysis of KANL1 or KANL2 has been reported.

1.13. Do KANL1 and KANL2 regulate the middle domain?

On the abaxial side, the middle domain genes *WOX1* and *PRS* are suppressed by *KAN1* and *KAN2*, working together with *ARF2, ARF3*, and *ARF4* (Alvarez et al., 2016; Heisler, 2021; Pekker et al., 2005; Yu et al., 2017). There is a debate in the literature regarding the adaxial side. Some studies have shown that the *HDZIP III* gene *REV,* along with *AS2,* suppresses WOX1 and PRS on this side (Alvarez et al., 2016; Ram et al., 2020). However other studies conclude that low auxin levels repress WOX1 and PRS adaxially (Burian et al., 2022; Guan et al., 2017). This controversy is discussed in detail in (Fernando and Heisler, 2024). With the identification of *KANL1* and *KANL2* genes as downstream targets of the *HDZIP III* gene, the hypothesis can be proposed that WOX1 and PRS may be repressed in adaxial tissue by KANL1 and KANL2.

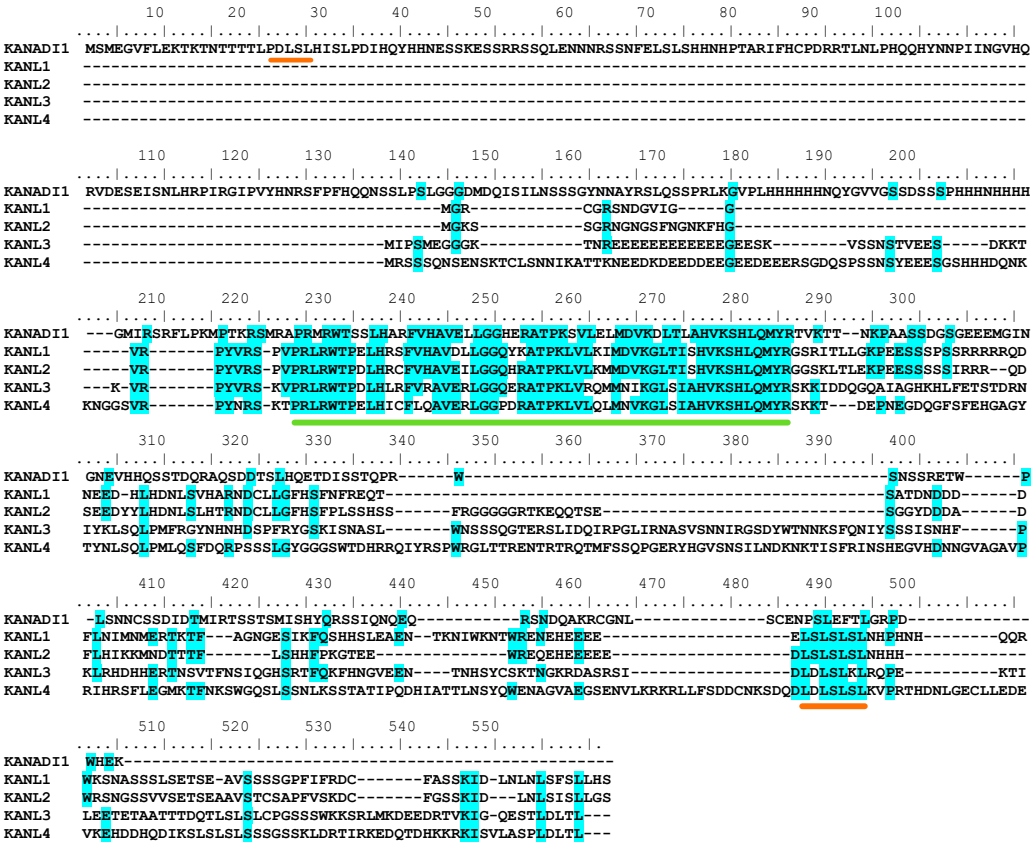

Figure 1.8 The multiple sequence alignment of protein sequences for KANADI1 and its orthologs KANLs

Identical amino acids are labelled in blue boxes. The MYB domain, containing the conserved SHLQMYF residue, is highlighted with a green underline. EAR motifs are underlined in orange. Other than the MYB domain, KANADI1 possess N- and C-terminal regions resembling ERF-associated amphiphilic repression (EAR) domains PDLSL and LEFTL. KANL1 and KANL2 possess only an LxLxL EAR domain, apart from the MYB domain. The figure is adapted with modifications from (Luo et al., 2024). The species and accession numbers corresponding to these transcription factors are provided in Table 1.1.

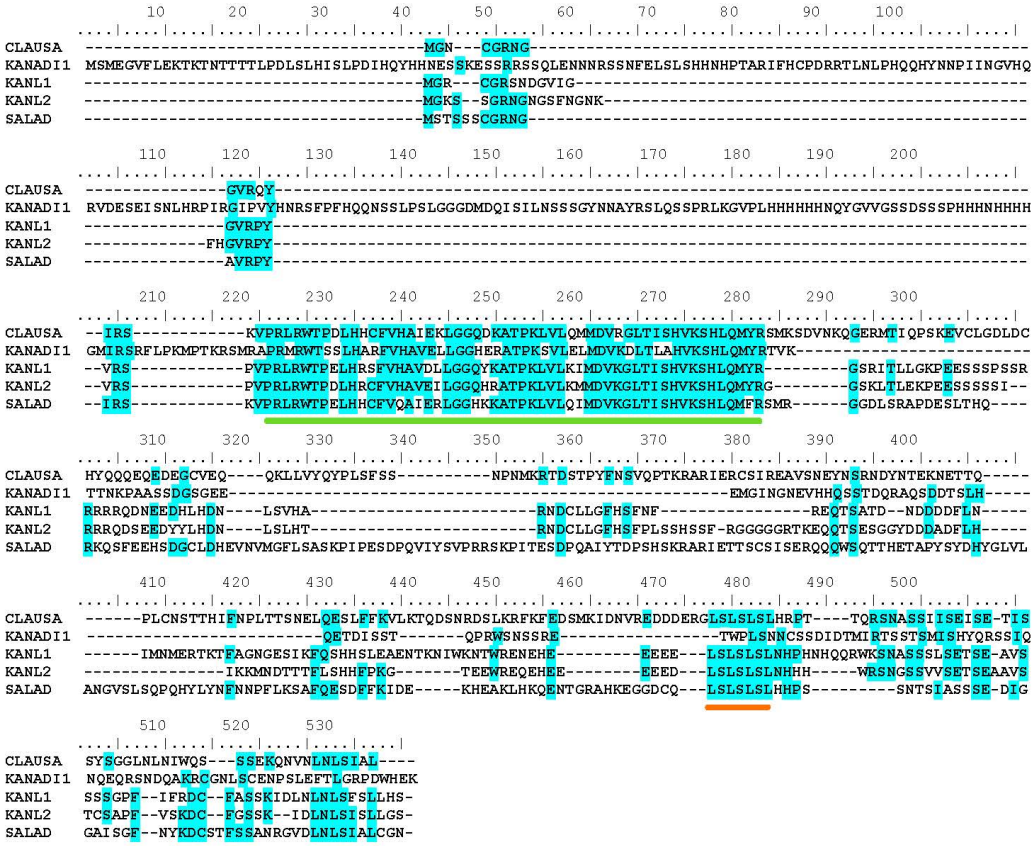

Figure 1.9 Multiple sequence alignment of protein sequences of KANADI1 and its orthologs KANLs, CLAUSA and SALAD

Identical amino acids are labelled in blue boxes. The MYB domain, containing the conserved SHLQMYF residue, is highlighted with a green underline. EAR motifs are underlined in orange. CALUSA, SALAD and the KANLs possess the same LxLxL EAR domain, apart from the MYB domain. The figure is adapted with modifications from *(Luo et al., 2024)*. The species and accession numbers corresponding to these transcription factors are provided in Table 1.1.

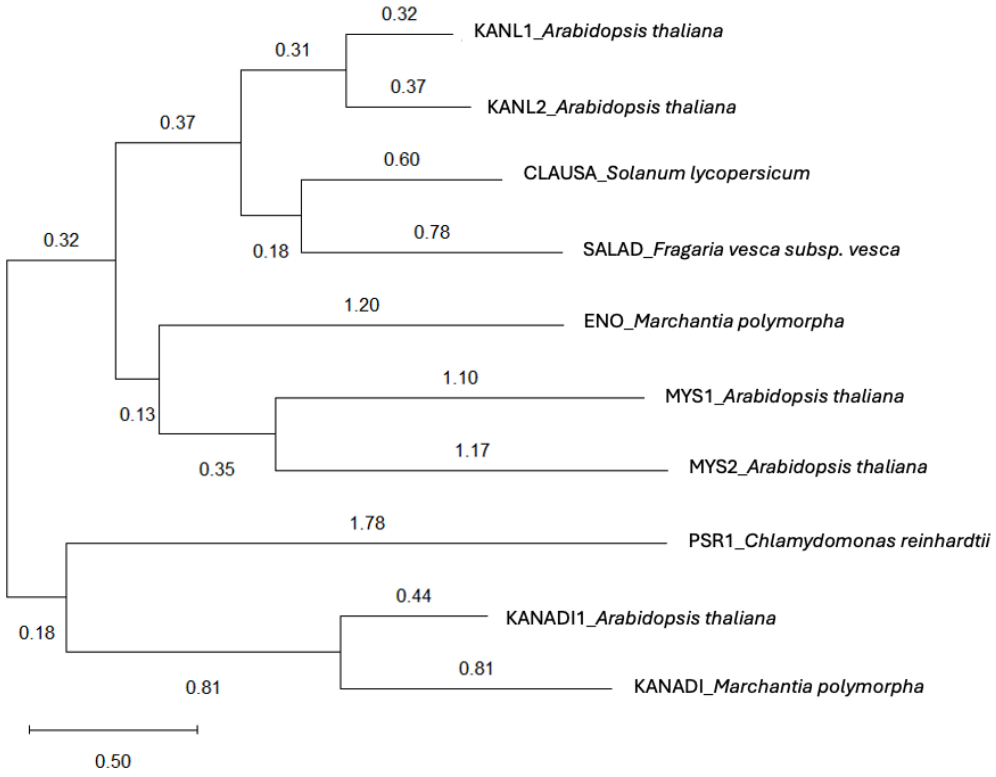

Figure 1.10 Evolutionary analysis of KANLs

The phylogenetic tree was inferred using MEGA 12 by the Maximum Likelihood method and the Jones-Taylor-Thornton (JTT) model of amino acid substitutions, and the tree with the highest log likelihood (-10,569.15) is shown. The tree is drawn to scale with branch lengths, shown next to the branches. The analysis was conducted using the amino acid sequence of the full protein, revealing the evolutionary relationship of KANLs among the members of GARP transcription factor family. Species and the accession numbers of the transcription factors are listed in table 1.1.

Table 1.1 Accession numbers of transcription factors discussed in this thesis

Accession Number	Transcription Factor name	Species
NP_568334.1	KANADI1	*Arabidopsis thaliana*
NP_1322279.1	KANADI2	*Arabidopsis thaliana*
NP_567535.1	KANADI3	*Arabidopsis thaliana*
NP_1119363.1	KANADI4	*Arabidopsis thaliana*
NP_172912.3	KANL1	*Arabidopsis thaliana*
NP_1324904.1	KANL2	*Arabidopsis thaliana*
NP_181364.2	KANL3 (MYS1)	*Arabidopsis thaliana*
NP_1324369.1	KANL4 (MYS2)	*Arabidopsis thaliana*
XP_004236899	CLAUSA	*Solanum lycopersicum*
XP_004297794	SALAD	*Fragaria vesca subsp. vesca*
Mp4g08700.1	ENO	*Marchantia polymorpha*
PNW74555.1	PSR1	*Chlamydomonas reinhardtii*
Mp3g04970.1	KANADI	*Marchantia polymorpha*

1.14. This thesis

The *KANL1* and *KANL2* genes described are novel genes potentially involved in adaxial/abaxial tissue development and patterning. While an analysis of their mutant phenotype has been published (Luo et al., 2024), this analysis was relatively limited in scope. It did not include any kind of genetic or expression analysis in *Arabidopsis* and was focused mainly on the leaf margin, even though other aspects of the phenotype are visible from the published images presented. Given the distinct expression domains of *KANL1* and *KANL2* compared to *CLAUSA* and *SALAD*, it remains to be seen whether the *KANLIKEs* exhibit unique functional roles compared to *CLAUSA* and *SALAD*, or if they share functional similarities. This project's main aim is to further investigate the regulation of *KANLIKEs* by *HD-ZIP III* genes and to investigate their role within the already established adaxial-abaxial regulatory framework governing leaf development described in the literature. To begin with, Chapter 3 further investigates whether *HD-ZIP III* genes regulate *KANLIKEs* as immediate and direct targets. In Chapter 4, I investigate the developmental functions of *KANL1* and *KANL2* using loss-of-function mutants. The final results chapter focuses on genetic interactions between *KANL1* and *KANL2* and other genes involved in adaxial-abaxial leaf patterning. Chapter 6 summarises the function of *KANL1* and *KANL2* in leaf polarity establishment.

Chapter 2 – Materials and Methods

2.1. Plant Materials

Unless stated otherwise, the Ara*bidopsis thaliana* ecotype Landsberg *erecta* (L*er*) was utilized as the wild type (WT), for the mutant backgrounds and in the generation of transgenic lines in this research.

2.1.1. Transgenic lines

Dr. Carolyn Ohno generated all the transgenic lines analysed in this research.
Table 2.1 lists the plant lines containing translational fusions with fluorescent proteins and all the genotypes analysed with the respective plant selection.

2.1.1. Mutant alleles

The single mutant alleles, *kanl1-1 (kanl1)* in *pPIN1::PIN1 CFP* and *kanl2-1 (kanl2)* in *pPIN1::PIN1 GFP* were available in the Heisler lab. The *as2-1* (Col) (Semiarti et al., 2001) and *wox1-101 prs-2* (Col) (Nakata et al., 2012b) were available in the Heisler lab. The *as2-101*(L*er*) (Yi et al., 2002) was obtained from the Arabidopsis Biological Resource Center (ABRC). The *kan1-2 kan2-1*, *rev-9, phb-6, phv-5*, and *phb-6, phv-5 rev-9/+ (*L*er*) alleles (Emery et al., 2003) were kindly provided by Prof. John Bowman. The *wox1* allele in L*er* ecotype and *kanl1 kanl2* background was generated by Dr. Carolyn Ohno in the Heisler lab.
All the multiple mutants combined with the *kanl1 kanl2* double mutant ((*as2 kanl1 kanl2, rev kanl1 kanl2, phb phv kanl1 kanl2, phb phv rev kanl1 kanl2, wox prs kanl1 kanl2* (Col + L*er* introgressed ecotype)) were generated by the mutants mentioned above and are described in the Methods section 2.2.2.

Table 2.1 Transgenic lines used in this research for gene expression by confocal microscopy

T-DNA construct	Analysed background/genotype	Plant selection
pPIN1;::PIN1-CFP	WT, *kanl1 kanl2*	Glufosinate
pKANL1::KANL1-2XYPET (H.Ram and C.Ohno, unpublished)	*pPIN1::PIN1-CFP,* *as2-1*(Col), *pPIN1::PIN1 GFP* in *kan1 kan2* (Col), *wox1-101 prs-2* (Col), *kanl1 kanl2*	Glufosinate
pKANL2::KANL2-2XGFP (H.Ram and C.Ohno, unpublished)	*wox1-101 prs-2* (Col), *pKANL1::KANL1-2YPET* with *pPIN1::PIN1 CFP,* *pPIN1::PIN1 CFP* in *kanl1 kanl2*	Glufosinate
pKANL2::KANL2-2XYPET (H.Ram and C.Ohno, unpublished)	*pPIN1::PIN1-GFP,* as2-1(Col), *pPIN1::PIN1 GFP* in *kan1 kan2* (Col)	Hygromycin
pCUC2::CUC2-VENUS (Heisler et al., 2005)	*pPIN1::PIN1-GFP,* *kanl1 kanl2*	Glufosinate
pWOX1::2XYPET-WOX1 (C.Ohno, unpublished)	*pPIN1::PIN1-CFP,* *as2-101*, *as2-1* (Col) *pPIN1::PIN1 GFP* in *kan11 kan12*	Glufosinate
pPRS::PRS-2XYPET (C.Ohno, unpublished)	*pPIN1::PIN1-CFP,* *as2-10*1, *as2-1* (Col) *pPIN1::PIN1 GFP* in *kan11 kan12*	Glufosinate
pAS2::AS2-GFP (C.Ohno, unpublished)	WT, *kanl1 kanl2*	Glufosinate
pWOX1::2XGFP-WOX1 (Caggiano et al., 2017)	*pPIN1::PIN1-CFP,* *kanl1 kanl2*	Glufosinate
pREV::REV-2XYPET (Caggiano et al., 2017)	WT, *pPIN1::PIN1-GFP,* *kanl1 kanl2*	Glufosinate
pKAN::KAN1-2XGFP (Caggiano et al., 2017)	WT, *kanl 1kanl2*	Glufosinate

2.2. Methods

2.2.1. Plant growth conditions

The seeds were sterilised with 70% ethanol and initially planted on GM media or GM media containing antibiotics for plant selection. The composition of the GM medium is detailed in Table 2.2. After two days of stratification at 4°C in the dark, the plants were grown on plates for seven days before being transferred to soil. The seedlings analysed with confocal microscopy were continuously grown on GM media for the required duration.

Plants were grown in a uniform soil mixture made up of Jiffy Multiplication High Demand soil, vermiculite (fine, grade 2), and perlite (medium) at a ratio of 4:3:2 and supplemented with Exact Mini Osmocote 3-4 month (ICL), within a growth room that received continuous light from cool white-fluorescent lamps (approximately 130-150 µE m^2 sec^1). The temperature was kept at 22°C, and the humidity was maintained between 30% and 50%, with an air exchange rate of 2 to 3 times per hour.

The plants cultivated for the phenotypic analysis of rosette leaves were grown for 28 days in a growth cabinet with long daylight (16 hours of light and 8 hours of dark) at 18°C.

Table 2.2 GM medium components

Component	Amount (for 1L)
Sucrose	10 g
MS salts (Sigma M5524)	4.33 g
MES-2-(N-morpholino)-ethane sulfonic acid (Sigma M2933)	0.5 g
Bacto Agar	9 g
MS Vitamins (Sigma M3900)	1 ml
Sulfadiazine (optional)	7.5 mg
Carbenicillin (optional)	300 mg
Basta (optional)	7.5 mg
Hygromycin (optional)	35 mg

2.2.2. Generation of *kanl1 kanl2* double mutant and combinatorial mutants

CRISPR-Cas9 induced mutant alleles, *kanl1-1(kanl1)* in background *pPIN1::PIN1 CFP* and *kanl2-1(kanl2)* in background *pPIN1::PIN1 GFP,* were outcrossed to WT three times to generate the *kanl1 kanl2* double mutant in the absence of the *PIN1* marker. This was done to avoid the undesirable phenotype caused by multiple copies of PIN1 and any off-target Cas9-induced mutations. The homozygous plants for both the alleles *kanl1-1 and kanl2-2* were identified by PCR genotyping followed by restriction digestion, as described in method section 2.2.3.

The *as2-101* allele was crossed with *kanl1 kanl2* to generate the *as2 kanl1 kanl2* triple mutant; *wox1-101 prs-2* (Col) was crossed with *kanl1 kanl2* to generate the *wox1 prs kanl1 kanl2* quadruple mutant. The *rev-9* allele was crossed with *kanl1 kanl2* to generate the *rev kanl1 kanl2* triple mutant; *phb-6 phv-5* was crossed with *kanl1 kanl2* to generate the *phb phv kanl1 kanl2* quadruple mutant and *phb-6 phv-5 rev-9/+* was crossed with *kanl1 kanl2* to make the *phb phv rev kanl1 kanl2* quintuple mutant. The homozygous plants and mutants for all the loci were identified by PCR genotyping or PCR followed by restriction enzyme digestion, as described in method section 2.2.3.

2.2.3. Mutant analysis

2.2.3.1. DNA extraction

DNA was extracted from the leaf tissues as previously described by (Edwards, Johnstone and Thompson, 1991). One leaf from each plant was collected into a 1.5 ml tube. The tissue was ground with a pestle in 400 µl of extraction buffer (200 mM Tris, 50 mM NaCl, 25 mM EDTA, 0.5% SDS, pH 7.5) and then centrifuged at 13000 rpm for 2 minutes. The supernatant was mixed with 300 µl of isopropanol and combined before being centrifuged at 13000 rpm for 5 minutes. The resulting DNA pellet was washed with 70% ethanol and thoroughly air-dried. The pellet was dissolved in 100 µl of sterile TE (10 mM Tris, 1 mM EDTA).

2.2.3.2. Polymerase chain reaction (PCR), Restriction enzyme digestion and gel electrophoresis

PCR reactions were performed in a C1000 Thermal Cycler (Bio-rad) using One Taq DNA polymerase (NEB). The conditions were a 3-minute denaturation at 94℃ followed by 36 cycles of 94℃ for 10 seconds, 60℃ for 15-20 seconds, and extension at 68℃ for 1 minute per kb. The primer annealing temperature was set accordingly.

For some genotyping, both PCR and restriction enzyme digestion were used together.

If the resulting DNA fragment from PCR underwent digestion with a restriction enzyme, 5 µl of the DNA was treated with 1 µl of the restriction enzyme (NEB) and the supplied buffer. The reaction conditions included incubation at 37℃ overnight.

PCR-amplified or digested fragments were stained with Nancy-520 fluorescent dye (01494 Sigma-Aldrich) and separated by gel electrophoresis. Based on the fragment size, 1% or 3% agarose gels were run for 40 min at 70 V in 1X TAE buffer (0.04M Tris-acetate0.001M EDTA). The genotypes were determined by the desired fragment length or by observing the presence or absence of the fragment in a ChemiDoc MP Imaging System (BioRad).

Table 2.3 summarizes the different genotyping techniques used to determine the mutant alleles, including the oligonucleotides and restriction enzymes.

Table 2.3 Summary of mutant genotyping

Gene and allele	Oligonucleotides	Restriction enzyme (NEB)	Wild type allele vs mutant allele
kanl1-1	(F)CATCTTTCTTCCTCTACAGAAG (R)GGTCTTACTCCACCAATTATTACTCCA	BspDI	Wild type-137 bp, mutant cut into 115 bp, 22 bp
kanl2-1	(F)TTTTAATCCCAACCCACACACCTC (R)GCGTGAAGGTTTTGACTCGGTAAC	XcmI	Mutant-628 bp, wild type cut into 247 bp and 381 bp
kan1-2	(F) AAGAAGATCCTCCCAACTCGAAAA (R)AGCCGGAAGATGAGTTTTAGATTGAGA TTTT	MseI	Wild type cut into 117 bp and 216 bp, mutant cut into 117 bp, 118 bp and 30 bp
kan2-1	(F)AACAACAACAACAACATCATCATCCG (R)GGTATTCCTCTTATTGGTCTTAAGTGA	AciI	Mutant-161 bp, wild type cut into 135 bp and 26 bp
wox1-10 and *wox1-15* (L*er*)	(F) GACGATGGGTTACAACGAAGGAG (R) AGCATCATCAGCTCCCTCTTGTTC	Hyp166II	Mutant-283 bp, wild type cut in to 101 bp and 183 bp
wox1-101 (Col)	(1) TGTGGACGATGGGTTACAAC (2) CGTCAATTTGTTTACACCAC (3) GATATATACCTCTGGTTGCG	_	Primers 1 and 2 amplify mutant 650 bp fragment, Primers 1 and 3 amplify wild type 800 bp fragment
prs-2 (Col)	(1) CTAAGTGTTTGGAGATAGCATCAC (2) ACATGGGAGAAGGATGAGAGCAGC (3) AGCTGTTGCCCGTCTCACTGGTG	_	Primers 1 and 2 amplify wild type 500 bp fragment, Primers 1 and 3 amplify mutant 250 bp fragment
phb-6	(1) TCGAGATTGGCGTCTGAGATAAA (2) GGTTCCCGTCCGATTTCGACT (3) TTGGAAACGCATTCAAAGACAAT	_	Primer 1 and 2 only amplify the mutant allele, no amplification for wild type. Primer 1 and 3 only amplify the wild type, no amplification for mutant
phv-5	(1) GTTCCTTGTCCTTTCTCTCTCAG (2) ACGGTCGGGAAACTAGCTCTAC (3) GTTTGATTAGCTGTCACTTTTCC	_	Primer 1 and 2 only amplify the wild type allele, no amplification for mutant. Primer 1 and 3 only amplify the wild type, no amplification for mutant
rev-9	(1) CCTCTGTTCCAAAGTTCAGCAG (2) GCCTGCCCAACCTTTCGGTA	_	Primer 1 and 2 only amplify the mutant

	(3) GCCTGCCCAACCTTTCGGTA		allele, no amplification for wild type. Primer 1 and 3 only amplify the wild type, no amplification for mutant

2.2.4. ChIP (Chromatin extraction and immunoprecipitation) qPCR to determine *KANL1* and *KANL2* regulation by *REV*

Chromatin extraction and immunoprecipitation were conducted using the same buffers and solutions described by (Kaufmann et al., 2010). *pAtUBQ10>>REVr*-GFP in *ap1 cal1* was used as the plant line.

2.2.4.1. REV induction by Dexamethasone treatment of inflorescence meristem

Four distinct plant lines (T2) were chosen from the transformants by planting them on DEX plates. The seeds of selected plant lines were planted and allowed them to grow until bolting. The smooth inflorescences, devoid of floral organs, were treated with DEX for 6 hours (10 μM DEX + 0.015% Silwet L-77).

2.2.4.2. Tissue harvesting and fixation with formaldehyde

After 6 hrs of the DEX treatment, inflorescence tissue (900 mg) were harvested and collected in 50 ml falcon tubes on ice, and 25 ml of MC buffer (10 mM sodium phosphate, 50 mM NaCl, 0.1 M sucrose, pH 7) was added. The tissues were fixed by adding 1.56 ml of a 16% (w/v) methanol-free formaldehyde solution (28908, Thermo Scientific) under vacuum (0.8 bar) at room temperature for 30 minutes in the chemical fume hood. After 15 minutes, the tissue was mixed with the solution, and the vacuum was reapplied for another 14 minutes. The fixation was stopped by adding 2.5 ml of glycine from a 1.25 M stock. Before freezing, the fixed tissue was washed

three times with MC buffer (25 ml each wash), dried well on tissue papers, frozen in liquid nitrogen, and stored at -80 °C.

2.2.4.3. Nuclei isolation and Chromatin shearing

The tissue was ground in liquid nitrogen, and the homogenised tissue powder was resuspended in ice-cold M1 buffer (0.1 M NaCl, 10 mM β-mercaptoethanol, 10 mM sodium phosphate, pH 7, 1 M 2-methyl-2,4-pentanediol (8208191000 ,Merck), and a complete protease inhibitor cocktail (11697498001, Roche). Using a glass funnel, the resulting slurry was filtered through a clean nylon mesh (55 μm, Sefar). The flow-through was collected in 50 ml tubes placed on ice. The filtrate was centrifuged at 1000 x g for 20 minutes at 4°C. The supernatant was removed, and the nuclei pellet was kept.

The pellet was resuspended in ice-cold M2 buffer containing M1 buffer, 10 mM MgCl2, and 0.5% Triton X-100. It was then centrifuged at 1000 x g for 20 minutes at 4°C. The supernatant was removed, and this step was repeated five times. The final pellet was suspended in ice-cold M3 buffer (M1 buffer without 2-methyl-2,4-pentanediol) and centrifuged at 1000 x g for 10 minutes at 4°C.

The nuclear pellet was resuspended in 0.5 ml of ice-cold sonic buffer (0.1 M NaCl, 10 mM EDTA, 0.5% Sarkosyl,10 mM sodium phosphate, pH 7, and freshly added 21 μl of a complete protease inhibitor cocktail from a 25× stock) and transferred into a 1 ml Covaris sonication tube (milliTUBE 1 ml AFA Fiber, CatNo. *520135* (100)).

The DNA was sheared using a M220 focused-ultrasonicator (Covaris, USA), following a setup similar to that described by (Krizek et al., 2020). This setup involved 14 cycles at 75% peak power, a 5% duty factor, and 200 cycles per burst, all conducted at 7°C. The sonicated chromatin was then transferred to a 2 ml Low-DNA binding tube (Eppendorf) and the samples were centrifuged at full speed for 10 minutes at 4°C. The supernatant was transferred to a new tube,

and this step was continued until no debris was visible. 25 µl of sonicated chromatin was kept on ice to be used as the input control for qPCR.

2.2.4.4. Immunoprecipitation

The protein-DNA complexes were immunoprecipitated by adding 50 µl of anti-GFP microbeads from the µMACS^{TM} GFP isolation kit (130-091-288, Miltenyi Biotec). They were incubated on a rotating device (10 rpm) in a cold room for one hour. The lysate was separated using µ-columns in the µMACS^{TM} separator (130-042-701, Miltenyi Biotec). All washes were performed at room temperature. The µ-columns were pre-treated with 200 µl of cold IP buffer (0.05% SDS ,150 mM NaCl, 5 mM MgCl2, 50 mM HEPES, pH 7.5, 10 µM ZnSO4, and 1% Triton X-100). The lysate was allowed to pass through by gravity flow, and the immobilized beads were washed twice with 400 µl of cold IP buffer. The beads were then washed twice with 200 µl of high salt buffer (500 mM NaCl, 1 % Triton X-100, 0.1 % SDS, 2 mM EDTA, 20 mM Tris-Cl, pH 8). This was followed by two washes with 200 µl of LiCl buffer (0.25 M LiCl, 10 mM Tris–HCl, pH 8, 1 mM EDTA, 1 % NP-40, 1 % sodium deoxycholate) and finally washed with 200 µl of 1x TE (1 mM EDTA,10 mM Tris–HCl, pH 8). After the final wash, the columns were incubated for 5 minutes with 20 µl of hot elution buffer (95°C) containing 1% SDS, 10 mM EDTA, 50 mM DTT, and 50 mM Tris–HCl at pH 8. The cross-linked DNA was eluted three times with 50 µl of hot elution buffer.

2.2.4.5. Reverse cross-linking and DNA purification

150 µl of 1x TE was added to the eluate from the column, and 275 µl of 1x TE was added to the input DNA. Subsequently, 15 µl of 5 M NaCl was added to each sample to achieve a final NaCl concentration of approximately 250 mM. The samples were thoroughly mixed and incubated overnight at 65 °C. Then, 8 µl of proteinase K (20 mg/ml, 26160, Thermofisher) was added to the samples, which were incubated at 65 °C for 6 hours. The DNA was precipitated by adding 2.5 volumes of 100% ethanol, 0.1 volume of 3 M sodium acetate (pH 5.4), and 1 µl of glycogen,

followed by overnight incubation at -20 °C. The samples were centrifuged for 30 minutes at 4 °C at top speed. The supernatant was removed, and the pellet was resuspended in 100 µl of water. The DNA was purified using a ChIP DNA clean and concentrator kit (D5205 Zymo Research) as per the manufacturer's instructions and eluted with 50 µl of the elution buffer into 1.5 ml tube.

2.2.4.6. Determination of sonication efficiency

The sonication efficiency for the fragmented DNA was assessed using purified DNA from the input sample. 20 µl of the input DNA sample was loaded onto a 1.5 % agarose gel alongside the size marker. The size of the DNA smear and its maximum peak were evaluated (the desirable fragment sizes range from 200 to 1000 bp, with the maximum peak around 500 bp).

2.2.4.7. ChIP qPCR

qPCR was performed using the DNA instead of cDNA as described in the methods 2.2.6. The input DNA was diluted 1,000 times, while the ChIP DNA was diluted 4 times for qPCR reactions. The primers used to check the REV binding sites at *KANL1* and *KANL2* promoter regions are listed in Table 2.4.

2.2.4.7. Data normalisation

The normalisation was performed using the % input method described by (Yamaguchi et al., 2014). The qPCR signals obtained from the ChIP sample were divided by the qPCR signals obtained from the input sample and the graphs were created. The construction of graphs and statistical analysis were performed using GraphPad Prism version 10.4.1 (532) software.

Table 2.4 Oligonucleotides used in ChIP qPCR

Primer name	Sequence (5'-3')
ZPR3-F	AACGAAATAAATGCGACAAATGA
ZPR3-R	AACGAAATAAATGCGACAAATGA
ACTIN2-F	CGTTTCGCTTTCCTTAGTGTTAGCT
ACTIN2-R	AGCGAACGGATCTAGAGACTCACCTTG
KANL1-1-F	GTGCTGGATGATATTTTAGTGGCT
KANL1-I-R	ACAAAAATCAGATGAAAGTTGTATGCTT
KANL1-II-F	GGGCTACCACATAGGGAAATGAT
KANL1-II-R	ATGCCCCTATGCTTCTGCTT
KANL1-III-F	TGTATTATTTCAACCGCAAAGACT
KANL1-III-R	CCCATGTTTCGTTTGTCTTGGTT
KANL2-1-F	GAATGGGGTCACGAGTCAAGA
KANL2-I-R	ACAGAGAGGTGACATGTGTTTT
KANL2-II-F	TGTAGCCTTGTGTAGTTCTCTGG
KANL2-II-R	GTCTTGACTCGTGACCCCATT
KANL2-III-F	GCTGATACCACGTAAACCACG
KANL2-III-R	ACTGTTTTTAAATGATGTATGTATTTCTTGT
KANL2-IV-F	TAGAATTTGCCTTGTTCTTGCATGT
KANL2-IV-R	TGGGTCAATTTTCTCATCACCC

2.2.5. Phenotypic Analysis

2.2.5.1. Microscopy

The photos of rosette leaves, leaf series for all the genotypes, whole plants, and shoots were taken with a Nikon D3400 digital camera using a ruler as a scale bar. Detailed photos of single leaves, inflorescences, and seedlings were captured using a Zeiss Stemi 2000c dissection microscope and a Nikon Z6II camera.

2.2.5.2. Quantification of transverse curvature index

The curvature index was quantified as described by (Liu et al., 2010) with slight modifications. Unless specified otherwise, 28-day-old rosette leaves were used to quantify the rosette leaf phenotype. A minimum of eight replicates (rosettes) were used for all genotypes. The plants were maintained under consistent light, humidity, soil, and water conditions (the seeds harvested on the same day were planted for comparison to ensure equal germination). The dissected leaves from the rosettes, with or without cotyledons, were kept hydrated on wet tissue before imaging. The photos of each leaf before and after flattening were taken, with a ruler serving as the scale bar. A glass slide was used to flatten the leaf, and if necessary, cuts were made to ensure the leaf lay completely flat without damaging its shape (Figure 2.1).

The width of leaves (before and after flattening) was measured using the captured images with ImageJ software (Schneider, Rasband and Eliceiri, 2012). The transverse curvature index was calculated using the equations outlined by (Liu et al., 2010).

$$\text{Transverse Curvature Index (CI)} = (\text{AB} - \text{ab})/\text{AB}$$

Where AB is the flattened width and ab is the projected width.

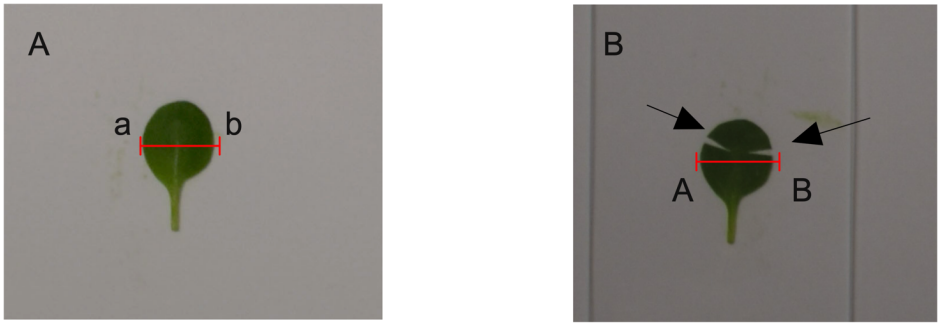

Figure 2.1 Quantification of leaf Transverse Curvature Index

Leaves (before flattening) were arranged on white paper using a ruler, and photographs were taken (A). They were flattened using glass slides. Before placing the glass slides, small cuts were made with a razor blade to ensure they lay completely flat on the sheet (black arrows in B). The red line ab in (A) shows the projected width of the leaf, the red line AB in (B) indicates the flattened width.

2.2.5.3. Quantification of divergence angle in rosette leaves

The divergence angles were measured as described by (Guenot et al., 2012). Images of fully grown rosettes at 28 days old were captured and the divergence angle was quantified using Image J software. A minimum of 20 plants from each genotype, all grown under the same conditions, were used for the analysis.

2.2.5.4. Statistical analysis

GraphPad Prism version 10.4.1 (532) software was used to generate all the graphs and perform the statistical analysis. Statistical significance was assessed using Student's t-test.

2.2.6. Gene expression analysis by qPCR

For RNA extraction, seedlings were grown vertically for 5 DAS. The leaves, along with the hypocotyl and excluding the roots, were harvested with a clean blade and stored at -80 °C. Three biological replicates were performed for one genotype, and RNA was isolated using the ISOLATE II RNA Plant Kit (MER-BIO-52077, Meridian Bioscience) following the manufacturer's instructions. The RNA was eluted in 60 µL of RNase-free water, and its quality was assessed by running it on a 1.5% agarose gel. The concentrations were measured using a Nanodrop 2000c spectrophotometer (Thermo Scientific). One microgram of RNA was converted to cDNA with 5X Trans Amp buffer and reverse transcriptase (SensiFAST cDNA synthesis kit (MER-BIO-65053)) in a C1000 Touch Thermal Cycler (Bio-Rad). Before the qPCR, all primers were validated for the desired efficiency. The primers used in the qPCR are listed in Table 2.5. Three independent experiments (biological replicates) were conducted, with each experiment being repeated three times (technical replicates) using a QuantStudio 7 Pro thermocycler (Applied Biosystems). Applied Biosystems 2X PowerUp™ SYBR Green Master Mix (A25742, Thermofisher) was utilised, and the qPCR was performed in an optical 384-well reaction plate (4309849, Thermofisher). The resulting transcript levels were normalised to *ACTIN2* transcript levels. Relative gene expression levels were calculated using the 2^–ΔΔCt method (Livak and Schmittgen, 2001)

Table 2.5 Oligonucleotides used in the qPCR

Primer Name	**Sequence (5'-3')**
KANL1-F	CGGCGGTCAATATAAAGCAACTC
KANL1-R	TGGTGAAGAACTCTCTTCTGGTT
KANL2-F	CCCCAAGGGAACAGAGGAGTG
KANL2-R	TCGTTTCGCTCACCACCGA
WOX1-F	ACCACGGATTCGACAAGAAAGA
WOX1-R	TCGCATCCGACCGAACATATC
PRS-F	CCTTCTCCCATGTGTCTTCCTC
PRS-R	TGCATCAATATCTCTTCAGCTCCA
KNAT1-F	GACCACTACCCTCGGCTACA
KNAT1-R	AAGCCCAAGGCCGTAGTAGT
ACTIN2-F	GCCATCCAAGCTGTTCTCTC
ACTIN2-R	CAGTAAGGTCACGTCCAGCA

2.2.7. Gene expression analysis by confocal

2.2.7.1. Sample preparation for live imaging

A minimum of three independent T2 or T3 plant lines homozygous for the reporter marker were used for the confocal analysis. The seedlings were grown on plates at 22 °C for 3-4 days under continuous light, while the plants grown in soil were used to image the inflorescence meristem. For live imaging, seedlings were mounted on agar plates. One cotyledon was gently removed using fine tweezers, as described by (Caggiano, 2013) to enable clear observation of the SAM. If necessary, one leaf was removed with a fine needle to achieve a clear view of the adaxial leaf surface. The inflorescence meristems were dissected and prepared for imaging as described in (Heisler et al., 2005).

2.2.7.2. Confocal microscopy settings

All live imaging was performed using hybrid detectors (HyDs) on a Leica TCS-SP5 upright confocal laser-scanning microscope with a 25X water objective (N.A. 0.95). The pixel format was set to 514 x 514, and the optical sections were spaced 1 μm apart. The bidirectional scanning speed was configured to 400 Hz, and line averaging was set to 2.

The fluorescence of CFP, GFP, VENUS, and YPET was imaged using an argon laser. The 458 nm laser was used to excite CFP, which was detected using a 465-500 nm window. The 488 nm laser was used to excite GFP, and the emission window was set to 493-513 nm. Both Venus and YPET were excited by 514 nm laser, and the emission window was set to 520-580 nm. Two different fluorescent proteins were imaged simultaneously using sequential scan mode, switching in between frames. The pinhole size was adjusted based on image brightness and contrast of the fluorescent protein.

2.2.7.3. Image analysis and processing

For the representative image, the similar expression pattern reported by at least three independent plant lines was selected. All the images were analysed and processed using Imaris Viewer. They were annotated and arranged using Adobe Illustrator (version 29.5.1).

2.2.8. Multiple sequence alignment

The amino acid sequences of KANADI, KANL1, KANL2, CLAUSA, and SALAD were downloaded from the NCBI database (https://www.ncbi.nlm.nih.gov/protein). BioEdit software (Hall, 1999) was used to create multiple sequence alignments with default settings.

2.2.9. Phylogenetic analysis

The amino acid sequences were downloaded from the NCBI database (https://www.ncbi.nlm.nih.gov/protein). Multiple sequence alignment was performed using the MUSCLE algorithm in MEGA12 with default parameters (Kumar et al., 2024). Evolutionary analysis was conducted in MEGA12 using the Maximum Likelihood method and Jones-Taylor-Thornton (1992) model (Jones, Taylor and Thornton, 1992).

Chapter 3 - The regulation of *KANL1* and *KANL2* genes

3.1. Introduction

As discussed in Chapter 1, two genes, *KANL1* and *KANL2* were identified in an experiment conducted in the Heisler lab to identify downstream targets of *HD-ZIP III* genes and *KANADI,* which are involved in leaf adaxial-abaxial patterning (Ram et al., 2020). In short, a FACS/RNA-seq approach was used to identify genes that are differentially expressed in cells within the shoot meristem that express *REV* vs *KAN1*. In addition, genes were identified that altered their expression in response to changes in *REV* and *KAN1* expression. From these experiments, *KANL1* and *KANL2* were selected for further study due to their co-expression with REV, their induction by REV, their repression by KAN1 and the presence of a similar MYB DNA binding domain to KANADI family proteins (Chapter 1, Figure 1.6 and 1.7). A second study by the Heisler lab also found *KANL1* and *KANL2* to be down-regulated after induction of miR165a*,* which represses expression of the HD-ZIP III family, in the SAM (Sinha et al., 2023).

This chapter investigates in more detail the expression and regulation of *KANL1* and *KANL2,* revealing differences in their expression patterns in the adaxial and abaxial domains. It also reports cross-regulation between the *KANL1* and *KANL2* genes.

3.2. Results

3.2.1. KANL1 and KANL2 expression patterns partially overlap with each other

As reported earlier, ectopic induction of REV in the epidermal layer of the shoot meristem upregulates both *KANL1* and *KANL2* (Ram et al., 2020). To investigate the expression of these genes during leaf development in detail, I used fluorescent protein reporters (reporter details are in section 4.2.3) to monitor their expression (Figure 3.1). I found the expression pattern of *pKANL1::KANL1-2XYPET* closely resembles that of *pREV::REV-2XYPET*, as it is found on the adaxial side of the leaves, including in the vasculature of the first two leaves (Figure 3.1, B and E, white arrow). However, KANL1-2XYPET expression does not extend throughout the centre of the SAM as REV does (Figure 3.1, E, white arrow at SAM). While *pKANL2::KANL2-2XGFP* expression is also detectable in the adaxial leaf domain, this expression is confined to the epidermal and subepidermal layers and is absent from the leaf vasculature. Additionally, KANL2-2XGFP expression was detected only weakly in the SAM (Figure 3.1, F, white arrow at SAM) compared to KANL1-2XYPET and REV-2XYPET. The reported expression patterns were noted in at least three independent plant lines.

However, a different expression pattern can be observed when the two *pKANL1::KANL1-2XYPET* and *pKANL2::KANL2-2XGFP* reporters are expressed together in the same plant (Figure 3.2, A and B). I found that KANL1-2XYPET expression was largely absent in KANL2-2XGFP expressing cells within the adaxial domain, with very few cells exhibiting co-expression. This observation suggests that increased levels of KANL2 expression can repress KANL1 expression. To investigate further, I used qPCR to monitor the levels of *KANL1* transcripts in the *kanl2* mutant, and *KANL2* transcripts in the *kanl1* mutant. However, I only detected higher levels of *KANL2* transcripts in the *kanl1* mutant, suggesting that *KANL2* suppresses *KANL1,* while no difference in transcript levels of *KANL1* was detected in *kanl2.*

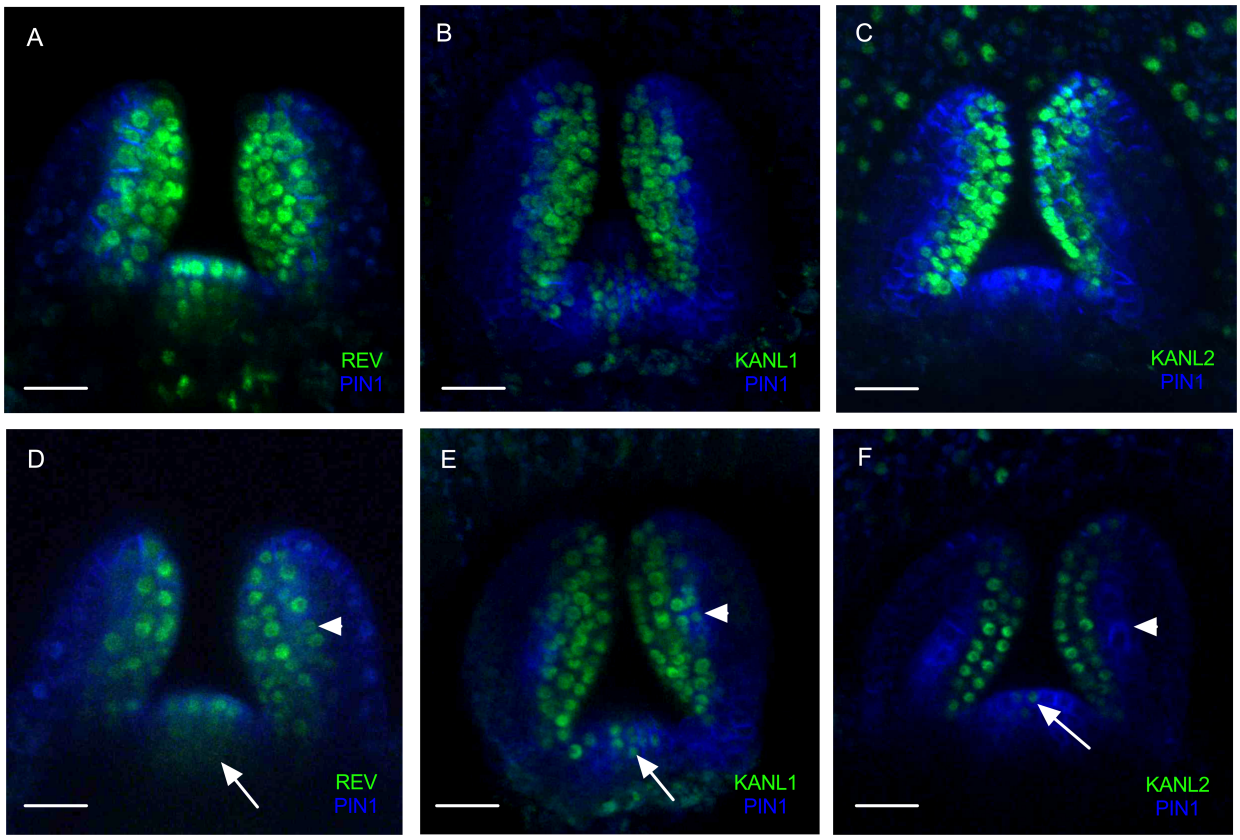

Figure 3.1 KANL1 and KANL2 expression partially overlap with each other

Confocal z-stack projections showing the expression of REV-2XYFP (A) KANL1-2XYFP (B) KANL2-2XYFP (C) with PIN1-GFP 4 days after stratification (DAS) in a vegetative shoot apical meristem. (D, E and F) Longitudinal sections of the seedlings are shown in (A, B and C). White arrows in (D and E) show the presence of REV-2XYFP and KANL1-2XYFP expression in the vasculature and SAM. White arrows in (F) show minimal expression of KANL2-2XYFP in the vasculature and SAM, respectively. Scale bars: 20µm.

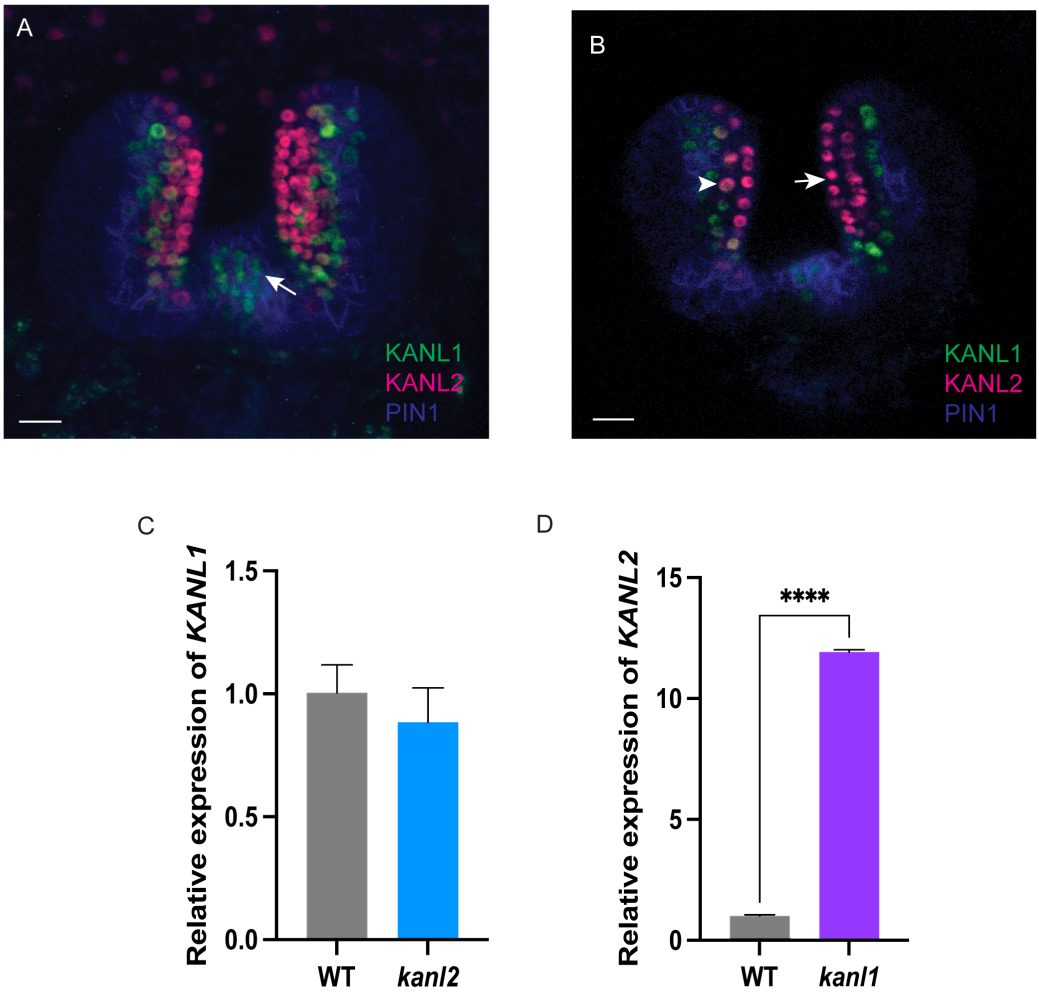

Figure 3.2 *KANL2* suppress the expression of *KANL1*

Confocal z-stack projections showing the expression of KANL1-2XYFP and KANL2-2XGFP together with PIN1-CFP at 4 DAS in a vegetative shoot apical meristem. (B) Longitudinal optical section of the seedlings shown in (A). White arrow in (A) indicates the presence of KANL1-2XYFP and the absence of KANL2-2XGFP in SAM. White arrow in (B) shows the absence KANL1-2XGFP in the outer epidermis cell layer which expresses KANL1-2XYFP. White arrowhead in B shows the expression of KANL1-2XYFP and KANL2-2XGFP both in one cell. (C and D) RT-qPCR analysis of *KANL1* and *KANL2* transcript levels in *kanl2* and *kanl1* single mutants. Data are mean ± SD calculated from three independent experiments. Each independent experiment was performed three times. Asterisks indicate statistically significant difference (***P ≤ 0.001) determined by Student's t test. Scale bars:15µm

3.2.2. *HD-ZIP III* genes regulate *KANL1* and *KANL2*

To further investigate the regulation of *KANL1* and *KANL2* by the *HD-ZIP III* genes**,** I analysed the expression of *KANL1* and *KANL2* in *HD-ZIP III* mutant seedlings (Figure 3.3). Firstly, the expression patterns of *pKANL1::KANL1-2XYPET* and *pKANL2::KANL2-2XYPET* were examined in *phb phv* mutant seedlings using fluorescent protein fusions. The KANL1-2XYPET and KANL2-2XYPET expression pattern in *phb phv* was found to be similar to that of the wild type (Figure 3.3, B and D). This was further analysed in other *HD-ZIP III* mutants by quantifying the transcript levels in *rev-9*, *phb-6 phv-5* and *phb phv rev* (Figure 3.3, E). Unexpectedly, I found that *KANL2* expression was significantly higher in *rev-9* compared to the wild type, while there was no difference in the *KANL1* transcript levels. The expression of both *KANL1* and *KANL2* was also found to be significantly higher in *phb-6 phv-5.* However, in the triple *phb phv rev* mutant*, KANL1* expression was significantly lower while *KANL2* was unchanged, compared to WT. These results reveal that under some circumstances, *KANL* expression is upregulated when HD-ZIP III expression is lacking and appear to contradict earlier findings that the expression of *KANLs* is dependent on the presence of HD-ZIP III expression (as inferred by published experiments involving the induction of miR165) (Sinha et al., 2023). However, there is a methodological difference between the two studies, and it may cause this fluctuation as well.

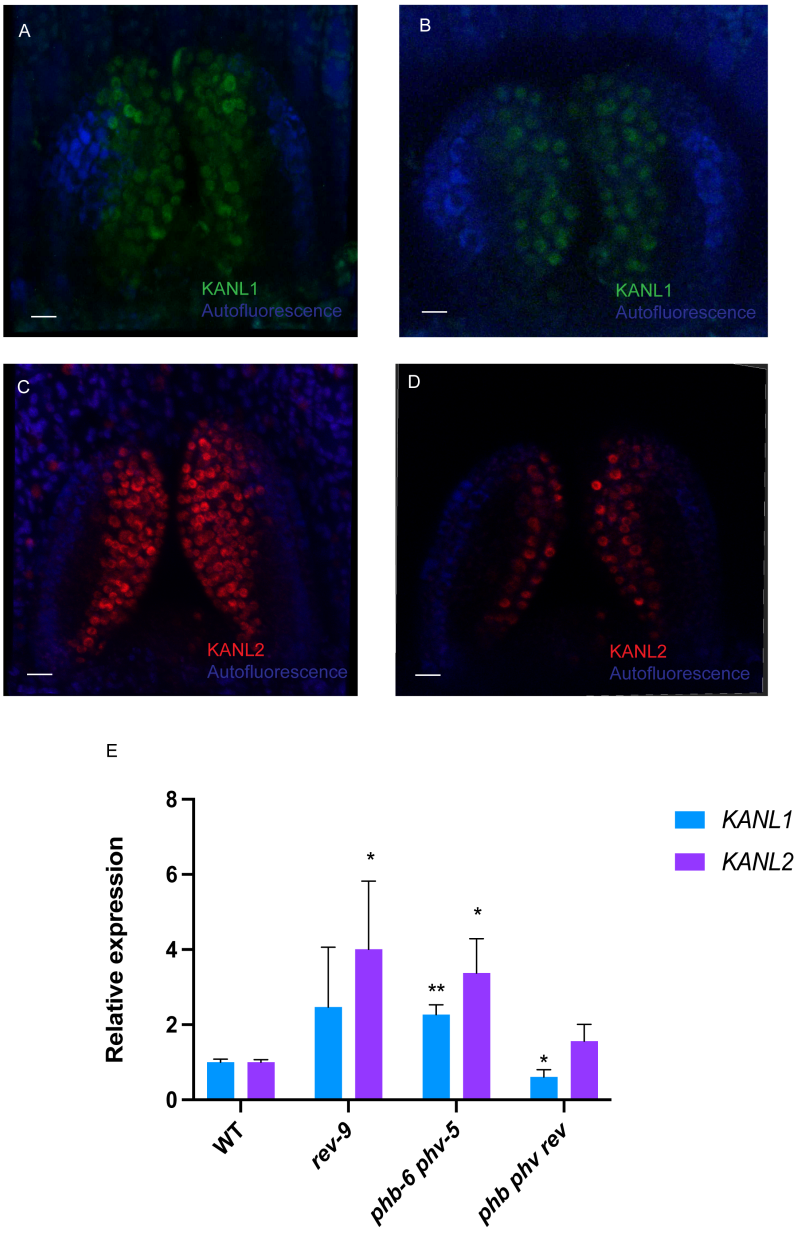

Figure 3.3 *KANL1* and *KANL2* expression in *HD-ZIP III* mutants

Confocal z-stack projections showing the expression of KANL1-2XYFP (A) and KANL2-2XYFP (C) in a vegetative SAM at 4 DAS in *phb phv* mutant background. (B and D) Longitudinal sections of the seedlings shown in (A and B). (E) RT-qPCR analysis of *KANL1* and *KANL2* transcript levels in WT, *rev-9*, *phb-6 phv-5* and *phb phv rev*. Data are mean ± SD from three independent experiments. Each independent experiment was performed three times. Asterisks indicate statistically significant difference (* $P \leq 0.05$, **$P \leq 0.01$) determined by Student's t test. Scale bars: 10 µm.

3.2.3. REV transcription factor binds to the *KANL1* and *KANL2* promoters *in vivo*

The previous results suggest that both *KANL1* and *KANL2* alter their expression in response to changes in *REV* expression. Therefore, to discover whether *KANL1* and *KANL2* are direct targets of REV, a ChIP experiment was conducted to determine whether REV binds sites within the promoter of the *KANL1* and *KANL2* genes. A dexamethasone-inducible two-component system was employed (*pAtUBQ10>>REVr-GFP*) to induce the miRNA-resistant mutated *REV* cDNA (Samalova, Brzobohaty and Moore, 2005) (Figure 3.4, A). The construct was transformed into the *Arabidopsis ap1 cal* double mutant background (Bowman et al., 1993) to increase chromatin yield per gram of fresh weight.

Four distinct plant lines (T2) were chosen from the transformants by planting them on DEX plates. The transformants displayed a strong phenotype of arrested meristem growth and radialised leaves in the seedlings (Figure 3.4, C) compared to the control (Figure 3.4, B). These phenotypes were consistent with earlier findings (Caggiano et al., 2017). The smooth inflorescences, devoid of floral organs, were selected and treated with DEX for 6 hours before tissue harvesting and fixation in 16% formaldehyde. DEX-treated inflorescences exhibited nuclear expression of the REVr-GFP fluorescent protein (Figure 3.6, E), confirming REVr-GFP induction.

The ChIP-qPCR was designed to analyse the REV binding sites in the genomic region upstream of the transcription starting site in the *KANL1* and *KANL2* genes, up to nearly 3 kb, using several primer pairs (Figures 3.5 and 3.6). The primer sets, three primers for *KANL1* and four primers for *KANL2,* cover at least one predicted REV binding site containing the "ATGAT" motif (Brandt et al., 2012). *ACT2* and *ZPR3* were used as negative and positive controls to validate the results (Merelo et al., 2016). Enrichment for REV-bound DNA was detected nearly 2 kb upstream (Figure 3.5, A III region) compared to surrounding locations in the *KANL1* genomic region. Similar results were obtained from two independent Chip-qPCR experiments (Figures 3.5, B and C). For *KANL2*, REV-bound DNA was detected at relatively high levels at all four locations

analysed. However, regions III and IV are significant as they were enriched in two independent experiments (Figures 3.6, B and C). However, in both the experiments, *ACT2* were expressed in high levels upon the DEX treatment (Figure 3.5, B and C and Figure 3.6 B and C), suggesting possible binding of REV to the *ACT2* promoter under these particular experimental conditions. Together, these data suggest that REV directly targets the *KANL1* and *KANL2* promoters, although further replicates and additional independent experimental evidence are required to gain further confidence.

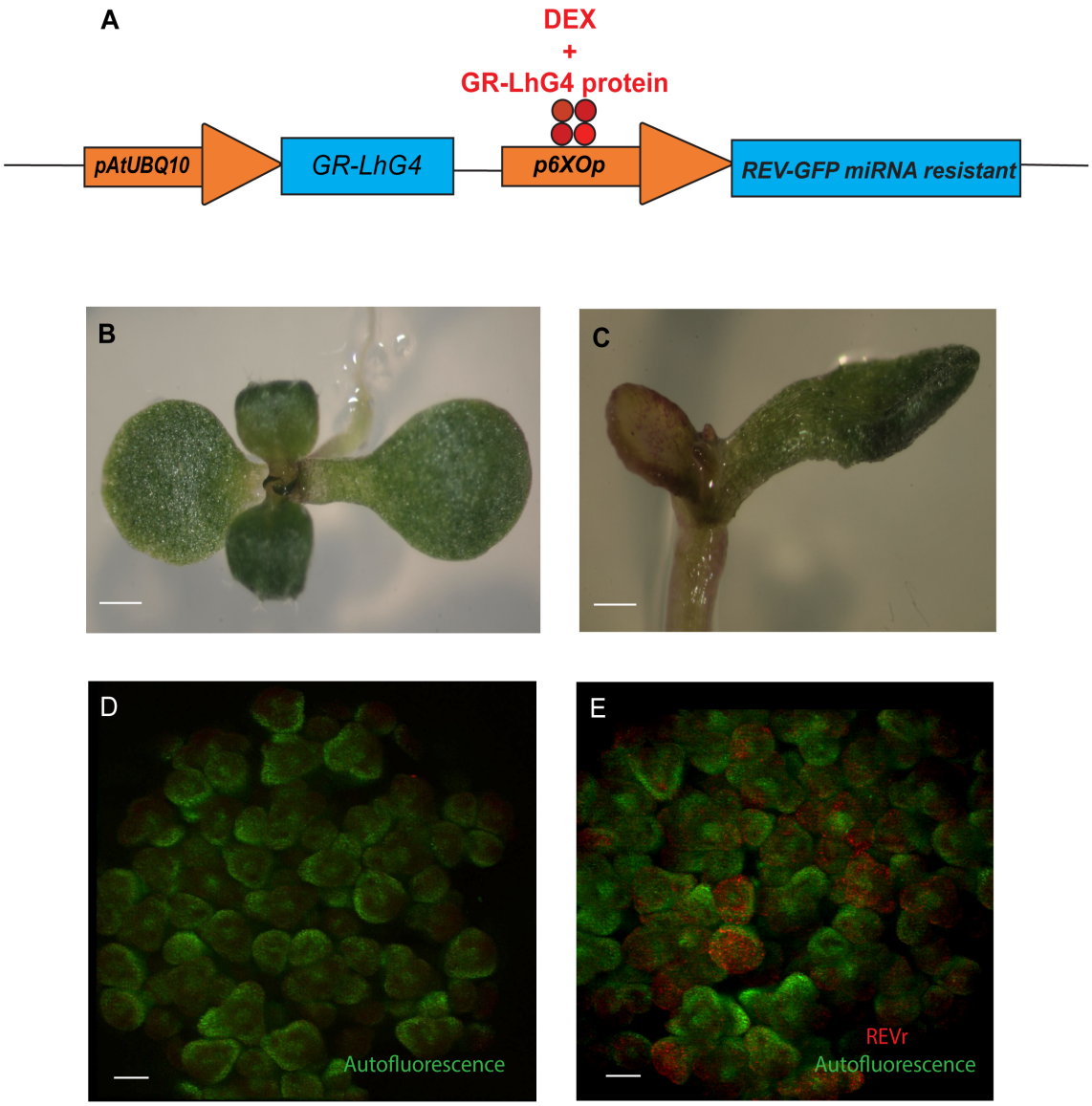

Figure 3.4 GR-Lhg4/6XOP two-component system used to induce miRNA resistant REV-GFP

Schematic representation of the construct used to induce REVr-GFP (A). The transgenic plant analysis of 8-day-old seedlings (B and C). Plants were grown on GM plates without DEX (B) and with DEX (C). (D and E) Verification of REVr-GFP induction by analysing the expression of REVr-GFP fluorescence of the DEX-treated inflorescence after 6 hrs prior to tissue harvesting. (D) Confocal projection of inflorescence without DEX treatment (Control). (E) Confocal projection showing the nuclear expression of REVr-GFP after 6 hrs of DEX treatment. Scale bars: 1 mm (B and C) and 50 µm (D and E).

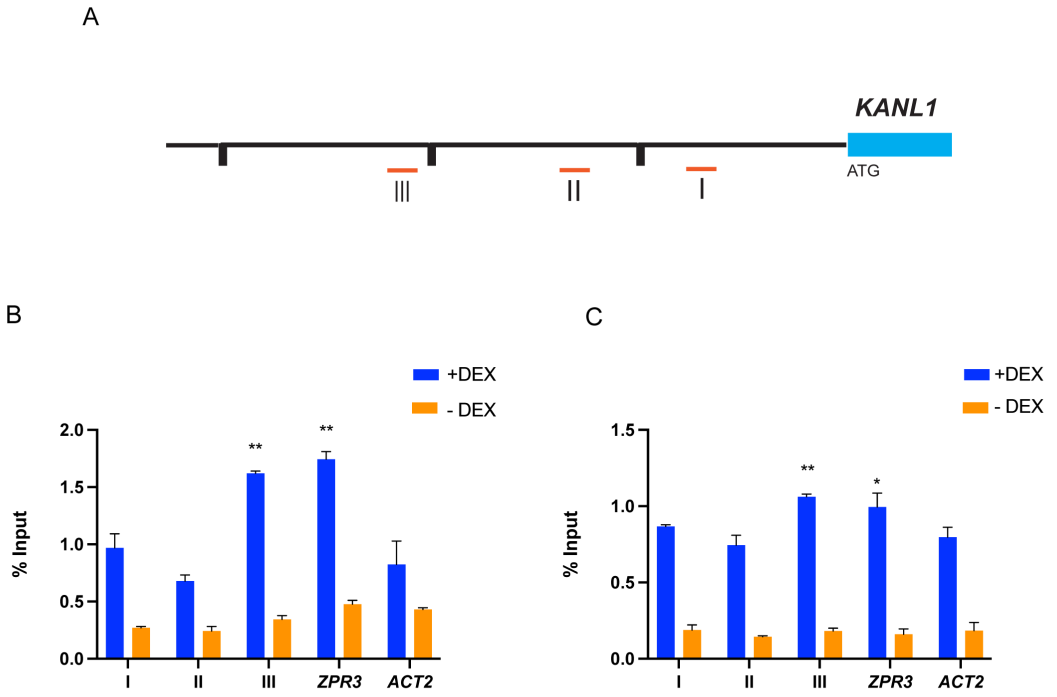

Figure 3.5 REV binds to the *KANL1* promoter

(A) A diagram of *KANL1* genomic region analysed by ChIP-qPCR. The black horizontal line represents the promoter region upstream of the *KANL1* predicted transcriptional start site. The black vertical lines separate the genomic region into 1000 pb. The orange lines mark the regions amplified by ChIP-qPCR. (B and C) ChIP qPCR data of two independent experiments obtained by % input method. The ChIP samples were normalized to the Input samples. Error bars show mean ± SD from three technical replicates. *ACT2* and *ZPR3* were tested as negative and positive controls. Asterisks indicate statistically significant difference (* $P \leq 0.05$, ** $P \leq 0.01$) determined by Student's t test.

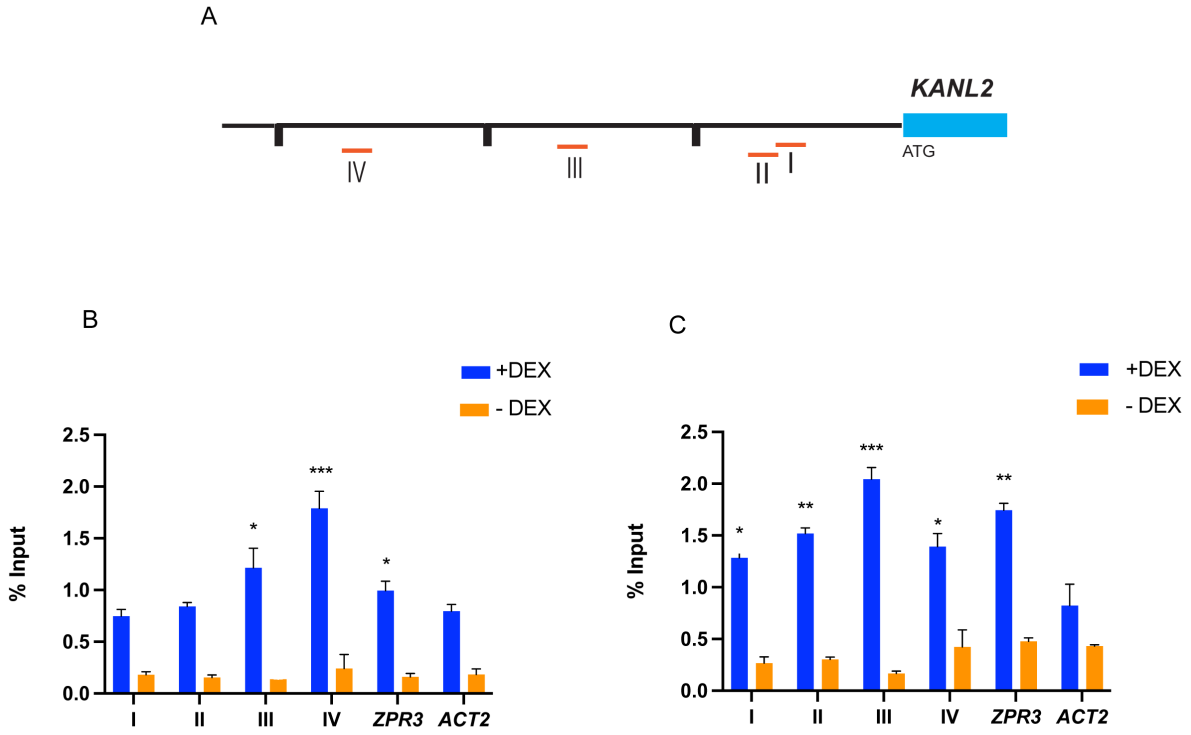

Figure 3.6 REV binds to the *KANL2* promoter

(A) A diagram of *KANL2* genomic region analysed by ChIP-qPCR. The black horizontal line represents the promoter upstream of *KANL2* transcriptional start site. The black vertical lines separate the genomic region into 1000 pb. The orange lines mark the regions amplified by ChIP-qPCR. (B and C) ChIP qPCR data of two independent experiments obtained by % input method. The ChIP samples were normalized to the Input samples. Error bars show mean ± SD from three technical replicates. *ACT2* and *ZPR3* were tested as negative and positive controls. Asterisks indicate statistically significant difference (* $P \leq 0.05$, ** $P \leq 0.01$, *** $P \leq 0.001$) determined by Student's t test.

3.2.4. KAN1 down regulates KANL2

In addition to being regulated by REV, the expression of both *KANL1* and *KANL2* is reported to be repressed by KAN1 (Ram et al., 2020). This was further investigated by examining the expression patterns of the *pKANL1::KANL1-2XYPET* and *pKANL2::KANL2-2XYPET* fluorescent proteins in the *kan1 kan2* mutant background (Figure 3.7). I could not detect any difference in KANL1-2XYPET expression compared to the WT in *kan1 kan2* seedlings examined (Figure 3.7, A and B). In contrast, KANL2-2XYPET exhibited ectopic expression in the abaxial epidermis of *kan1 kan2* seedling leaves (Figure 3.7, C-F). This was more obvious in older leaves, where KANL2-2XYPET was stronger throughout the abaxial epidermis (Figure 3.7, E and F). The reported expression patterns were noted in at least three independent plant lines. The mutant seedlings *kan1 kan2* were identified by observing the seedling phenotype; they possess narrow, spoon-shaped cotyledons that pointed upwards compared to WT (Eshed et al., 2001).

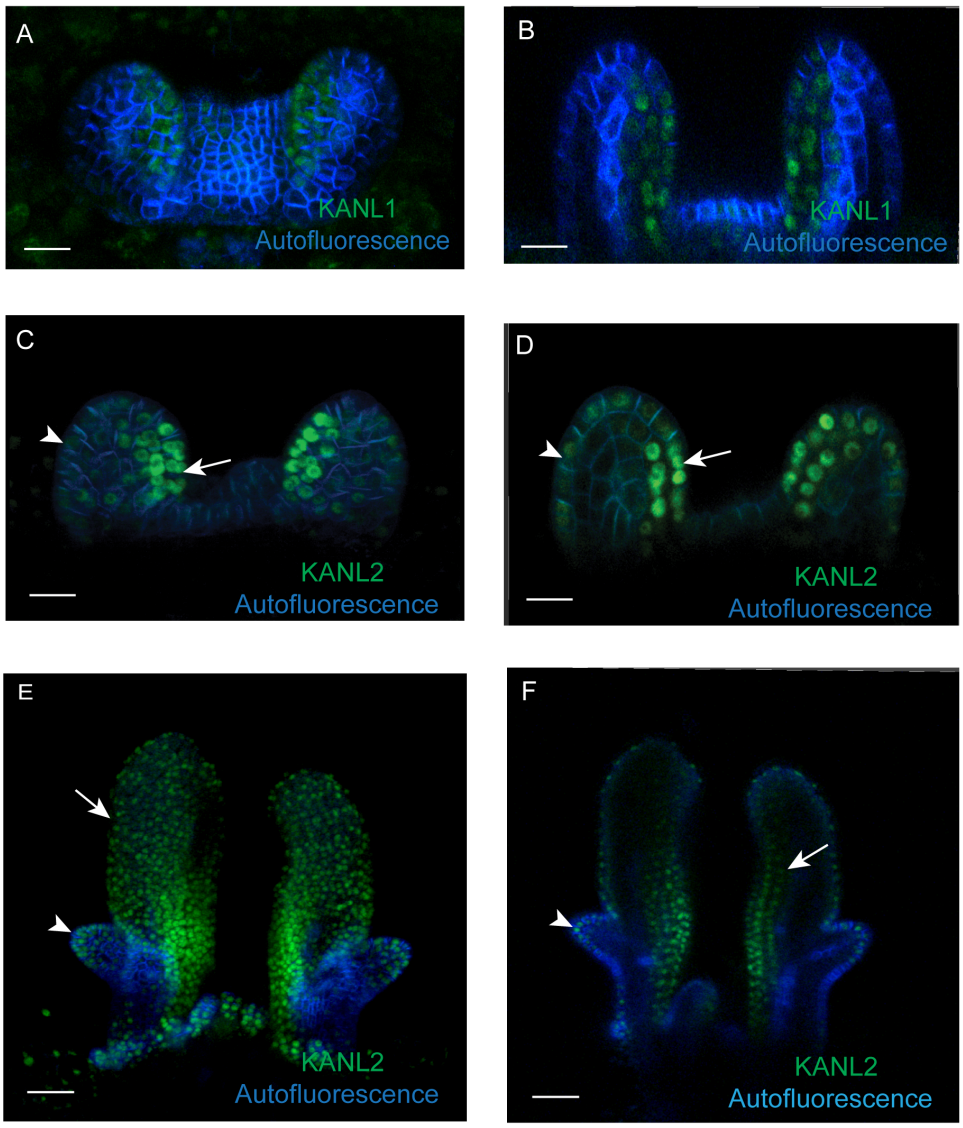

Figure 3.7 *KAN1* downregulate the KANL2 in abaxial domain

Confocal z-stack projections showing the expression of KANL1-2XYPET (A) and KANL2-2XYPET (C) together with PIN1-GFP in a *kan1 kan2* vegetative SAM at 3 DAS. (B and D) Longitudinal sections of the seedlings shown in (A and C). White arrows in (C and D) mark adaxial expression of KANL2-2XYPET in the seedlings of *kan1 kan2* leaves. White arrowheads in (C) and (D) mark the abaxial epidermal expression of KANL2-2XYPET in the seedlings of *kan1 kan2* leaves. (E) Confocal z-stack projections showing expression of KANL2-2XYFP in *kan1 kan2* together with PIN1-GFP at 7 DAS in a vegetative shoot apical meristem. (F) Longitudinal section of the seedling shown in (E). White arrow in (E) marks the expression of KANL2-2XYPET in the abaxial epidermis of the leaves in *kan1 kan2* seedling, white arrowhead in (E) marks the expression of KANL2-2XYPET on the outhgrowth of the *kan1 kan2* seedling. The white arrow in (F) shows the expansion of KANL2-2XYPET towards the cells in the vasculature. The white arrowhead in (F) indicates expression of KANL2-2XYPET in the epidermis of a *kan1 kan2* outgrowth. Scale bars, 15 µm (A, B, C and D) and 50 µm (E and F).

3.3 Discussion

As discussed in Chapter 1, previous studies from the Heisler lab indicate that REV promotes the expression of *KANL1* and *KANL2.* As reported by (Ram et al., 2020), the two genes *KANL1* and *KANL2* were identified through a FACS/RNA-seq approach as being differentially expressed in REV expressing cell types in the *Arabidopsis* shoot. The expression patterns of the *KANL* genes, as analysed here, support these earlier conclusions. For instance, both KANL reporters are expressed adaxially in patterns that resemble the *REV* expression pattern, which is complementary to that of the *KAN* genes (Figure 3.1). Surprisingly, however, the transcript levels of both *KANL1* and *KANL2* were not absent or downregulated in *rev-9* mutants; rather, *KANL1* showed no significant difference, while *KANL2* exhibited a significant upregulation compared to WT. Similarly, I found both *KANL1* and *KANL2* to be elevated in *phb-6 phv-5*. Finally, I analysed *KANL1* and *KANL2* expression in *phb phv rev* triple mutants and found *KANL1* to be downregulated but not completely absent, while *KANL2* exhibited no significant difference in expression level. Given the similarity between REV and other members of the HD-ZIP III family, the maintenance of *KANL1* and *KANL2* expression in *rev-9* or *phb phv* double mutants might be due to redundancy within the HD-ZIP III family, including *ATH15*. This proposal is specifically supported by the earlier finding that *KANL1* and *KANL2* were found to be downregulated after miR165 induction, which targets all HD-ZIP IIIs (Sinha et al., 2023). The significantly higher expression of *KANL2* in *rev* single and *phb phv* double mutants is more difficult to explain but may suggest the reduction of another factor that suppresses *KANL1* or some other uncharacterized compensatory mechanism. The complexity of *KANL1* and *KANL2* regulation is further underscored by the finding that these genes also negatively regulate each other (Figure 3.2).

Based on earlier studies, I also investigated whether the REV protein directly binds to the *KANL1* and *KANL2* promoters as direct targets of the REV protein. The ChIP method (Kuo & Allis, 1999) was used to identify the DNA-binding sites of the REV protein on the *KANL1* and *KANL2*

promoters. According to the ChIP-qPCR results, REV directly binds to the *KANL1* and *KANL2* promoters. (Figures 3.7 and 3 8). The primer pairs for *ZPR3* were used to validate the results as the positive control (positive binding site) and showed significant REV binding in both independent experiments over control, confirming the strength of the experimental design and the true ChIP enrichment. *ACT2*, a widely used housekeeping gene (Yamaguchi et al., 2014), was used as the negative control since REV rarely binds to it. Unexpectedly, in both independent experiments, the dexamethasone resulted in considerable enrichment for *ACT2* (negative control). This resulted in lower fold enrichment (2-3) of positive controls, compared to perhaps 8-16-fold enrichment expected for positive controls in ChIP-qPCR (Kaufmann et al., 2010). A possible explanation is that REV may bind the *ACT2* promoter to a limited degree, which could become significant if expression levels of REV are very high. Such binding may be further enhanced if dexamethasone influences general chromatin accessibility (Pajoro et al., 2014). This issue may potentially be improved by altering the construct, expressing REV in a non-inducible manner, such as transforming *pREV::REV-GFP* into *rev-9*. Despite this drawback, the results indicate REV does bind sites on the *KANL1* and *KANL2* promoters when compared to the positive control. Additional experiments, including tobacco transient expression analyses, Yeast One-Hybrid assays and CUT&RUN methods, may be further used to test this regulatory relationship.

As reported here, I found that REV binds to the *KANL1* and *KANL2* promoters according to the results of a ChIP-qPCR, and these results align with the already predicted and researched canonical REV recognition site (Brandt et al., 2012; Bertolotti et al., 2021). Further research with additional qPCR on ChIP DNA may reveal the sequence of cis-regulatory elements on the *KANL1* and *KANL2* promoters for HD-ZIP III binding. Additionally, other HD-ZIP III transcription factors may bind to the promoters of KANL1 and KANL2.

While *KANL1* and *KANL2* are very similar in sequence and expression, this chapter starts to reveal intriguing differences. KANL1-2XYPET expression is stronger compared to KANL2-2XYPEYT

(Figure 3.1) in the SAM. Also, there is a cross-regulation between these two genes (Figure 3.2). KANL1-2XYPET expression is minimum in the cells where KANL2-2XGFP was expressed (Figure 3.2, A and B). Also, based on transcripts analysis by qPCR in *kanl1* mutant seedlings, *KANL2* are high (Figure 3.2 C and D), suggesting a possible regulation of KANL1 by KANL2. As noted by (Ram et al., 2020), aside from the upregulation by REV, KAN1 was found to downregulate *KANL1* and *KANL2* genes. Analysis of *KANL* expression in the *kan1 kan2* mutant background was found to be consistent with these earlier findings regarding *KANL2* regulation. However, the observation that KANL1 was not noticeably changed in this mutant background points to additional important differences in KANL1 and KANL2 regulation. Future research involving *KANADI* will clarify how *KANL1* and *KANL2* genes are regulated in the abaxial domain. Additionally, ChIP-qPCR can be carried out to determine whether KAN1 directly binds to the promoters of *KANL1* and *KANL2*.

Chapter 4 -Developmental function of *KANL1* and *KANL2* genes

4.1. Introduction

While Chapter 3 investigates *KANL1* and *KANL2* expression and regulation, this chapter focuses on the developmental function of *KANL1* and *KANL2*. So far, one published study reports that the double mutant in the Col ecotype of *Arabidopsis* exhibits an increase in leaf serration (Figure 7 in Luo et al., 2024), consistent with the reported role of *CLAUSA* from tomato (Avivi et al., 2000; Bar et al., 2015; 2016) and *SALAD* from wild strawberry (Luo et al., 2024) in regulating leaf complexity. These previous studies also report that *CLAUSA* and *SALAD* expression in tomato and strawberry, respectively, is largely restricted to the leaf margin (Bar et al., 2016; Luo et al., 2024). In contrast, this thesis and other work from the Heisler lab reveal that *KANL1* and *KANL2* are expressed on the adaxial side of *Arabidopsis* leaves and that these genes are also regulated by genes involved in adaxial-abaxial leaf polarity, suggesting a novel role in this process. Considering these findings, this chapter extends the analysis of *KANL1* and *KANL2* developmental function beyond previous published work to reveal new roles.

4.2. Results

4.2.1. CRISPR-Cas9 generated *kanl1* and *kanl2* mutant alleles

The *kanl1 kanl2* double mutant was created by crossing two single mutants, *kanl1-1* and *kanl2-1*, which had already been generated in the Heisler lab. These alleles were created using the CRISPR-Cas9 genome editing system with the pkir1.1 vector system (Tsutsui & Higashiyama, 2016). For *KANL1*, the gRNA targeted the first exon. In the *kanl1-1* mutant, a T was inserted at the 24th nucleotide of the first exon, which causes a frameshift, resulting in an early stop codon. The protein stops at amino acid position 41, disrupting the MYB domain, which spans amino acids 25 to 83 in the wild type. For *KANL2*, the gRNA also targeted the first exon. In the *kanl2-1*

mutant, 5 nucleotides were deleted at position 92. This causes a frameshift, resulting in a protein with the first 31 amino acids the same as wild type, followed by 30 missense amino acids before stopping early. This also disrupts the MYB domain, which spans amino acids 25 to 89 in the wild type.

4.2.2. *kanl1 kanl2* mutants in the L*er* ecotype do not exhibit leaf altered serrations but have downward curved leaves

No phenotype for *kanl1-1* and *kanl2-1* single mutants was detected in *Arabidopsis* rosette leaves. In examining the *kanl1 kanl2* double mutant, however, I found it exhibited a phenotype of downward-curved leaves compared to the wild type along their mediolateral axis. In contrast, it did not have a visible leaf serration phenotype, as previously described (Figure 7C in Luo et al., 2024) for the double mutant in the Col ecotype, This is illustrated in a comparison of rosettes and single leaves (Figure 4.1). The downward curvature of the leaves was quantified by measuring the transverse curvature index (CI) (Liu et al., 2010; Ren et al., 2018) (Figure 4.2). The transverse curvature index was measured in the first to tenth leaves in WT, *kanl1,* and *kanl2* single mutant alleles, as well as in *kanl1 kanl2* rosettes. All genotypes were grown under the same conditions. Compared to the wild type (WT), single mutant alleles of either *kanl1* or *kanl2* do not exhibit transverse curvature; however, *kanl1 kanl2* showed a significant transverse curvature difference for the first, second, fifth, and seventh leaves. The leaves bend downward from the middle to the margin. The highest CI was observed in the seventh leaf of the 28-day-old rosette, which was 0.34 (Figure 4.2). Although the curvature index was higher only for the first, second, fifth, and seventh leaves, limited replicates may have prevented some differences from reaching significance. More replicates could improve statistical power and clarify these effects.

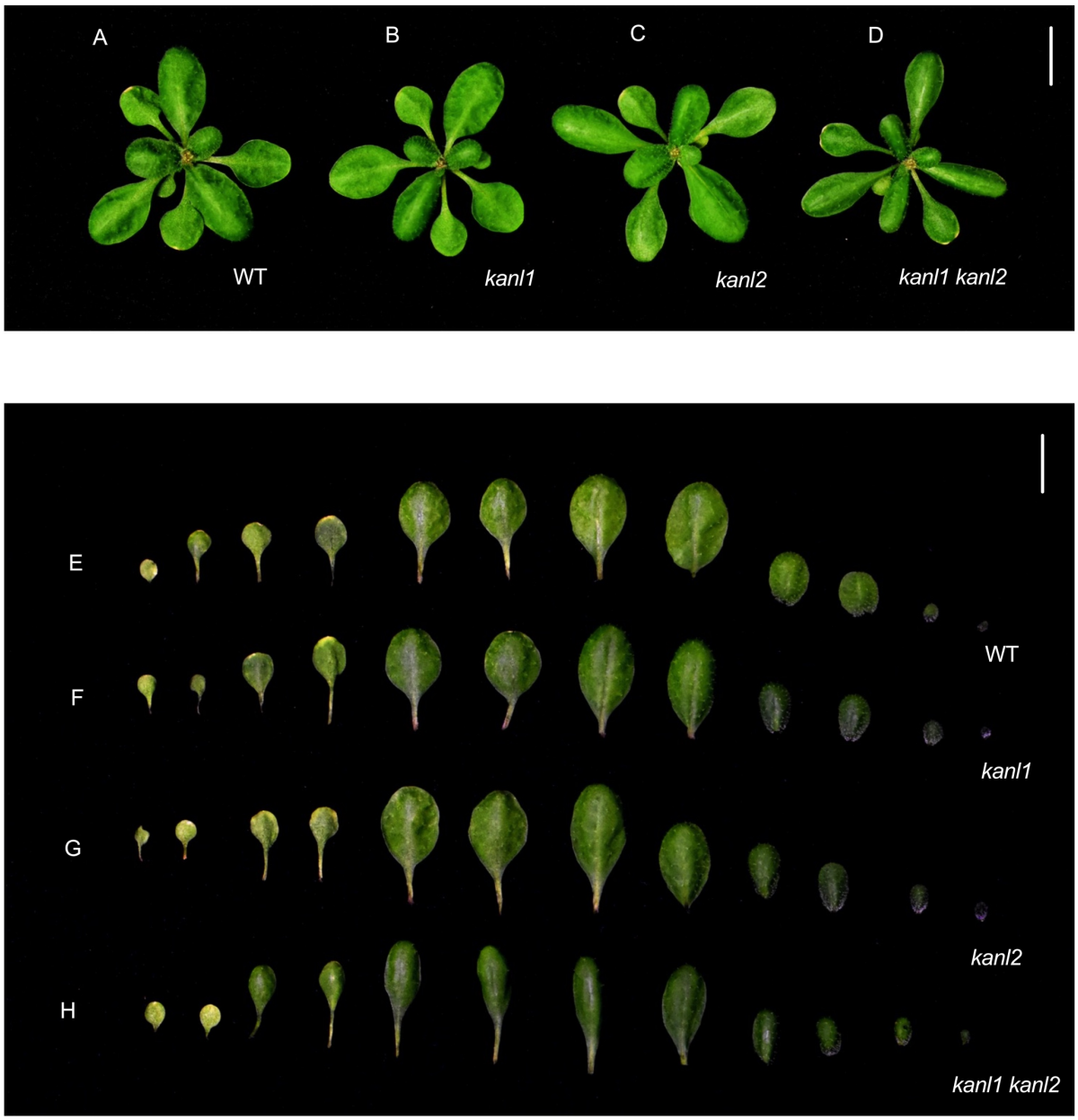

Figure 4.1 Rosette leaves phenotype in *kanlike* mutants

A-D) 4-week-old rosettes of wild type (A), *kanl1* (B), *kanl2* (C), and *kanl1 kanl2* (D). (E-H) Leaf series (2 cotyledons and 10 leaves from left to right) of 4-week-old wild type (E), *kanl1* (F), *kanl2* (G), and *kanl1 kanl2* (H). Bars indicate 1 cm.

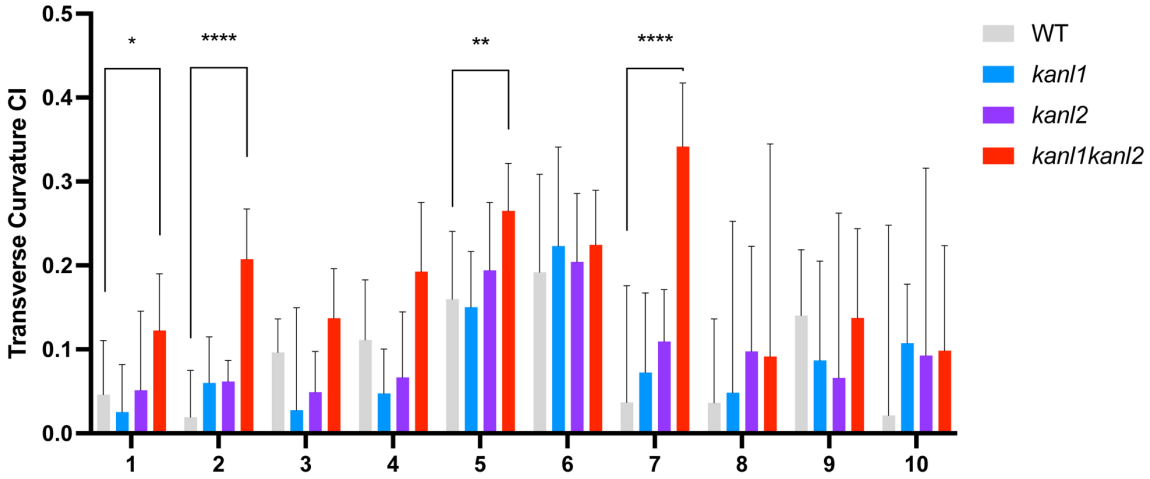

Figure 4.2 Quantification of transverse curvature indices of rosette leaves in *kanlike* mutants

Transverse curvature indices for 28-day-old rosette leaves of *kanlike* mutants are presented as mean ± SD. The first ten leaves of each rosette were measured separately. The number of rosettes measured for each genotype was ≥ 8. Statistically significant differences in CI compared to the wild type were determined by Student's t-test for each leaf number separately. Asterisks indicate statistical significance (*P ≤ 0.5, ** P ≤ 0.01, **** P ≤ 0.0001).

4.2.3. Complementation of the double mutant phenotype by transforming *KANL1* and *KANL2* wild-type genes independently to *kanl1 kanl2*

To confirm that the phenotype of the *kanl1 kanl2* double mutant is due to the absence of the *KANL1* and *KANL2* genes, complementation experiments were performed using C-terminal KANL-double fluorescent protein fusions under the control of KANL promoter regions. These constructs were designated *pKANL1:KANL1-2XYPET* and *pKANL2:KANL2-2XGFP*. The *pKANL1:KANL1-2XYPET* clone comprises 7.02 kb of *KANL1* genomic sequence with 4.855 kb promoter, while *pKANL2:KANL2-2XGFP* contains 5.645 kb of *KANL2* genomic sequence with 2.638 kb promoter. Multiple homozygous transgenic lines expressing either KANL1-2XYPET or KANL2-2XGFP fluorescent protein fusions in the *kanl1 kanl2* double mutant were screened for the presence of the respective fluorescent protein using confocal microscopy (Figure 4.3, A and B). Plants selected based on fluorescence were grown alongside WT and the *kanl1 kanl2* untransformed mutants to compare their phenotypes (Figure 4.3). The transverse curvature of the rosette leaves of the complemented lines was quantified using the CI method (Figure 4.4). In the complemented lines, CI was not measured to be significantly different to wildtype for the first, second, fifth, and seventh leaves, whereas the CI of the untransformed *kanl1 kanl2* double mutants was found to be significantly greater. These data confirm that the rosette leaf phenotype (downward-curved leaves) of the *kanl1 kanl2* CRISPR-generated alleles arises from the absence of functional *KANL1* and *KANL2* genes. This further confirms that the two genes are redundant, as expressing *KANL* gene in the double mutant *kanl1 kanl2* background can restore wild-type leaf curvature.

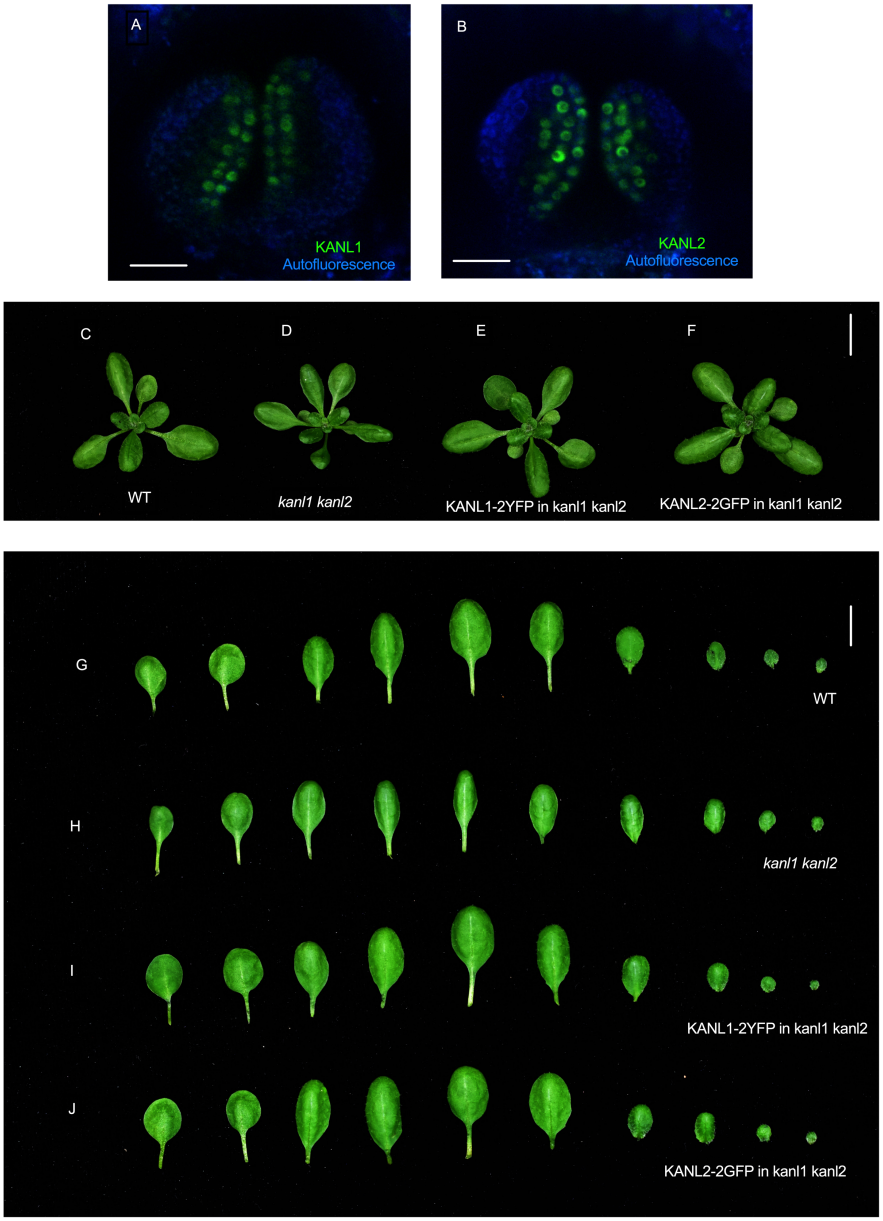

Figure 4.3 Complementation of the double mutant phenotype by transforming *KANL1* and *KANL2* wild-type genes independently into the *kanl1 kanl2* double mutant

Confocal z-stack projections of KANL1-2XYPET in *kanl1 kanl2* and KANL2-GFP in *kanl1 kanl2* (B), respectively, in a vegetative meristem at 3 DAS. (C-F) 4-week-old rosettes of wild type (C), *kanl1 kanl2* (D), complemented line of KANL1-2XYPET in *kanl1 kanl2* (E), complemented line of KANL2-GFP in *kanl1 kanl2* (F). (G-J) Leaf series of 4-week-old wild type (G), *kanl1 kanl2* (H), complemented line of KANL1-2XYPET in *kanl1 kanl2* (I), complemented line of KANL2-GFP in *kanl1 kanl2* (J). Scale bars: 20 µm (A and B) and 1 cm (C-J).

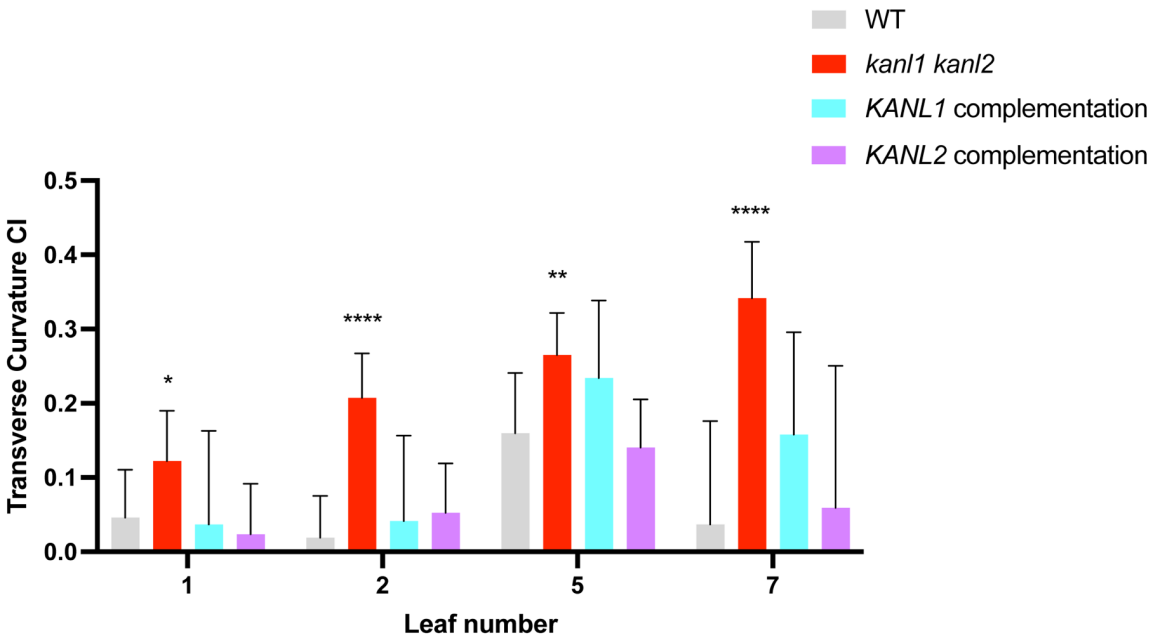

Figure 4.4 Quantification for the Complementation of the double mutant phenotype by transforming *KANL1* and *KANL2* wild-type genes into *kanl1 kanl2*

Transverse curvature indices for 28-day-old rosette leaves of WT, *kanl1 kanl2, KANL1*-complemented lines, and *KANL2*-complemented lines were quantified. The mean ± SD of CI is shown for the first, second, fifth, and seventh leaves of each rosette. The number of rosettes measured for each different plant line and genotype was ≥ 8. Statistically significant difference compared to the respective WT was determined by Student's t-test for each leaf number separately. Asterisks indicate statistical significance (*P ≤ 0.5, ** P ≤ 0.01, **** P ≤ 0.0001).

4.2.4. The transverse curvature of *HD-ZIP III* mutants and *HD-ZIP III* mutants in *kanl1 kanl2* double mutant background

Similarly to *kanl1 kanl2* double mutants, *HD-ZIP III* mutants also exhibit downwardly curved leaves and their transverse curvature indices have been reported (Liu et al., 2010). As discussed in Chapter 3, the evidence gathered so far indicates *KANL1* and *KANL2* are downstream targets of the *HD-ZIP III* genes. Therefore, I investigated this proposal further by generating combinatorial mutants. *kanl1 kanl2* multiple mutants with *HD-ZIP III* genes were generated by crossing the mutant alleles (Figure 4.5). *rev-9* plants were crossed with *kanl1 kanl2* to generate *rev kanl1 kanl2*. *phb-6 phv-5* was crossed with *kanl1 kanl2* to produce *phb phv kanl1 kanl2* and *phb-6 phv-5 rev-9/+* was crossed with *kanl1 kanl2* to obtain; *phb phv rev kanl1 kanl2* mutants. Plants homozygous mutant at all these loci were identified by planting several generations and performing PCR genotyping, or by PCR followed by restriction enzyme digestion (see methods 2.2.2).

Plants identified as *rev kanl1 kanl2* displayed significantly downward-curved leaves (Figure 4.7). The transverse curvature indices of *rev-9* and *rev kanl1 kanl2* were measured and compared to WT (Figure 4.8). The results show significant differences in curvature indices compared to the wild type for *kanl1 kanl2, rev-9*, and *rev kanl1 kanl2.* In *rev kanl1 kanl2* triple mutants, the leaves curved more downward than those of either the *kanl1 kanl2* or *rev-9* single mutants (Figure 4.5, E, arrowheads). Similarly, in *phb phv kanl1 kanl2,* the leaves curved downward compared to either *kanl1 kanl2* or *phb pbv* (Figure 4.5, F, white arrows). The finding that *rev kanl1 kanl2* mutants are more severely affected than *rev* single mutants indicates that *KANL1* and *KANL2* are still functioning in the *rev* single mutant background consistent with the detection of significant *KANL1* and *KANL2* expression also in this mutant background.

As previously reported (Emery et al., 2003) *phb phv rev* triple mutants develop abaxialised cotyledons without a SAM (Figure 4.6, A and B). Unexpectedly, *phb phv rev kanl1 kanl2*

quintuple mutants developed two expanded cotyledons, and a single radialised leaf in the centre replaced the SAM (Figure 4.6, C). Also, *phb phv rev/+* (Figure 4.6, D) and *phb phv/+ rev* (Figure 4.6, E) showed a similar phenotype to *phb phv rev kanl1 kanl2* quintuple mutant (Figure 4.6, C), suggesting that KANL1 and KANL2 compensate somewhat the loss of *HD-ZIP III* genes in SAM. Further interpretations in this background are difficult as there are five alleles segregating and multiple genotypes and variations are possible; for instance, see Figure 4.6, F. However, it can be concluded that for the SAM, *KANL1* and *KANL2* do not show an additive genetic interaction with *HD-ZIP III* genes as shown for the leaves (Figure 4.5 and 4.7).

All together, these findings indicate that the *KANLs* and *HD-ZIP III* genes act somewhat additively in terms of regulating leaf curvature. Such a result is consistent with the two families of protein sharing a common function and the finding that in single and double *HD-ZIP III* mutants, the KANLs are still expressed. In contrast, the lack of synergistic interaction in terms of SAM phenotype may suggest that the *KANLs* genes do not contribute the same way to SAM maintenance, although a more extensive comparison of *phb phv rev* vs *phb phv rev kanl1 kanl2* mutant plants is warranted.

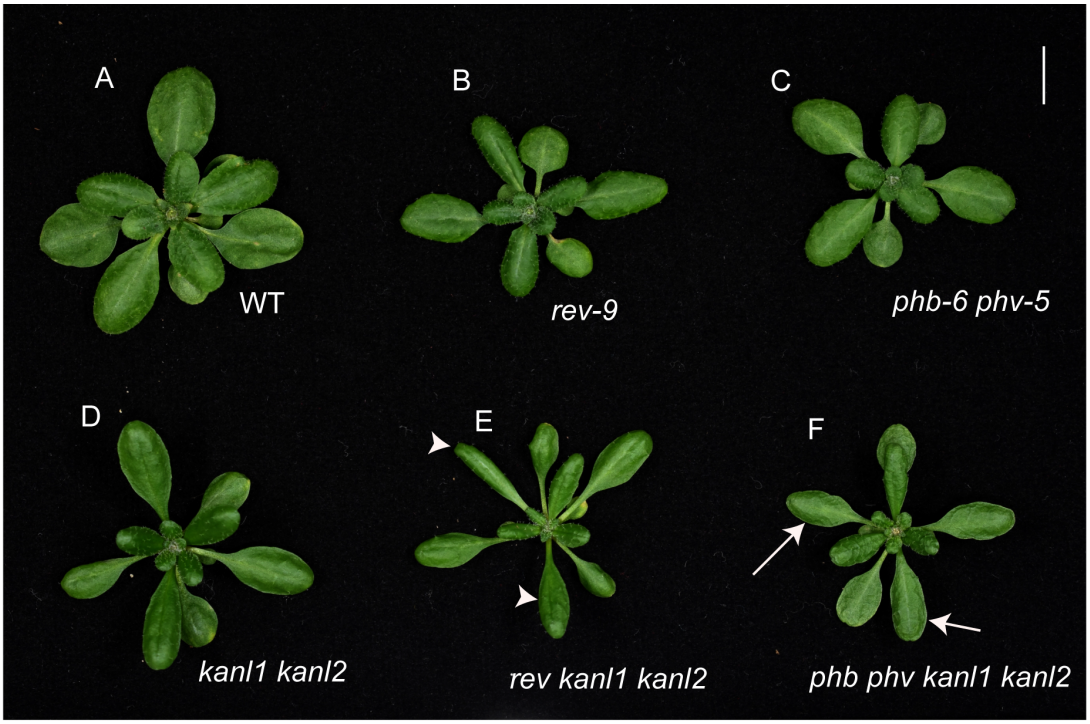

Figure 4.5 *kanl1 kanl2* combinatorial mutants with *HD-ZIP III* mutants

(A-F) 4-week-old rosettes of WT (A), *rev-9* (B), *phb-6 phv-5* (C), *kanl1 kanl2* (D), *rev kanl1 kanl2* (E), *phb phv kanl1 kanl2* (F). Scale bar:1 cm.

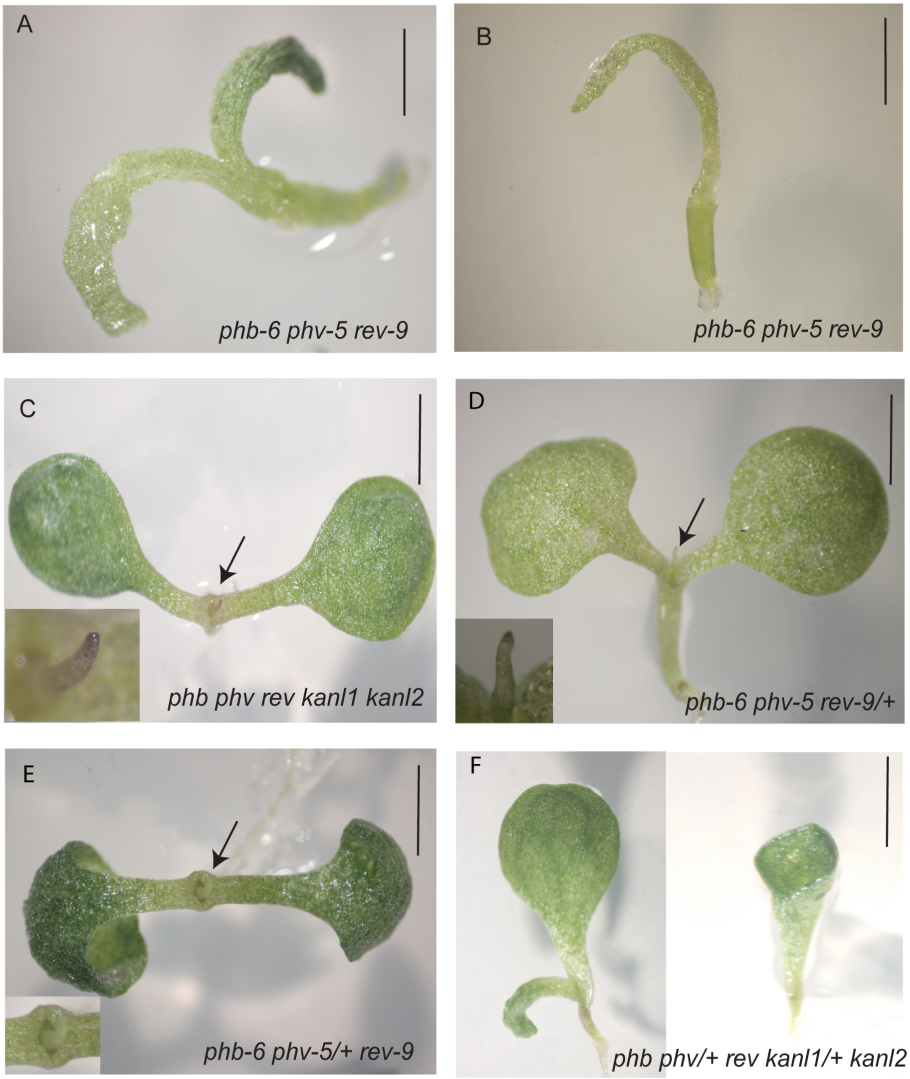

Figure 4.6 *KANL1* and *KANL2* interaction with *HD-ZIP III* genes in the SAM

(A-F) Phenotypes of the seedlings, 7 DAS. (A and B) *phb-5 phv-6 rev-9,* (C) *phb phv rev kanl1 kanl2,* (D) *phb-5 phv-6 rev-/+,* (E) *phb-5 phv-6/+ rev-9* and (F) *phb phv/+ rev kanl1+ kanl2.* Scale bars: 1cm.

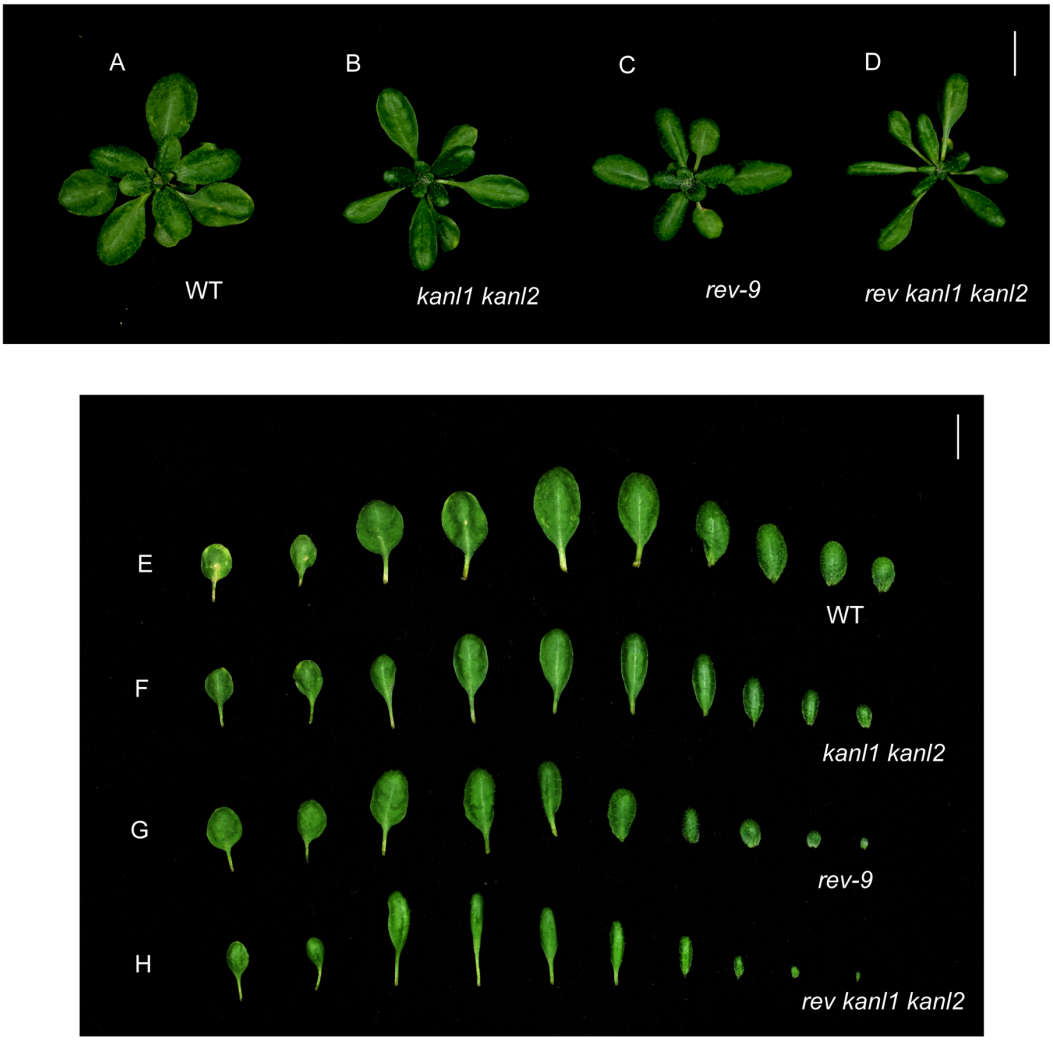

Figure 4.7 Rosette leaves phenotype in *rev-9, rev kanl1 kanl2*
(A-D) 4-week-old rosettes of wild type (A), *kanl1 kanl2* (B), *rev-9* (C) and *rev kanl1 kanl2* (D). (E-H) Leaf series (10 leaves) of 4-week-old wild type (E), *kanl1 kanl2* (F) *rev-9* (G) and *rev kanl1 kanl2* (H). Bars indicate 1 cm.

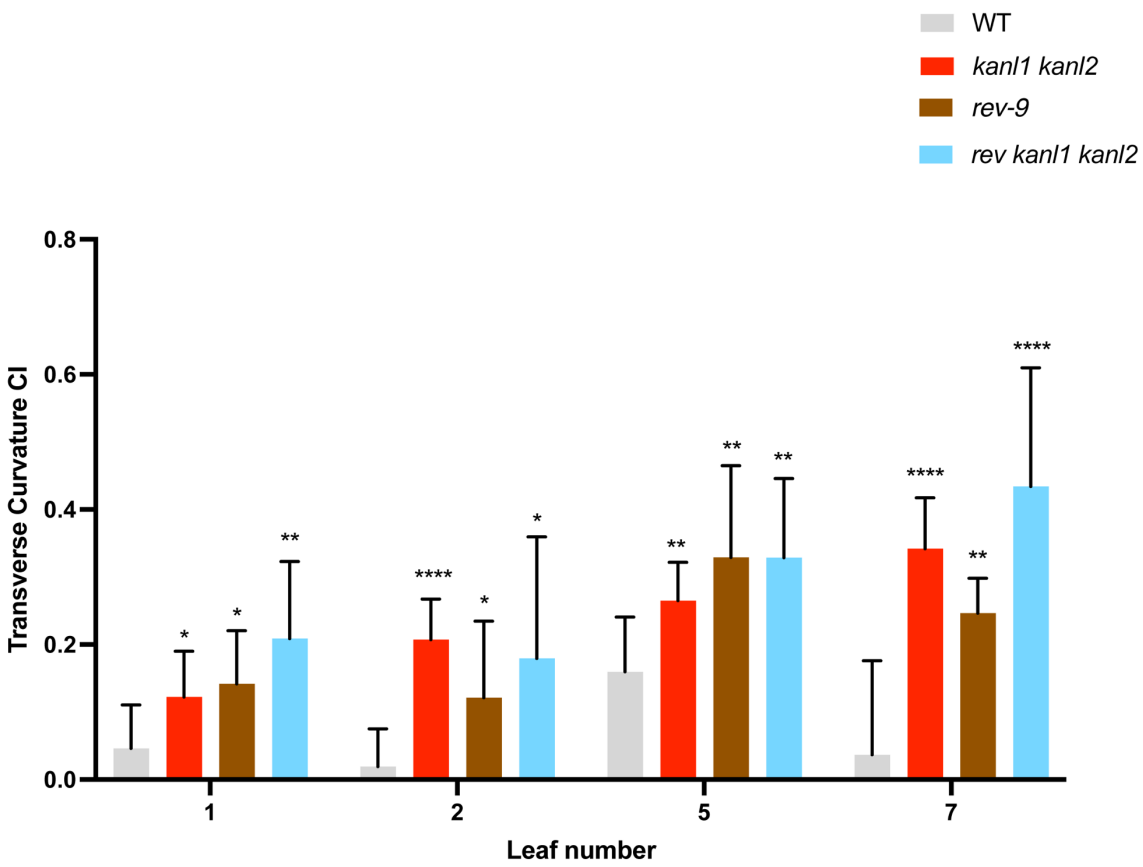

Figure 4.8 Quantification of transverse curvature indices of rosette leaves in *rev-9, rev kanl1 kanl2*

Transverse curvature indices for 28-day-old rosette leaves (first, second, fifth and seventh) of the genotypes are presented as mean ± SD. The number of rosettes measured for each genotype was ≥ 8. Statistically significant difference compared to the respective WT was determined by Student's t-test for each leaf number separately. Asterisks indicate statistical significance (*P ≤ 0.5, ** P ≤ 0.01, **** P ≤ 0.0001).

4.2.5. Evolutionary conserved role of *KANL1* and *KANL2* genes

Both *CLAUSA* and *SALAD* have been reported to suppress orthologs of *CUC2*, which specifies boundary formation in the SAM. *CLAUSA* has also been reported to repress *KNOX1* gene expression (Bar et al., 2015; 2016; Luo et al., 2024). To test whether the *Arabidopsis KANL* genes play a similar role, the expression of *pCUC2:CUC2-VENUS* was examined in *kanl1 kanl2* mutants. In the WT, CUC2-VENUS is expressed in the proximal area of the epidermis in the first two leaves (Figure 4.8, A, white arrows), but it is absent in the inner cells and on the adaxial side (Figure 4.9, B, white arrows). In *kanl1 kanl2* seedlings CUC2-VENUS was detected ectopically in the leaf epidermis near the leaf base (Figure 4.8, C, white arrows) and in the adaxial epidermis and inner cells (Figure 4.9, D, white arrows). Additionally, to test whether *KANL1* and *KNAL2* repress KNOX1 gene expression levels, I measured *KNAT1* mRNA levels by qPCR (Figure 4.10). The results revealed higher than wild type *KNAT1* transcript levels in *kanl1 kanl2* mutant seedlings in all three independent experiments indicating that *KANL1* and *KANL2* suppress *KNOX1* genes in *Arabidopsis*, as has been found for the orthologous in tomato and strawberry.

Both *clau* and *salad* mutants exhibit deeper serration depths in their compound leaves. The leaflet number in *salad* mutants, in their trifoliate leaf structures, remains constant, while *clau* has a higher leaflet number (Bar et al., 2015; 2016; Luo et al., 2024). Additionally, *clau* mutants have been reported to possess more leaves than the WT before flowering, a wider SAM, abnormal phyllotaxy, and a broader inflorescence meristem (Bar et al., 2015).

In *kanl1 kanl2*, there were no significant differences detected for the number of leaves formed in the rosettes. However, the arrangement of leaves in *kanl1 kanl2* in the shoot differs from that of the wild type. In wild-type plants, successive lateral organs arise in a predictable pattern known as “phyllotaxy.” To analyse the differences of phyllotaxy, I measured the divergence angles between the first pair of leaves in the WT, *kanl1*, *kanl2* and *kanl1 kanl2*. In the WT, the divergence angle between the first pair of leaves is approximately 140.2^0 (Figure 4.10). In *Arabidopsis*

thaliana, the divergence angle between two successive lateral organs is around 137.5^0 (Byrne et al., 2003). In *kanl1 kanl2*, the divergence angle between the first pair of leaves is approximately 168.3^0 (Figure 4.11), indicating that the phyllotaxy is disrupted in *kanl1 kanl2*.

Though there were no differences in the number of leaves in *kanl1 kanl2* rosettes at the vegetative stage when leaves were initiated, a significant difference was observed in the number of flowers produced by the inflorescence meristem. The number of flower buds initiated from the inflorescence meristem is comparatively high in *kanl1 kanl2* (Figure 4.12).

These similarities in the developmental functions of *KANLIKE* orthologs across different species indicate an evolutionarily conserved role for the *KANLIKEs*.

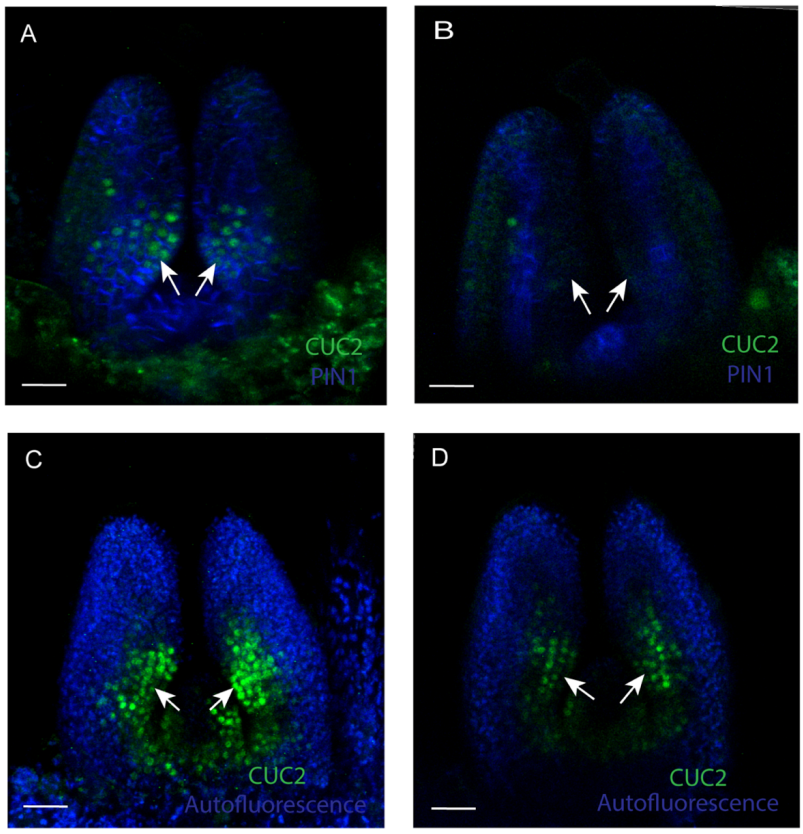

Figure 4.9 *KANL1* and *KANL2* attenuate CUC2 expression
Confocal z-stack projections showing the expression of CUC2-VENUS (green), and PIN1-GFP (blue) in a vegetative meristem of WT 4 DAS (A) and a transverse optical section of (A) to visualise the inner cell layers (B). White arrows in (A) indicate the expression of CUC2-VENUS in the abaxial epidermis at the base of the leaf. White arrows in (B) show the absence of CUC2-VENUS in the adaxial cells and inner cell layers. Confocal projections exhibit the expression of CUC2-VENUS (green) in a vegetative meristem of *kanl1 kanl2* in 4 DAS (C) and a transverse optical section of (C) to visualise the inner cell layers (D). White arrows in (C) show the expression of CUC2-VENUS in abaxial epidermis. White arrows in (D) show the expression of CUC2-VENUS in adaxial epidermis and inner cells. The reported expression patterns were noted in at least three independent plant lines. Scale bars: 15 μm.

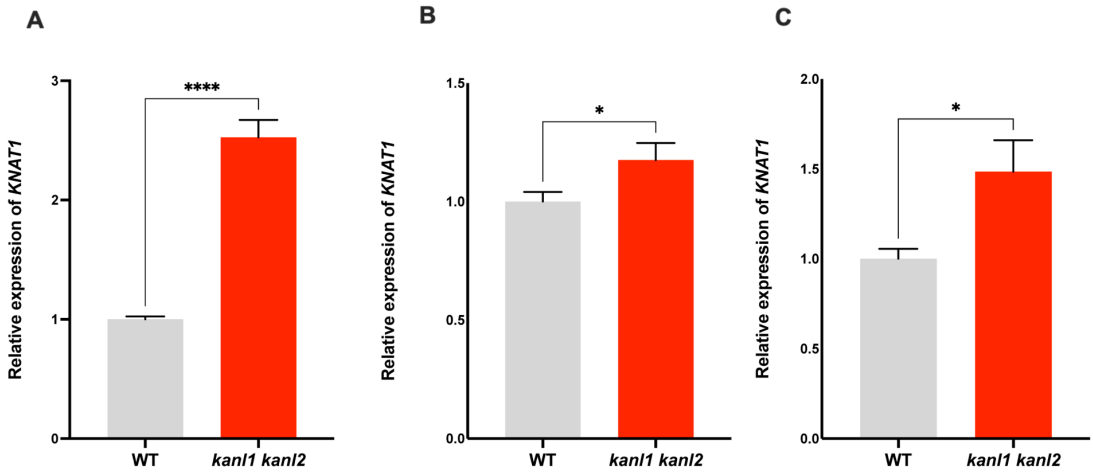

Figure 4.10 *KANL1* and *KANL2* suppress KNAT1 expression

RT-qPCR analysis of *KNAT1* transcripts levels in WT, *kanl1 kanl2* in three independent experiments (A-C). Data are mean ± SD from three technical replicates. Asterisks indicate statistically significant difference compared to the WT (* $P \leq 0.05$, ****$P \leq 0.0001$) determined by Student's t test. Scale bar is 15 μm.

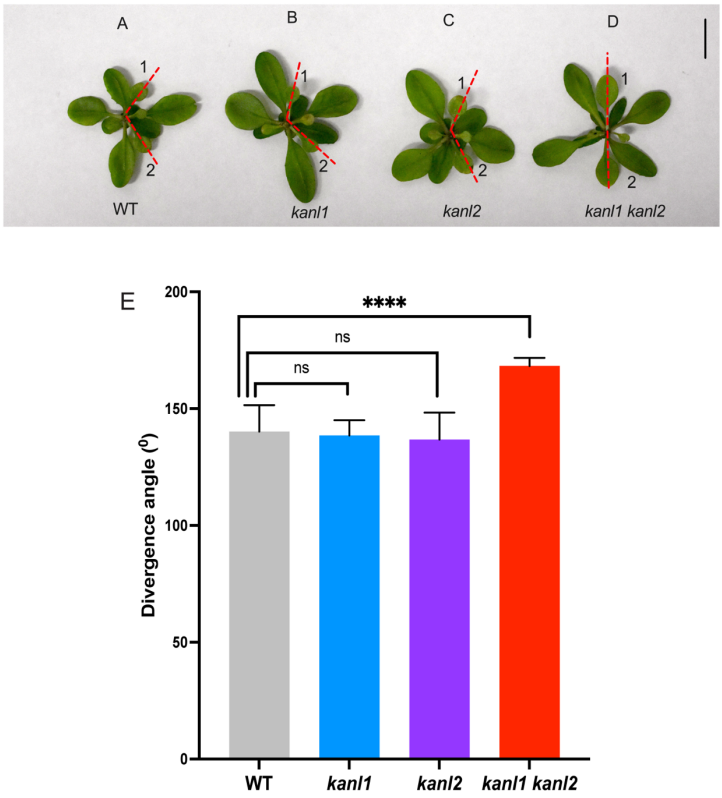

Figure 4.11 *kanl1 kanl2* plants show a different divergence angle compared to the wild type

(A-D) 4-week-old rosettes of wild type (A), *kanl1* (B), *kanl2* (C), and *kanl1 kanl2* (D). The first and second leaves were labelled. Red dashed lines mark the divergence angle between the first two leaves. (E) Quantification of the divergence angle between the first and second leaves of WT, *kanl1, kanl2, kanl1 kanl2.* Mean ± SD are shown. Asterisks indicate statistical significance compared to WT. (**** $P \leq 0.0001$, ns: not significant). Scale bar is 1 cm.

Figure 4.12 *kanl1 kanl2* plants appear to have a larger number of flower buds

(A-D) 8-week-old whole plants of WT (A), *kanl1* (B), *kanl2* (C), and *kanl1 kanl2* (D). (E-H) Inflorescences of 8-week-old WT (E), *kanl1* (F), *kanl2* (G), and *kanl1 kanl2* (H). Scale bars, 1 cm (A-D) and 5 mm (E-H).

4.3. Discussion

In this chapter, I investigate the developmental function of the *KANL1* and *KANL2* genes by assessing *kanl1 kanl2* double mutant and found that these genes act to prevent the downward curving of leaves. In *Arabidopsis thaliana,* the *HD-ZIP III* mutants *rev-9, rev-6, phb-5, and phb-6* were reported to also exhibit downward transverse curvature. Among these, *rev-6* is noted to have a high transverse curvature index (Liu et al., 2010).

Here, *kanl1 kanl2* rosette leaves were found to exhibit downward curvature similar to that of *HD-ZIP III* mutants (Figure 4.1 and 4.5). This downward curvature was restored by introducing the wild-type *KANL1* or *KANL2* genes (Figure 4.3), indicating that the lack of the *KANL1* and *KANL2* genes led to the downward curving phenotype. Multiple mutants of *kanl1 kanl2,* along with *HD-ZIP III* mutants, resulted in intriguing phenotypes; *rev kanl1 kanl2* leaves curved downwards more severely compared to *rev-9 or kanl1 kanl2* single mutants. *The phb phv kanl1 kanl2* quadruple mutant exhibited the same behaviour, curving downwards more severely compared to *phb-6, phv-5,* or *kanl1 kanl2*. These results reveal a shared developmental function between the *KANL* and *HD-ZIP III* genes and is consistent with the finding that KANL1 and KANL2 expression was still detected by qPCR analysis in *rev-9*, *phb-6 phv-5* and *phb-6 phv-5 rev-9* plants (Chapter 3, Figure 3.3).

Mutations in other regulatory factors involved in leaf differentiation and morphogenesis lead to curved leaf shapes. Among these, miRNAs play a crucial role in leaf flatness in *Arabidopsis* (Ren et al., 2018). Consistent with the *HD-ZIP III* loss-of-function phenotypes, the gain-of-function mutant of miRNA166g, which represses HD-ZIP III expression, causes *Arabidopsis* leaves to bend downward. Other than the regulation by miRNA 165/166, DOF (DNA-binding with One Finger) transcription factor Dof5.1 also regulates leaf curvature by directly binding to the REV promoter (Kim et al., 2010). Another recent study shows that SPL10 (SQUAMOSA PROMOTER

BINDING PROTEIN-LIKE 10) also binds to the REV promoter and enhances its activity in leaf curvature (Xu et al., 2025).

In contrast to the loss-of-function phenotype, overexpression of *HD-ZIP III* genes can result in upward-curling leaves. For instance, an adaxialised phenotype was observed in the cross-section of the leaves that exhibited upward curvature after ectopic miRNA-resistant REV in *Arabidopsis* (Xu et al., 2025). However, *HD-ZIP III* genes and the miRNAs are not the only adaxial-abaxial factors linked to leaf curvature in *Arabidopsis.* Adaxial domain genes *AS2* and *AS1* also influence leaf curvature; *as2-1* and *as1-1* exhibit a downward curling of the cotyledons compared to the wild type and produce a larger number of epidermal cells on the adaxial side than on the abaxial side (Iwakawa et al., 2007). Therefore, it would be intriguing to analyse the cellular structure of the *kanl1 kanl2* leaves to test for differences between the cells (number and size) of the adaxial and abaxial sides of the leaves.

CLAUSA from tomato contributes to severe phenotypic effects not only in leaves but also in fruits and inflorescences (Avivi et al., 2000). Tomato *clau* mutant leaves exhibit higher complexity and deeper leaf margin serrations (Bar et al., 2015; 2016). Strawberry *salad* mutants do not show altered trifoliate leaf complexity but do have deeper serrations on their leaflets (Luo et al., 2024). *CLAUSA* is reported to suppress leaf complexity by negatively regulating the *KNOX1* gene *LeT6/Tkn2,* and attenuating cytokinin levels. *CUC* (*GOBLET*) levels are also high in *clau* mutants (Bar et al., 2015; 2016). In *salad* mutants, there is no difference in *KNOXI* levels; however, *CUC2* (*FveCUC2a*) levels are high, and they report that the regulation of *FveCUC2a* is indirect (Luo et al., 2024). In the *Arabidopsis kanl1 kanl2* mutant, both *CUC2* expression and *KNOX1* gene, *KNAT1* levels are high. Also, in *kanl1 kanl2* Col ecotype, also known as *atsalad,* shows more serrations than the WT (Col) (Figure 7C in Luo et al., 2024). There is likely a natural variation in leaf margin morphology in L*er* ecotype and Col ecotype that is associated with *ERECTA* allele (Torii et al., 1996; Shpak et al., 2004). This study utilised L*er* ecotype, hence, no serration was

observed in either WT or *kanl1 kanl2.* This reveals that despite differences in expression patterns between *Arabidopsis* and other species, the orthologous *KANL1/KANL2*, *SALAD*, and *CLAUSA* genes retain partially conserved developmental functions.

Apart from leaf morphology, *kanl1 kanl2* mutants also exhibited phyllotaxy defects (Figure 4.10). Similar results were reported in *clau* mutants. The *clau* mutant was reported to possess a larger SAM compared to the respective WT and caused the abnormalities in the phyllotaxy (Bar et al., 2015). It is possible *kanl1 kanl2* may also possess a broader SAM that leads to the larger divergence angles in leaf initiation. This could be monitored by comparing the size of the CLV3 expression (*pCLV3::CLV3-GFP*) domain by confocal microscopy (Uzair et al., 2024), since CLV3 expression is confined to the stem cell domain of the apex of SAM. Apart from changes in SAM size, ectopic CUC2 in *kanl1 kanl2* may cause abnormal phyllotaxy. It has been reported that misexpression of CUC2 causes abnormal phyllotaxy in *Arabidopsis* (Hibara et al., 2006). Also, ectopic KNAT1 is reported to cause abnormal phyllotaxy (Lincoln et al., 1994).

Chapter 5 - Genetic interactions of *KANL1* and *KANL2* genes with other genes known to be involved in adaxial-abaxial patterning

5.1. Introduction

The data presented so far support the proposal that *KANL1* and *KANL2* are downstream targets of *HD-ZIP III* genes and that they are expressed on the adaxial side of leaves. Their double mutant phenotype indicates that they promote leaf flatness by preventing downward curvature. Given these findings, it is important to determine the regulatory relationship between *KANL1* and *KANL2* and other genes known to function in a related manner. Therefore, this chapter aims to investigate the genetic and regulatory relationship between the *KANLs* and middle domain-specific transcription factors *WOX1* and *PRS* (Nakata et al., 2012b), as well as adaxial-specific *AS2* (Iwakawa et al., 2002).

5.2. Results

5.2.1. *KANL1* and *KANL2* suppress WOX1 on the adaxial side of the leaf

In *Arabidopsis thaliana*, two genes, *WOX1* and *WOX3/PRS*, redundantly regulate leaf curvature and margin development. *wox1 prs* double mutants, for example develop narrow leaves that curve upward, opposite to the *kanl1 kanl2* phenotype (Vandenbussche et al., 2009; Nakata and Okada, 2012; Nakata et al., 2012b). The expression domain of PRS and WOX1 has been designated as the middle domain of the leaf, corresponding to the middle mesophyll layers and margin cells (Nakata et al., 2012b). To test whether *KANL1* and *KANL2* regulate WOX1 or PRS expression, I analysed the expression of *pWOX1::2XGFP-WOX1* and *pPRS::PRS-2XYPET* in the WT and in the *kanl1 kanl2* double mutant. In the wild type, 2XGFP-WOX1 was detected only in the leaf margin, as reported previously (Nakata et al., 2012b); however, in *kanl1 kanl2*, 2XGFP-WOX1 was detected ectopically (Figure 5.1, F, white arrows), appearing throughout the adaxial side of

the leaf epidermis. Consistent with this finding, *WOX1* transcripts in *kanl1 kanl2* seedlings at 5 DAS were higher compared to the wild type as determined by qPCR (Figure 5.1, G). In contrast to WOX1, the expression domain of *pPRS::PRS-2XYPET* in *kanl1 kanl2* appeared similar to that in the wild type (Figure 5.2, C and D, white arrows). Additionally, to test whether *WOX1* and *PRS* regulate *KANL1* and *KANL2* expressions, I analysed the expression of *pKANL1::KANL1-2XYPET* and *pKANL2::KANL2-2XGFP* in the *wox1-101 prs-2* double mutant (Figure 5.3). The results indicated no differences in the expression domains of KANL1-2XYPET and KANL2-2XGFP in *wox1-101 prs-2* compared to the respective wild-type domains (Figure 5.3). KANL1-2XYPET expression is adaxial (Figure 5.3, A and C, white arrows) and present in the SAM (Figure 5.3, A and C, white arrowheads) in both WT and *wox1 prs*. KANL2-2XGFP expression is also adaxial (Figure 5.3, B and D, white arrows) in both WT and *wox1 prs*. This suggests that WOX1 and PRS do not suppress *KANL1* and *KANL2.*

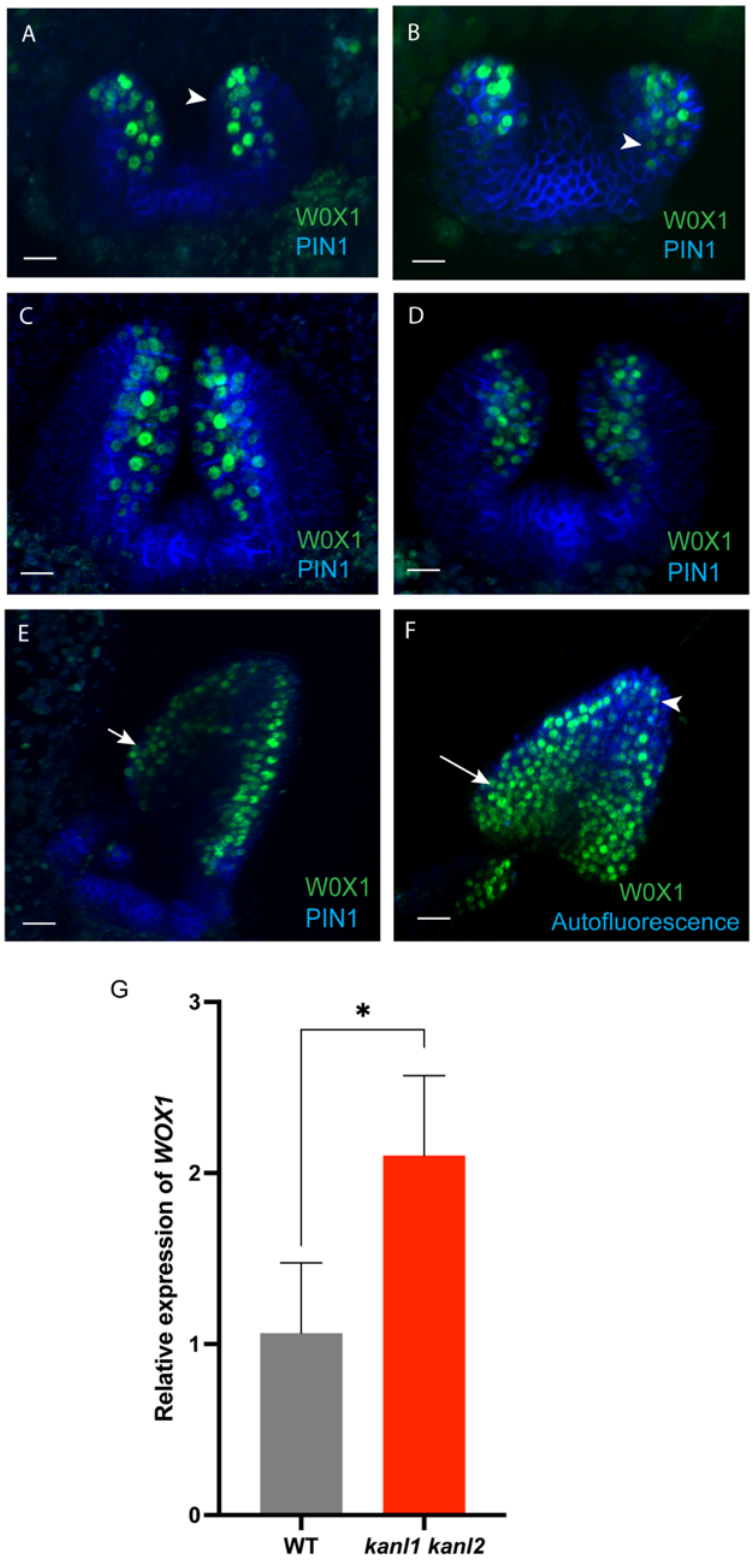

Figure 5.1 *KANL1* and *KANL2* suppress WOX1

Confocal z-stack projections showing the expression of 2XGFP-WOX1 (green) and PIN1-CFP (blue) in a vegetative meristem at 3 DAS in WT (A) and in *kanl1 kanl2* (B). The white arrowhead in (A) shows the absence of 2XGFP-WOX1 on the adaxial side of the leaf, and the white arrowhead in (B) shows expanded 2XGFP-WOX1 expression in the adaxial side. Confocal projections showing the expression of 2XGFP-WOX1 (green) and PIN1-CFP (blue) in a vegetative meristem at 4 DAS in WT (C) and in *kanl1 kanl2* (D). Confocal projection (E) showing the expression of 2XGFP-WOX1 (green) and PIN1-CFP (blue) in the first leaf from a vegetative meristem at 5 DAS. The white arrow in (E) shows the 2XGFP-WOX1 expression is only in the leaf margin. Confocal projection (F) showing the expression of 2XGFP-WOX1 (green) and Autofluorescence (blue) in the first leaf from a vegetative meristem of 5 DAS. The white arrows in (F) show the 2XGFP-WOX1 expression is throughout the epidermis of the adaxial side of the leaf. (G) RT-qPCR analysis of *WOX1* transcript levels in WT and *kanl1 kanl2.* Data are mean ± SD from three independent biological experiments. Each independent experiment was performed three times. Asterisks indicate statistically significant difference (* $P \leq 0.05$) determined by Student's t test. Scale bars: 10 μm.

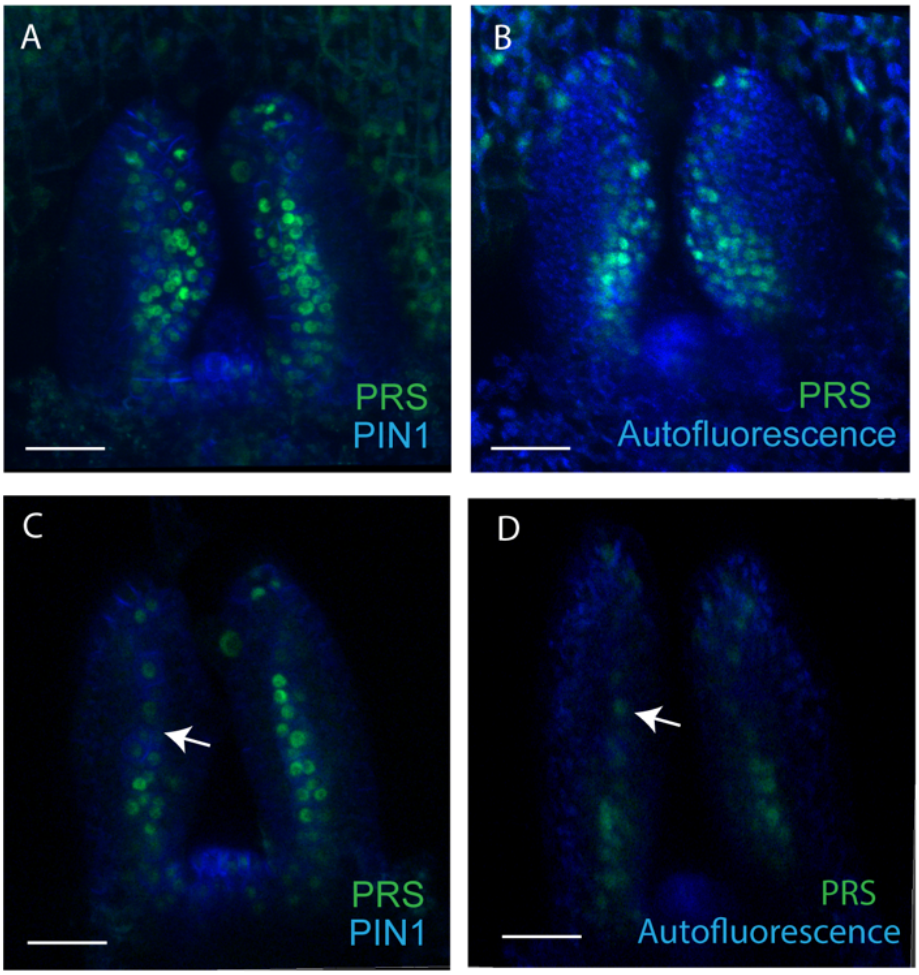

Figure 5.2 PRS expression pattern in *kanl1 kanl2* is similar to WT

(A) Confocal z-stack projection showing the expression of PRS-2XYPET (green) and PIN1-CFP (blue) in a vegetative SAM at 4 DAS in WT. (C) Longitudinal sections of the seedling shown in (A). (B) Confocal projection showing the expression of PRS-2XYPET (green) and autofluorescence (blue) in a vegetative SAM at 4 DAS in *kanl1 kanl2*. (D) Longitudinal sections of the seedling shown in (C). White arrows in (C and D) show that the PRS-2XYPET expression is limited to the leaf margin. Scale bars: 20 μm.

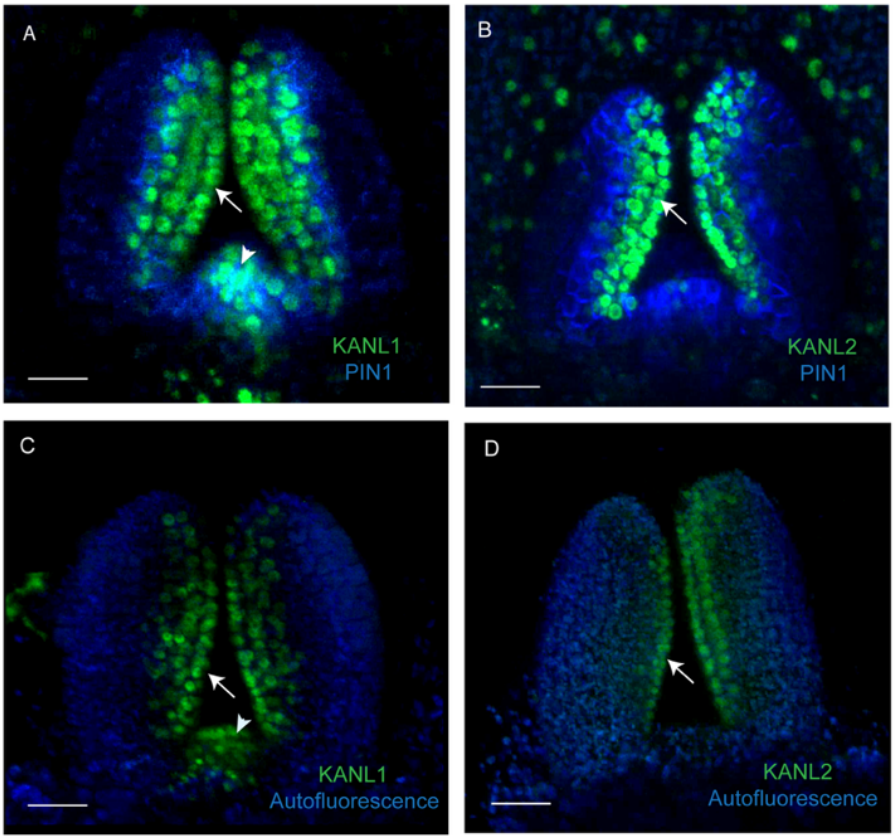

Figure 5.3 KANL1 and KANL2 expression pattern in *wox1 prs* is similar to that of the WT
Confocal projections showing the expression of KANL1-2XYPET (green) in WT (A), in *wox1 prs* (C) and KANL2-2XYPET (green) in WT (B), in *wox1 prs* (D) in a vegetative SAM at 4 DAS. White arrow in (A and C) shows the adaxial expression of KANL1-2XYPET in WT and *wox1prs*, respectively. The white arrowhead in (A and C) shows KANL1-2XYPET expression in WT and *wox1 prs,* respectively. The white arrow in (B and C) shows the adaxial expression of KANL2-2XYPET in WT and *wox1 prs,* respectively. Scale bars: 20 μm.

5.2.2. *wox1-10* (L*er*) and *wox1-15 kanl1 kanl2* (L*er*) mutant alleles used in this study

The finding that WOX1 is ectopically expressed in *kanl1 kanl2* across the entire upper side of the leaf epidermis suggests the possibility that this ectopic expression may contribute to the downward curvature of *kanl1 kanl2* leaves. To test this, I compared *wox1* (L*er*) single mutant leaves to the leaves of *wox1 kanl1 kanl2*. The *wox1* mutant alleles used for this preliminary analysis were generated by Dr. Carolyn Ohno in the Heisler lab. Dr. Ohno used the CRISPR-Cas9 genome editing system with the pkir1.1 vector system (Tsutsui and Higashiyama, 2016) and the same gRNA to target mutations in the *WOX1* gene of L*er* and in *kanl1 kanl2* independently. Thus, two new mutant alleles were created: *wox1-10* in the L*er* background and *wox1-15* in the *kanl1 kanl2* background. In the *wox1-10* mutant, a T is inserted at the 105th nucleotide position. The protein encodes the first 35 amino acids, which are identical to WT, followed by 8 nonsense amino acids that result in a premature stop codon. For *wox1-15* in the *kanl1 kanl2* background, four nucleotides were deleted from positions 102 to 105. The resulting protein encodes the first 34 amino acids, which are similar to WT, followed by 12 nonsense amino acids that lead to a premature stop codon. Thus, both alleles are similar and likely correspond to full loss-of-function mutations.

5.2.3. WOX1 is not required for the downward curving of *kanl1 kanl2* leaves

The alleles mentioned above were used to analyse the *wox1 kanl1 kanl2* triple mutant phenotype. The reported phenotypes of rosettes for *wox1-10* and *wox1-15 kanl1 kanl2* (Figure 5.4, B and D) are derived from F2 progeny resulting from a backcross. The backcross was conducted with either WT or *kanl1 kanl2* to reduce the possibility of off-target mutations caused by the CAS-9 protein in the T2 CRISPR-edited lines. Due to the backcross, the parent lines of these reported rosettes (Figure 5.4, B and D) were heterozygous for the *wox1* allele. PCR genotyping was performed to identify homozygous plants (See methods 2.2.2). The resulting phenotype for both *wox1* and *wox1 kanl1 kanl2* was similar across all homozygous plants (6/20) in the *wox1* segregating population. According to my phenotypic analysis, the *wox1-10* single mutant (Figure 5.4, B) is indistinguishable from WT, consistent with the previously reported phenotype for *wox1-101*, in the Col ecotype (Nakata et al., 2012b). The *wox1-15 kanl1 kanl2* phenotype resembled that of *kanl1 kanl2*, as leaves displayed the downward curving phenotype (Figure 5.4, C and D, white arrow), although due to time constraints, curvature was not quantified. This suggests that ectopic WOX1 does not cause the downward curving of *kanl1 kanl2* leaves.

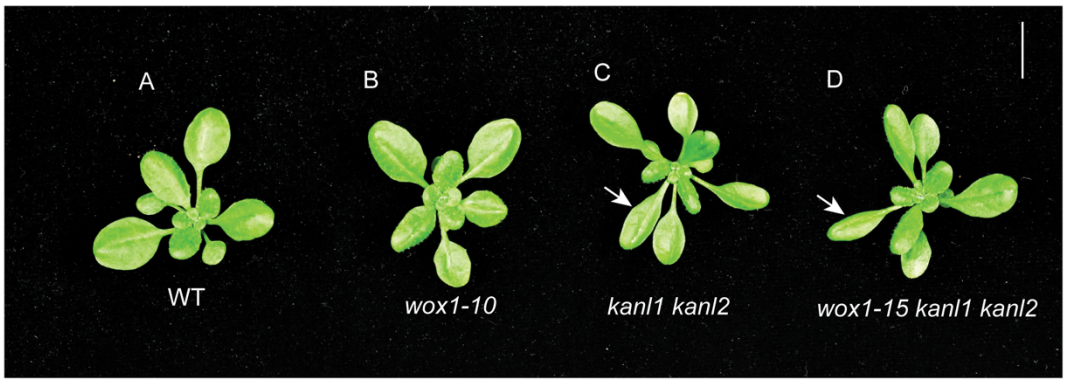

Figure 5.4 Rosette leaves phenotype in *wox1-15 kanl1 kanl2* (L*er*)
(A-D) 4-week-old rosettes of WT (A), *wox1-10* (B), *kanl1 kanl2* (C), *wox1-15 kanl1 kanl2* (D). The white arrows in (C) and (D) show downward curved leaf phenotype in *kanl1 kanl2*. Bar indicates 1 cm.

5.2.4. *wox1 prs* is epistatic to *kanl1 kanl2*

To investigate any potential genetic interaction between the *KANL* genes and WOX1 and PRS, I analysed the phenotype of *wox1 prs kanl1 kanl2* (Figure 5.5). The *wox1 prs kanl1 kanl2* was generated by crossing *wox1-101 prs-2* (Col) (Nakata et al., 2012b) with *kanl1 kanl2* (L*er*) (See methods 2.2.2). The leaves of *wox1 prs kanl1 kanl2* (mixed ecotypes of Col and Ler) quadruple mutants were narrow and curved upwards (Figure 5.5, D) similar to those of the *wox1-101 prs-2* double mutant (Figure 5.5, C). This indicates that *wox1 prs* is epistatic to *kanl1 kanl2,* although due to time constraints the curvature was not quantified.

Figure 5.5 Rosette leaves phenotype in *wox prs kanl1 kanl2*
(A-D) 3-week-old rosettes of WT (A), *kanl1 kanl2* (B), *wox1-101 prs-2* (C), *wox1 prs kanl1 kanl2* (D). Bars indicate 1 cm.

5.2.3. *AS2* acts synergistically with *KANL1* and *KANL2* to promote leaf flatness and to prevent abnormal outgrowths

Like the *KANLs* genes, *AS2* and *AS1* function to prevent the downward curvature of *Arabidopsis* leaves (Iwakawa et al., 2007). Additionally, it has been reported that *AS2* suppresses WOX1 and PRS expression (Satterlee and Scanlon, 2019). These similarities suggest that *AS2* and *KANL1/2* might either act in the same or parallel pathways. To distinguish between these possibilities, I began analysing the phenotypes of the *as2 kanl1 kanl2* triple mutant. Given the KANL mutant alleles were generated in a L*er* ecotype, the *as2 kanl1 kanl2* triple was generated by crossing *as2-101*, which is also in Ler (Yi et al., 2002), to *kanl1 kanl2* (Chapter 2, Materials and Methods, 2.1.1). However, since the *as2* phenotype has been reported to be stronger in the Col ecotype (Semiarti et al., 2001), I also grew the Col *as2-1* allele for an additional comparison of the phenotypes with *as2 kanl1 kanl2.*

as2-101 single mutants develop bilaterally asymmetric leaves with lobed structures, malformed venation, and outgrowths on the petioles (Semiarti et al., 2001). The lobed leaf structure is displayed in Figure 5.6 (K, white arrow). Overall, *as2 kanl1 kanl2* triple mutant plants were relatively shorter and exhibited a dwarf phenotype compared to WT, *as2-101*, *kanl1 kanl2* (Figure 5.10, D). At 28 days, no outgrowths on the leaf petiole of the 5th leaf of *as2-101* mutants were observed (Table 5.1). However, 22.2% of the 5th leaves of *as2-1* plants developed outgrowths on the leaf petiole (at 28 days in Table 5.1). As *as2* mutant leaves mature, more outgrowths become visible in both *as2-1* and *as2-101* single mutants (at 35 days in Table 5.1). Strikingly, the *as2 kanl1 kanl2* exhibits a much stronger phenotype than either *as2* single mutant allele at 28 days. When the leaves mature at 35 days, all 5th leaves of both single mutant *as2* alleles, as well as the *as2 kanl1 kanl2* plants, show outgrowths on the petiole (Table 5.1). However, *as2 kanl1 kanl2* triple mutants not only display lobed leaves and outgrowths on the petiole (Figure 5.6, L white arrow) but also, outgrowths on the leaf mid-vein (Figure 5.6, M, white arrow), which are not

found in either single *as2* mutant allele (compare Figure 5.7 C and D). The triple mutant leaves are not only distinguished by these outgrowths, but also by greater downward curvature compared to the *as2-101* single mutant (Figure 5.7, leaf series, C and D). At 35 days, in the *as2-101* single mutants, outgrowths are only evident on the leaf petiole (Figure 5.8, white arrows on A, B, C), whereas in *as2 kanl1 kanl2*, outgrowths occur on the leaf petiole (Figure 5.8, D and E, white arrows) and also on the 6th leaf midvein, where a leaf lamina-like structure appears top the midvein (Figure 5.8, F, white arrow). Additionally, leaf margins are twisted, and upward curvature is noticeable on the 5th leaf near the base (Figure 5.8, E, arrowhead). These phenotypes become even more pronounced when the leaves reach a more mature state, such as at 45 days old (Figure 5.9). In single *as2* mutants, outgrowths are exhibited on the leaf petiole across all the leaves at 45 days (Figure 5.9, A). However, in *as2 kanl1 kanl2*, outgrowths are seen on the petiole and in the mid-vein, as mentioned previously (Figure 5.9, F and G, white arrows). As the leaves mature, these outgrowths become significantly more pronounced (Figure 5.9, D, arrowhead). As noted earlier, on the 6th leaf, a leaf lamina-like structure appeared on the mid vein at 35 days old (Figure 5.8, F, white arrow). When more mature, at 45 days, these lamina-like structures further divide into several leaf laminae (Figure 5.9, H and I, white arrow and arrowhead). All together, these findings suggest that *AS2* acts in parallel with *KANL1* and *KANL2* to prevent leaf curving and abnormal outgrowths on the adaxial side of the leaf. In addition to enhanced leaf phenotypes, *as2 kanl1 kanl2* flowers also displayed a significant phenotype with narrow petals and sepals compared to the *as2-101* single mutants (Figure 5.11, D, white arrow and arrowhead).

5.2.4 Expression analysis

To investigate whether AS2 regulates *KANL1* or *KANL2*, I analysed the expression of *pKANL1::KANL1-2XYPET* and *pKANL2::KANL2-2XGFP* in *as2-1* (Figure 5.12). No differences in the expression domains of KANL1-2XYPET and KANL2-2XGFP in *as2-1* were detected compared to the respective wild type expression patterns (Figure 5.12). KANL1-2XYPET expression is adaxial (Figure 5.12, A and C, white arrows) and present in the SAM (Figure 5.12, A and C, white arrowheads) in both wild type and *as2-1*. KANL2-2XGFP expression is also adaxial (Figure 5.12, B and D, white arrows) in both wild type and *as2-1*. These data suggest *AS2* does not regulate the *KANL1* and *KANL2* expression domains.

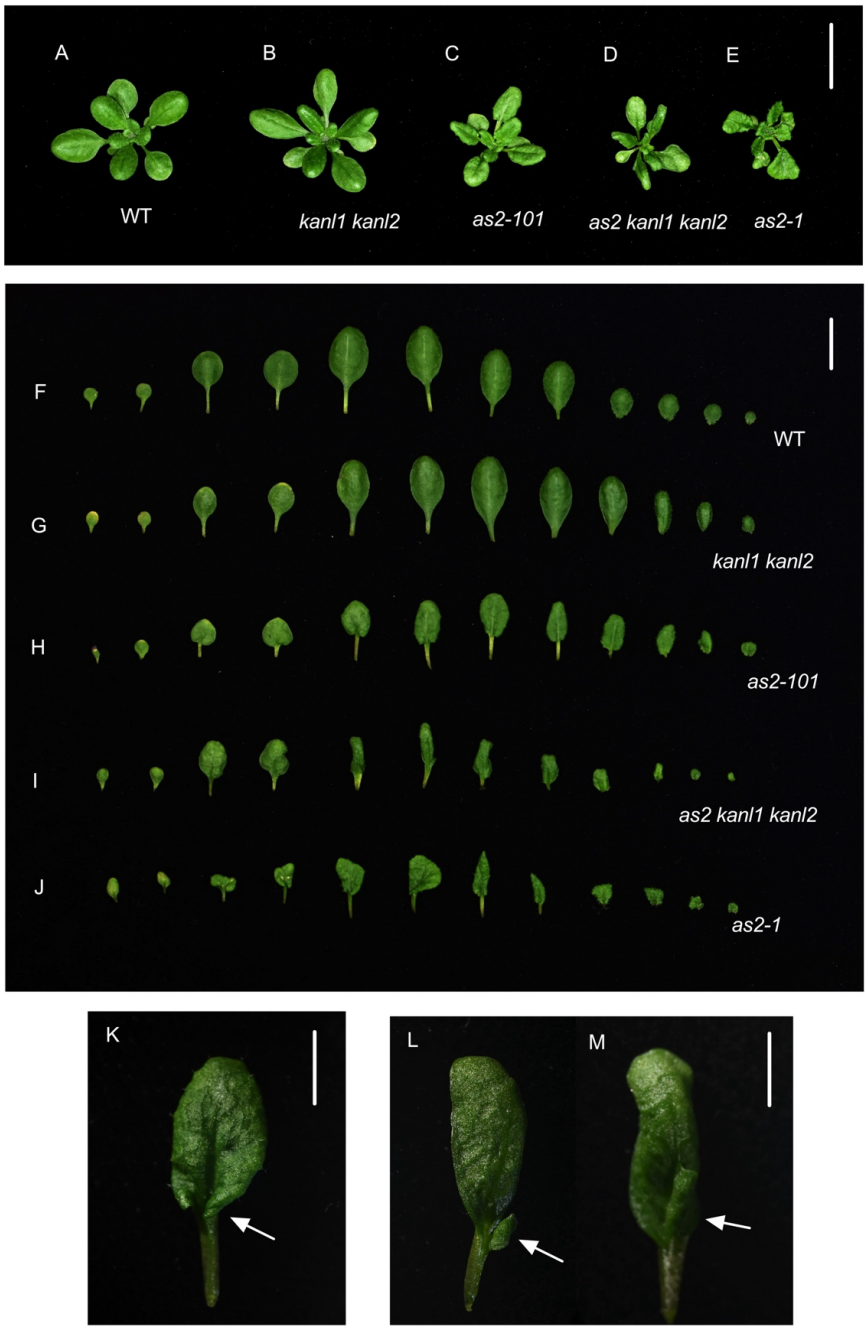

Figure 5.6 *as2* and *as2 kanl1 kanl2* triple mutant phenotype (28-days-old)

(A-E) 4-week-old rosettes of WT (A) *kanl1 kanl2* (B), *as2-101* (C), *as2 kanl1 kanl2* (D) and *as2-1* (F). (F-J) Leaf series (2 cotyledons and 10 leaves from left to right) of 28-day-old WT (F) *kanl1 kanl2* (G), *as2-101* (H), *as2 kanl1 kanl2* (I) and *as2-1*(J). (K) 5th Leaf of *as2-101*.The white arrow in (K) indicates the leaf lobe structure. (L) two different 5th leaves observed in *as2 kanl1 kanl2*. The white arrow in (L) indicates the leaflet-like structure on the 5th leaf petiole of *as2 kanl1 kanl2*. White arrow in (M) indicates the leaflet-like structure on the 5th leaf mid vein of *as2 kanl1 kanl2*. Bars indicate 1 cm.

Table 5.1 Proportions of *as2-1*, *as2-101* and *as2 kanl1 kanl2* plants which showed phenotypes in the 5th leaf at 28 days and 35 days old rosettes

Genotype with the ecotype	Age	The number of plants examined	Lotus leaves	Leaves that have outgrowths on petiole	Leaves that have outgrowths on mid vein
as2-1 (Col)	28 days	18	18 (100%)	4 (22.2%)	0 (0%)
as2-101 (L*er*)		20	20 (100%)	0 (0%)	0 (0%)
as2 kanl1 kanl2 (L*er*)		22	22 (100%)	11 (50%)	10 (45%)
as2-1 (Col)	35 days	18	18 (100%)	18 (100%)	0 (0%)
as2-101 (Ler)		20	20 (100%)	20 (100%)	0 (0%)
as2 kanl1 kanl2 (L*er*)		22	22 (100%)	22 (100%)	22 (100%)

Age indicates DAS, and percentages indicate the frequencies of the 5th leaf for the observed phenotype

Figure 5.7 The leaf phenotype of *as2* and *as2 kanl1 kanl2* triple mutant (35-days-old)
(A-B) 35 days-old rosettes of *as2-101*(A) *as2 kanl1 kanl2* (B). (C-D) Leaf series of 10 leaves of 35-days-old *as2-101* (C), *as2 kanl1 kanl2* (D). Bars indicate1 cm.

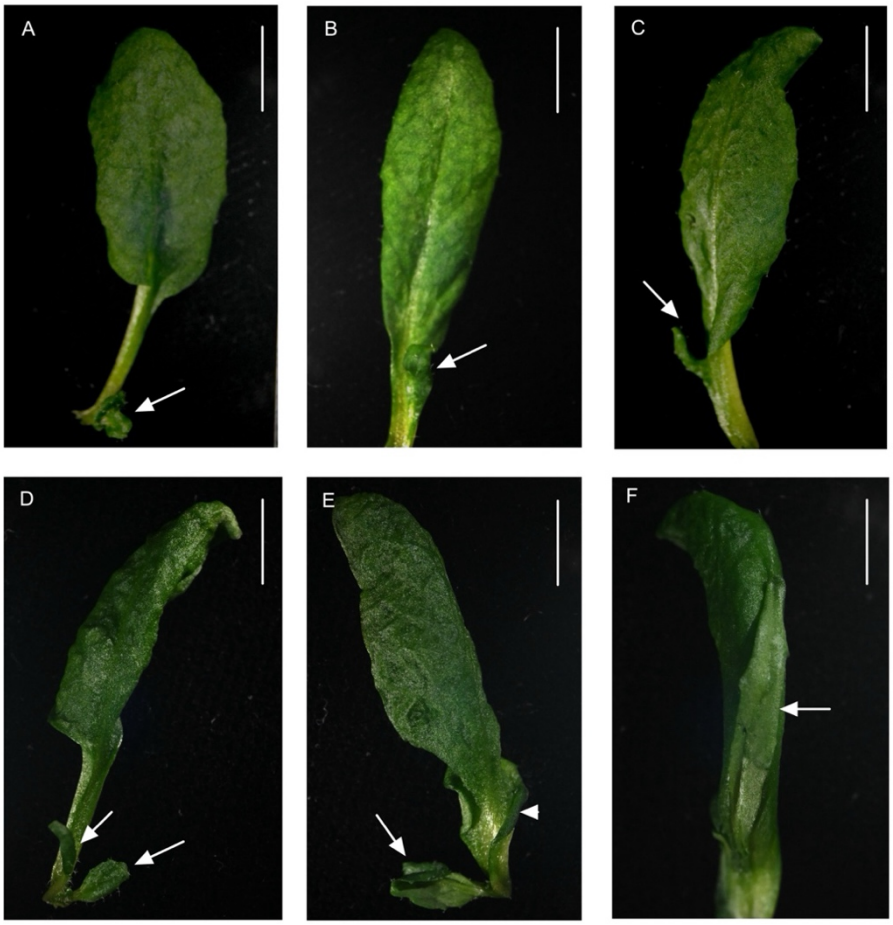

Figure 5.8 The 4th, 5th and 6th leaf phenotype of *as2* and *as2 kanl1 kanl2* (35-days-old) plants

35 days old 4th (A), 5th (B) and 6th (C) leaves of *as2-101*. The white arrow in (A) indicates the outgrowths on the petiole of the 4th leaf of *as2-101*. The white arrow in (B) indicates the outgrowth on the petiole near the leaf base of the 5th leaf of *as2-101*. The white arrow in (C) shows the outgrowth near the leaf base of 6th leaf of *as2-101*. The reported phenotypes were observed in all the plants (20) observed in *as2-101.* 35 days old 4th (D), 5th (E) and 6th (F) leaves of *as2 kanl1 kanl2*. The white arrows in (D) show the leaflet-like structures on the petiole of the 4th leaf of *as2 kanl1 kanl2*. The white arrow in (E) shows the leaflet-like structures on the petiole near the leaf base of the 5th leaf of *as2 kanl1 kanl2*. The white arrowhead in (E) shows the upward curved leaf margin at the leaf base of *kanl1 kanl2* (E). The white arrow in (F) shows the leaf-lamina like structure on the 6th leaf of *as2 kanl1 kanl2* mid vein. The reported phenotypes were observed in all (22) *as2-101 kanl1 kanl2* plants observed. Bars indicate 1 cm.

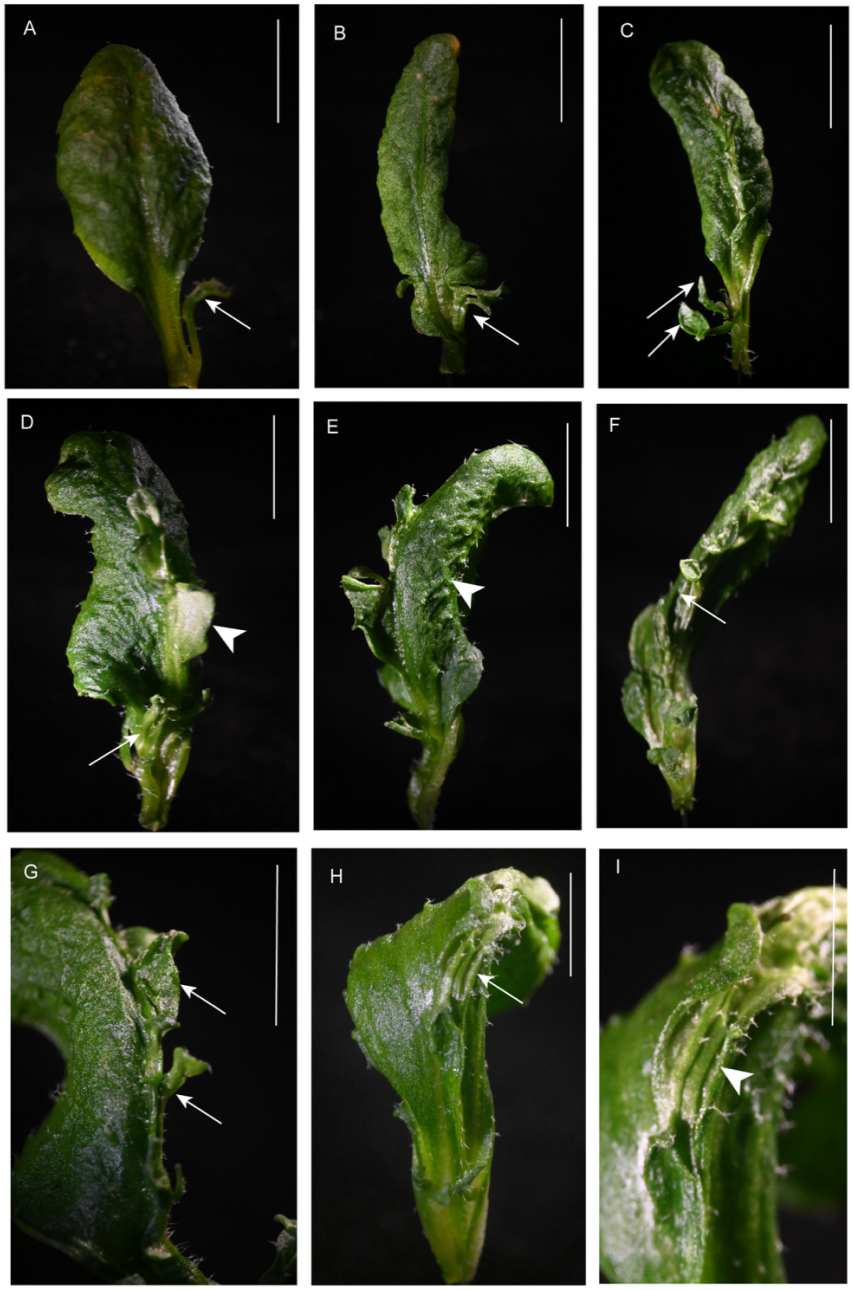

Figure 5.9 Different leaf phenotypes in *as2 kanl1 kanl2* at 45-days-old

(A) 5th leaf of 45-day-old *as2-101* plants. (B-I) Various leaf phenotypes of *as2 kanl1 kanl2* at 45 days old. The white arrow in B marks the outgrowths near the leaf base on the 4th leaf of *as2 kanl1 kanl2*. White arrows in (C) point to the outgrowths on the petiole of the 5th leaf of *as2 kanl1 kanl2*. The white arrow in (D) indicates the outgrowths on the petiole, while the white arrowhead on the mid vein denotes an ectopic lamina outgrowth on the 5th leaf of *as2 kanl1 kanl2*. The white arrowhead in (E) illustrates leaf protrusions on the adaxial side near the leaf margin identified on the 5th leaf of *as2 kanl1 kanl2*. The white arrow in (F) shows the outgrowth on the mid-vein of the 5th leaf of *as2 kanl1 kanl2*. (G) A closer view of the outgrowths noted in (F). The white arrow in (H) indicates that the mid-vein is divided into several leaf lamina structures on the 6th leaf of *as2 kanl1 kanl2*. (I) A closer view of the phenotype described in (H). The noted phenotypes were observed in all the plants at 45 days old. Bars indicate 1 cm.

Figure 5.10 The *as2 kanl1 kanl2* is comparatively a shorter plant
(A-D) 8-week-old whole plants of WT (A), *kanl1 kanl2* (B), *as2-101* (C), and *as2 kanl1 kanl2* Scale bar is 1 cm.

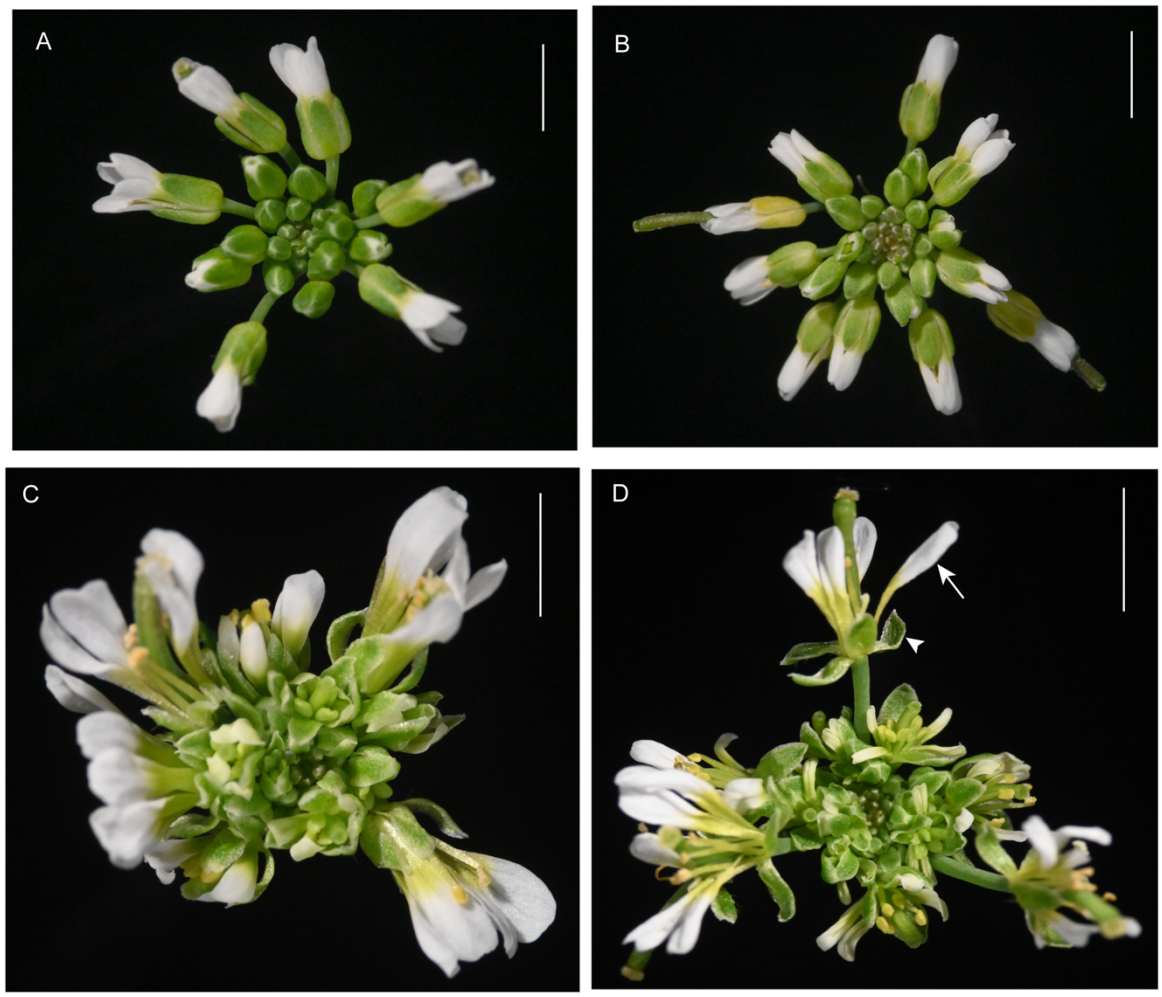

Figure 5.11 Flower phenotype in *as2 kanl1 kanl2*

(A-D) Inflorescences of 8-week-old WT (A), *kanl1 kanl2* (B), *as2-101* (C), and *as2 kanl1 kanl2.* The white arrow in (D) shows narrow petals, and the white arrowhead in (D) shows narrow sepals in *as2 kanl1 kanl2* inflorescence. Scale bars: 5mm.

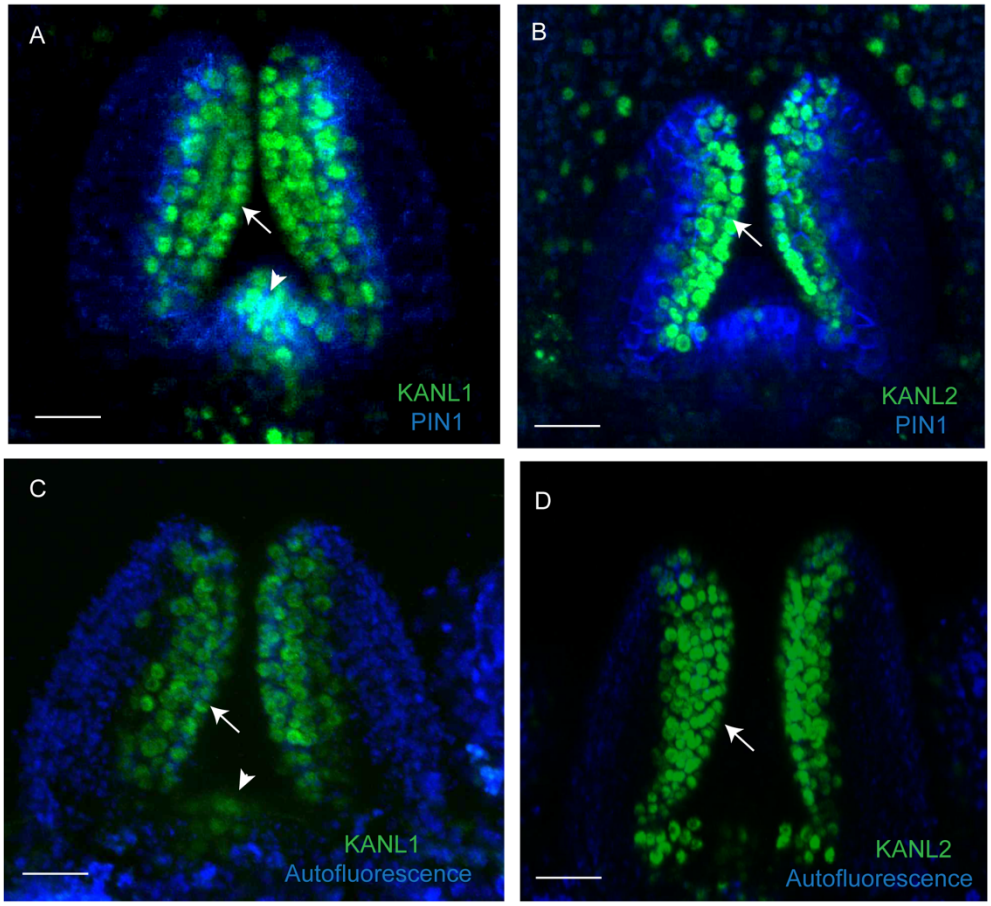

Figure 5.12 KANL1 and KANL2 expression patterns in leaves of *as2-1* plants are similar to that of the WT

Confocal projections showing the expression of KANL1-2YFP (green) in WT (A), in *as2-1* (C) and KANL2-2YFP (green) in WT (B), in *as2-1* (D) in a vegetative SAM at 4 DAS. White arrow in (A and C) shows the adaxial expression of KANL1-2YFP in WT and *as2-1*, respectively. The white arrowhead in (A and C) shows KANL1-2YFP expression in WT and *as2-1,* respectively. The white arrow in (B and C) shows the adaxial expression of KANL2-2YFP in WT and *as2-1,* respectively. Scale bars: 20 μm.

5.3. Discussion

A major finding from this chapter is that *KANL1* and *KANL2* regulate the expression of middle-domain gene *WOX1*. The results show that *KANL1* and *KANL2* suppress *WOX1* in the adaxial epidermis. According to my analysis, PRS-2XYPET was not ectopic in *kanl1 kanl2.* However, it has been confirmed in the Heisler lab that *KANL1* and *KANL2* suppress PRS, as shown by digital droplet PCR, which indicated that the number of transcripts of *PRS* was greater in *kanl1 kanl2* (Unpublished data, Dr. C.Ohno). Though there were no detectable differences in the spatial expression domain of PRS in *kanl1 kanl2*, the overall mRNA/protein levels are high within those cells.

Analysis of the *wox1 kanl1 kanl2* triple mutant indicates a similar phenotype with curved leaves to *kanl1 kanl2*, suggesting that ectopic WOX1 alone, expressed throughout the adaxial epidermis in *kanl1 kanl2,* is not required for the downward curvature of the double mutant leaves. However, analysis of the quadruple mutant *wox1 prs kanl1 kanl2* indicates upward curving leaves similar to the *wox1 prs* double phenotype indicating that *wox1 prs* is epistatic. Given WOX1 and PRS are functionally redundant (Nakata et al., 2012b), and that *KANL* expression is still present in *wox1 prs* double mutants, these findings indicate that the *KANL* genes function to prevent downward curving leaves, likely in part, by restricting the expression of both *WOX1* and *PRS*. Future experiments assessing *WOX1* and *PRS* expression in *as2 kanl1 kanl2* triple mutants and additional multiple mutant analysis may help test this hypothesis. Interestingly, past work has shown that the related but abaxially expressed *KANADI* genes also suppress WOX1 and PRS (Nakata et al., 2012b; Ram et al., 2020). Given *KANL1* and *KANL2* share a similar MYB DNA binding domain and EAR motif to the KAN proteins*,* an intriguing possibility to be tested in future work is whether both KAN and KANL transcription factors repress *WOX1* and *PRS* expression via the same cis-regulatory motifs.

In chapter 4, I discussed the role of both the *HD-ZIP III* and *KANLs* genes in promoting leaf flatness by preventing downward curvature of the leaf lamina. Another set of adaxially expressed genes that prevent downward curvature of the lamina are *AS2* and *AS1* (Iwakawa et al., 2007). To explore the functional relationship between the *KANLs* and *AS2*, this chapter reports the triple mutant phenotype. My analysis of *as2 kanl1 kanl2* demonstrates a much stronger phenotype than the *as2* single or *kan11 kanl2* double phenotypes alone, suggesting that *KANL1, KANL2,* and *AS2* prevent downward curvature through parallel pathways. Given *AS2* is known to repress *WOX1* and *PRS* (Satterlee and Scanlon, 2019), as found for the *KANLs* in this thesis, a likely possibility is that all three genes contribute to the repression of *WOX1* and *PRS* in adaxial tissues and that the more severe phenotype of the *as2 kanl1 kanl2* triple mutant reflects in part, a greater degree of ectopic WOX1 and PRS expression, compared to single *as2* or *kanl1 kanl2* double mutants. In this scenario, an analogy can be made between the ectopic outgrowths of the *as2 kanl1 kanl2* triple mutant on the adaxial side with outgrowths on the abaxial side in the *kan1 kan2* double mutant (Eshed et al., 2004). In the latter, WOX1 and PRS are expressed ectopically and are required for the ectopic outgrowth phenotype (Nakata et al., 2012b).

In *Arabidopsis* leaf primordia, two BTB-POZ domain proteins, BLADE-ON-PETIOLE1 (BOP1) and BOP2 are linked to the regulation of AS2 and adaxial-abaxial patterning (Ha et al., 2007; Jun, Ha and Fletcher, 2010). *AS2* in turn, represses *KNOX* genes to ensure proper leaf development. In *as2* mutants, *KNOX* genes, *KNAT1* and *KNAT2* are ectopic in leaves and flowers (Ori et al., 2000; Guo et al., 2008). In this study, I also found that *KANL1* and *KANL2* suppress *KNAT1* (Chapter 4, Figure 4.9). Therefore, mis-regulation of KNAT1 expression may also help explain the strong phenotype of *as2 kanl1 kanl2* mutants. It will be important to conduct further research on *KNOX1* levels (*KNAT1*, *KNAT2*, and *KNAT6*) in the *as2 kanl1 kanl2* mutant background and to examine plants mutant for all three *AS2*, *KANLs* and *KNOX-class* genes.

Lastly, I found CUC2 is ectopic in *kanl1 kanl2*. Given that *CUC2* is required for the outgrowths of *kan1 kan2* mutant on the abaxial side (Abley et al., 2016), it may be that ectopic CUC2 contributes to the outgrowths on the adaxial side of the *as2 kanl1 kanl2.* This can be analysed by generating plants mutant for *CUC2, AS2, KANL1*, and *KANL2*.

Chapter 6 – General Discussion

Adaxial-abaxial patterning in leaf development: Controversies in the literature

In 1955, Sussex's wounding experiment suggested that a signal from the SAM governs adaxial-abaxial patterning, thereby affecting the lamina structure of leaves (Sussex, 1955). This is clearly illustrated in (Figure 2 in Fernando and Heisler, 2024) attached here in the appendix. Since then, several studies have both supported and contradicted Sussex's proposal. Despite controversies, some key findings stand out. For example, leaf adaxial-abaxial patterning is now thought to be prepatterned in the SAM via the expression domains of transcription factors that specify adaxial-abaxial identity (Caggiano et al., 2017; Yu et al., 2017; Burian et al., 2022). However, one unresolved issue is the role of auxin in adaxial-abaxial patterning. Some studies have proposed that low auxin levels on the adaxial side are necessary for proper specification of adaxial cell fate (Figure 4 in Fernando and Heisler, 2024); otherwise, leaves become radialised and consist only of abaxial cell types (Qi et al., 2014; Guan et al., 2017). Additionally, these reports link these low levels of auxin to the lack of WOX1 and PRS expression in adaxial leaf tissues (Guan et al., 2017; Burian et al., 2022). A deeper discussion of this issue (Fernando and Heisler, 2024), without consideration of the *KANL* genes, is attached at the end of this thesis (appendix) and followed up, including consideration of the *KANL* genes, below.

Where do KANL1 and KANL2 fit into the adaxial-abaxial patterning of the leaf? And future directions

The findings presented in this thesis have important implications for understanding how the middle-domain WOX1 and PRS expression domain is defined. On the abaxial side, there has been little controversy. The middle domain genes *WOX1* and *PRS* are repressed by *KAN1* and *KAN2*, acting together with *ARF2*, *ARF3* and *ARF4* (Pekker, Alvarez and Eshed, 2005; Alvarez et al.,

2016; Yu et al., 2017; Heisler, 2021). On the adaxial side however, the literature consensus has not been as clear. Some reports have indicated the *HD-ZIP III* gene *REV* as well as *AS2* suppress WOX1 and PRS on the adaxial side (Alvarez et al., 2016; Ram et al., 2020). As mentioned above, other studies have indicated that low levels of auxin repress WOX1 and PRS adaxially (Guan et al., 2017; Burian et al., 2022). However, no data directly demonstrating that auxin levels are limiting for WOX1 and PRS has been reported, while increasing auxin levels does not result in ectopic WOX1 or PRS expression in *Arabidopsis* (Caggiano et al., 2017) arguing against this hypothesis. By revealing that *KANL1* and *KANL2* are required to restrict WOX1 expression to the middle domain, likely in conjunction with *AS2,* this thesis now adds considerable new evidence against the low auxin proposal.

Interestingly, despite the arguments above, low levels of auxin do seem important for leaf adaxial/abaxial patterning - just not in *Arabidopsis*. In tomato, a relatively recent study reports that wound-induced auxin depletion on the adaxial side of the leaf primordium causes a reduction in the expression of *SILAM1,* the tomato ortholog of *WOX1* (Wang et al., 2022). This finding is consistent with the known role of auxin in promoting WOX1 and PRS expression (Caggiano et al., 2017). The more surprising result however is that applying exogenous auxin to intact leaf primordia clearly caused ectopic expression of *SILAM1* in adaxial leaf tissues (Wang et al., 2022), in contrast to similar experiments in *Arabidopsis* (Caggiano et al., 2017). This indicates that the regulation of middle domain genes is different between the two species, which also correlates with different wound responses, since wounds abaxialise tomato and potato leaves but not those of *Arabidopsis* (Caggiano et al., 2017; Zhao and Traas, 2021). One specific difference in regulation revealed by this thesis is that KANL orthologs in different species, which I show can regulate middle-domain genes, are expressed in distinct patterns. For instance, both *CLAUSA* and SALAD are expressed along leaf margins (Bar et al., 2015; 2016; Luo et al., 2024) whereas in *Arabidopsis*, *KANL1* and *KANL2* are expressed adaxially. An important hypothesis to be tested

in future experiments, therefore, is whether differences in KANL ortholog expression account for species-specific differences in the sensitivity of middle domain gene expression patterns and leaf development in general, to wounding and exogenous auxin.

KANL clade and future directions

As mentioned in chapter 1, (Ram et al., 2020) reported that *KANL1*, *KANL2, KANL3,* and *KANL4* possess similar MYB DNA binding domains to that of *KANADI*. While *KANL1* and *KANL2* were chosen for this study because they exhibit similar expression patterns to REV, respond similarly to REV and KAN perturbations and are closely related to each other (Ram et al., 2020). KANL3/MYS1 and KANL4/MYS2 show a different expression pattern and function (Liu et al., 2022) than those found for KANL1 and KANL2 in this thesis. Also, KANL3 and KANL4 showed a separate divergence in the evolution (Figure 1.10 in Chapter 1).

Although they differ significantly in expression, function, and evolutionary background, the significant sequence similarity among the four genes indicates some level of redundancy may still exist. To assess whether these genes continue to serve compensatory or interconnected roles, as well as possible co-regulation, the analysis of quadruple mutants for their function and phenotype will be useful.

Such an analysis will be interesting to follow up not only in *Arabidopsis* but also in other species, including in non-flowering plants. For instance, in *Marchantia polymorpha*, such findings may reveal ancestral features and evolutionary changes related to the colonisation of land by plants.

More future directions

A major finding of this research is that KANLs suppress WOX1 and PRS on the adaxial side, similar to KAN on the abaxial side. This suggests that *KAN* and *KANL* may act through the same cis-regulatory elements to repress WOX1/PRS. This can be investigated by analysing the *WOX1* and *PRS* promoters for KANL and KAN binding. Additionally, it indicates that KANL transcription factors may downregulate many of the same targets as KAN. This could be examined through Chromatin Immunoprecipitation followed by sequencing (ChIP-seq) by comparing genome-wide KAN and KANL1 binding profiles.

Renaming KANLs

Initially, these genes were designated as *KANL1, KANL2, KANL3,* and *KANL4* based on the BLAST results and their close homology to the *KANADI* genes in *Arabidopsis. KANL3* and *KANL4* have been published under the designations of *MYS1* and *MYS2* (Liu et al., 2022). Also, these genes belong to the ENO group of the GARP transcription factor family (Bowman et al., 2017; Briginshaw, 2020). Therefore, giving these two genes new, distinctive names would help avoid confusion in the future.

In Summary

This study explored the regulation and functions of two newly identified genes involved in adaxial-abaxial leaf patterning, *KANL1* and *KANL2.* I provided evidence that the *KANLs* are direct downstream targets of the *HD-ZIP III* genes and demonstrated that their main function is to prevent the downward curving of *Arabidopsis* leaf lamina. Additionally, I found that *KANL1* and *KANL2* likely prevent this downward curving, in part, by suppressing the expression of the middle-domain genes *WOX1* and *PRS*, likely in conjunction with *AS2* (Figure 6.1). Comparing to other orthologous genes, I also found that *KANLIKEs* retain conserved functions in repressing

CUC and *KNOX* encoding genes. These findings not only add new players to the complex genetic regulatory network governing leaf development but also shed light on species-specific differences relevant to the understanding of leaf diversity and developmental responses to the environment.

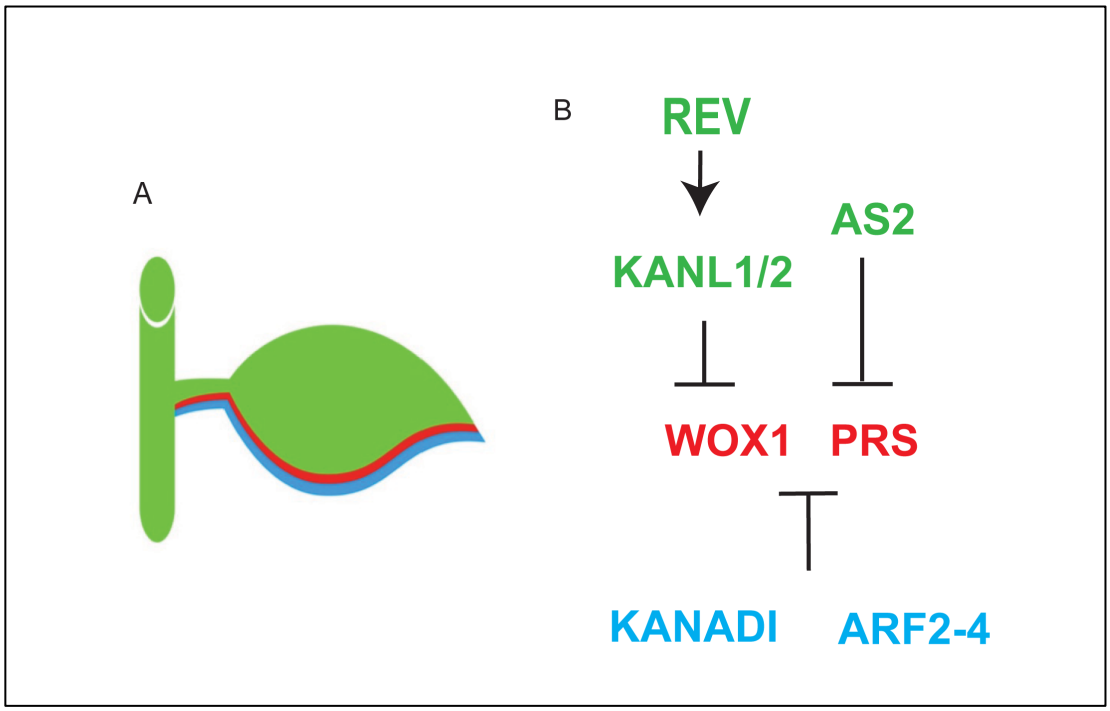

Figure 6.1 Schematic presentation of *KANLs* function in leaf development
(A) Three different domains in leaf development. Adaxial transcription factors (HD-ZIP III, KANLS, AS2) are expressed at the top of the leaf (green), while abaxial transcription factors (KANADI, ARFS) are expressed at the bottom (blue). The middle domain, where WOX1 and PRS are expressed and which responds to auxin, is located in between (red). (B) Model for the regulation of WOX1 and PRS by adaxial and abaxial domains. REV suppresses WOX1 and PRS via KANL1 and KANL2. Simultaneously, AS2 also suppresses WOX1 and PRS. KANADI and ARF2-4 suppress WOX1 and PRS on the abaxial side.

References

Abley, K., Sauret-Güeto, S., Marée, A.F. and Coen, E., 2016. Formation of polarity convergences underlying shoot outgrowths. *eLife*, 5, p.e18165. https://doi.org/10.7554/elife.18165.

Aida, M., Ishida, T., Fukaki, H., Fujisawa, H. and Tasaka, M., 1997. Genes involved in organ separation in Arabidopsis: an analysis of the cup-shaped cotyledon mutant. *The Plant cell*, 9(6), pp.841–857. https://doi.org/10.1105/tpc.9.6.841.

Alvarez, J.P., Furumizu, C., Efroni, I., Eshed, Y. and Bowman, J.L., 2016. Active suppression of a leaf meristem orchestrates determinate leaf growth. *eLife*, 5. https://doi.org/10.7554/elife.15023.

Avivi, Y., Lev-Yadun, S., Morozova, N., Libs, L., Williams, L., Zhao, J., Varghese, G. and Grafi, G., 2000. Clausa, a Tomato Mutant with a Wide Range of Phenotypic Perturbations, Displays a Cell Type-Dependent Expression of the Homeobox Gene LeT6/TKn2 1. *Plant Physiology*, 124(2), pp.541–552. https://doi.org/10.1104/pp.124.2.541.

Baima, S., Nobili, F., Sessa, G., Lucchetti, S., Ruberti, I. and Morelli, G., 1995. The expression of the Athb-8 homeobox gene is restricted to provascular cells in Arabidopsis thaliana. *Development*, 121(12), pp.4171–4182. https://doi.org/10.1242/dev.121.12.4171.

Bar, M., Ben-Herzel, O., Kohay, H., Shtein, I. and Ori, N., 2015. CLAUSA restricts tomato leaf morphogenesis and GOBLET expression. *The Plant Journal*, 83(5), pp.888–902. https://doi.org/10.1111/tpj.12936.

Bar, M., Israeli, A., Levy, M., Gera, H.B., Jiménez-Gómez, J., Kouril, S., Tarkowski, P. and Ori, N., 2016. CLAUSA is a MYB Transcription Factor that Promotes Leaf Differentiation by Attenuating Cytokinin Signaling. *The Plant Cell*, 28(7), p.tpc.00211.2016. https://doi.org/10.1105/tpc.16.00211.

Beerling, D.J. and Fleming, A.J., 2007. Zimmermann's telome theory of megaphyll leaf evolution: a molecular and cellular critique. *Current Opinion in Plant Biology*, 10(1), pp.4–12. https://doi.org/10.1016/j.pbi.2006.11.006.

Bertolotti, G., Unterholzner, S.J., Scintu, D., Salvi, E., Svolacchia, N., Mambro, R.D., Ruta, V., Scaglia, F.L., Vittorioso, P., Sabatini, S., Costantino, P. and Ioio, R.D., 2021. A PHABULOSA-Controlled Genetic Pathway Regulates Ground Tissue Patterning in the Arabidopsis Root. *Current Biology*, 31(2), pp.420-426.e6. https://doi.org/10.1016/j.cub.2020.10.038.

Bharathan, G., Goliber, T.E., Moore, C., Kessler, S., Pham, T. and Sinha, N.R., 2002. Homologies in Leaf Form Inferred from KNOXI Gene Expression During Development. *Science*, 296(5574), pp.1858–1860. https://doi.org/10.1126/science.1070343.

Bilsborough, G.D., Runions, A., Barkoulas, M., Jenkins, H.W., Hasson, A., Galinha, C., Laufs, P., Hay, A., Prusinkiewicz, P. and Tsiantis, M., 2011. Model for the regulation of Arabidopsis thaliana leaf margin development. *Proceedings of the National Academy of Sciences*, 108(8), pp.3424–3429. https://doi.org/10.1073/pnas.1015162108.

Bowman, J.L., Alvarez, J., Weigel, D., Meyerowitz, E.M. and Smyth, D.R., 1993. Control of flower development in Arabidopsis thaliana by APETALA1 and interacting genes. *Development*, 119(3), pp.721–743. https://doi.org/10.1242/dev.119.3.721.

Bowman, J.L., Kohchi, T., Yamato, K.T., Jenkins, J., Shu, S., Ishizaki, K., Yamaoka, S., Nishihama, R., Nakamura, Y., Berger, F., Adam, C., Aki, S.S., Althoff, F., Araki, T., Arteaga-Vazquez, M.A., Balasubrmanian, S., Barry, K., Bauer, D., Boehm, C.R., Briginshaw, L., Caballero-Perez, J., Catarino, B., Chen, F., Chiyoda, S., Chovatia, M., Davies, K.M., Delmans, M., Demura, T., Dierschke, T., Dolan, L., Dorantes-Acosta, A.E., Eklund, D.M., Florent, S.N., Flores-Sandoval, E., Fujiyama, A., Fukuzawa, H., Galik, B., Grimanelli, D., Grimwood, J., Grossniklaus, U., Hamada, T., Haseloff, J., Hetherington, A.J., Higo, A., Hirakawa, Y., Hundley, H.N., Ikeda, Y., Inoue, K., Inoue, S., Ishida, S., Jia, Q., Kakita, M., Kanazawa, T., Kawai, Y., Kawashima, T., Kennedy, M., Kinose, K., Kinoshita, T., Kohara, Y., Koide, E., Komatsu, K., Kopischke, S., Kubo, M., Kyozuka, J., Lagercrantz, U., Lin, S.-S., Lindquist, E., Lipzen, A.M., Lu, C.-W., Luna, E.D., Martienssen, R.A., Minamino, N., Mizutani, M., Mizutani, M., Mochizuki, N., Monte, I., Mosher, R., Nagasaki, H., Nakagami, H., Naramoto, S., Nishitani, K., Ohtani, M., Okamoto, T., Okumura, M., Phillips, J., Pollak, B., Reinders, A., Rövekamp, M., Sano, R., Sawa, S., Schmid, M.W., Shirakawa, M., Solano, R., Spunde, A., Suetsugu, N., Sugano, S., Sugiyama, A., Sun, R., Suzuki, Y., Takenaka, M., Takezawa, D., Tomogane, H., Tsuzuki, M., Ueda, T., Umeda, M., Ward, J.M., Watanabe, Y., Yazaki, K., Yokoyama, R., Yoshitake, Y., Yotsui, I., Zachgo, S. and Schmutz, J., 2017. Insights into Land Plant Evolution Garnered from the Marchantia polymorpha Genome. *Cell*, 171(2), pp.287-304.e15. https://doi.org/10.1016/j.cell.2017.09.030.

Brandt, R., Salla-Martret, M., Bou-Torrent, J., Musielak, T., Stahl, M., Lanz, C., Ott, F., Schmid, M., Greb, T., Schwarz, M., Choi, S.B., Barton, M.K., Reinhart, B.J., Liu, T., Quint, M., Palauqui, J.C., Martínez-García, J.F. and Wenkel, S., 2012. Genome-wide binding-site analysis of REVOLUTA reveals a link between leaf patterning and light-mediated growth responses. *Plant Journal*, 72(1), pp.31–42. https://doi.org/10.1111/j.1365-313x.2012.05049.x.

Briginshaw, L., 2020. The role of *KANADI* in the liverwort *Marchantia polymorpha* (Doctoral Dissertation). MONASH University.

Burian, A., Paszkiewicz, G., Nguyen, K.T., Meda, S., Raczyńska-Szajgin, M. and Timmermans, M.C.P., 2022. Specification of leaf dorsiventrality via a prepatterned binary readout of a uniform auxin input. *Nature Plants*, 8(3), pp.269–280. https://doi.org/10.1038/s41477-022-01111-3.

Byrne, M.E., 2006. Shoot meristem function and leaf polarity: The role of class III HD-ZIP genes. *PLoS Genetics*, 2, pp.0785–0790. https://doi.org/10.1371/journal.pgen.0020089.

Byrne, M.E., Barley, R., Curtis, M., Arroyo, J.M., Dunham, M., Hudson, A. and Martienssen, R.A., 2000. Asymmetric leaves1 mediates leaf patterning and stem cell function in Arabidopsis. *Nature*, 408(6815), pp.967–971. https://doi.org/10.1038/35050091.

Byrne, M.E., Groover, A.T., Fontana, J.R. and Martienssen, R.A., 2003. Phyllotactic pattern and stem cell fate are determined by the Arabidopsis homeobox gene BELLRINGER. *Development*, 130(17), pp.3941–3950. https://doi.org/10.1242/dev.00620.

Caggiano, M.P., 2013. Dorso-ventral patterning and lateral organ positioning in *Arabidopsis thaliana* (Doctoral Dissertation). University of Heidelberg, Germany.

Caggiano, M.P., Yu, X., Bhatia, N., Larsson, A., Ram, H., Ohno, C.K., Sappl, P., Meyerowitz, E.M., Jönsson, H. and Heisler, M.G., 2017. Cell type boundaries organize plant development. *eLife*, 6. https://doi.org/10.7554/elife.27421.

Chitwood, D.H., Headland, L.R., Filiault, D.L., Kumar, R., Jiménez-Gómez, J.M., Schrager, A.V., Park, D.S., Peng, J., Sinha, N.R. and Maloof, J.N., 2012. Native Environment Modulates Leaf Size and Response to Simulated Foliar Shade across Wild Tomato Species. *PLoS ONE*, 7(1), p.e29570. https://doi.org/10.1371/journal.pone.0029570.

Edwards, K., Johnstone, C. and Thompson, C., 1991. A simple and rapid method for the preparation of plant genomic DNA for PCR analysis. *Nucleic Acids Research*, 19(6), pp.1349–1349. https://doi.org/10.1093/nar/19.6.1349.

Emery, J.F., Floyd, S.K., Alvarez, J., Eshed, Y., Hawker, N.P., Izhaki, A., Baum, S.F. and Bowman, J.L., 2003. Radial Patterning of Arabidopsis Shoots by Class III HD-ZIP and KANADI Genes. *Current Biology*, 13(20), pp.1768–1774. https://doi.org/10.1016/j.cub.2003.09.035.

Eshed, Y., Baum, S.F., Perea, J.V. and Bowman, J.L., 2001. Establishment of polarity in lateral organs of plants. *Current Biology*, 11(16), pp.1251–1260. https://doi.org/10.1016/s0960-9822(01)00392-x.

Eshed, Y., Izhaki, A., Baum, S.F., Floyd, S.K. and Bowman, J.L., 2004. Asymmetric leaf development and blade expansion in Arabidopsisare mediated by KANADI and YABBY activities. *Development*, 131(12), pp.2997–3006. https://doi.org/10.1242/dev.01186.

Fernando, H. and Heisler, M.G., 2024. Wounding and the establishment of leaf polarity: From historical perspectives to present controversies. *Trends in Developmental Biology*.

Friedman, W.E., Moore, R.C. and Purugganan, M.D., 2004. The evolution of plant development. *American Journal of Botany*, 91(10), pp.1726–1741. https://doi.org/10.3732/ajb.91.10.1726.

Fritz, M.A., Rosa, S. and Sicard, A., 2018. Mechanisms Underlying the Environmentally Induced Plasticity of Leaf Morphology. *Frontiers in Genetics*, 9, p.478. https://doi.org/10.3389/fgene.2018.00478.

Greb, T. and Lohmann, J.U., 2016. Plant Stem Cells. *Current Biology*, 26(17), pp.R816–R821. https://doi.org/10.1016/j.cub.2016.07.070.

Guan, C., Wu, B., Yu, T., Wang, Q., Krogan, N.T., Liu, X. and Jiao, Y., 2017. Spatial Auxin Signaling Controls Leaf Flattening in Arabidopsis. *Current Biology*, 27, pp.2940-2950.e4. https://doi.org/10.1016/j.cub.2017.08.042.

Guenot, B., Bayer, E., Kierzkowski, D., Smith, R.S., Mandel, T., Žádníková, P., Benková, E. and Kuhlemeier, C., 2012. PIN1-Independent Leaf Initiation in Arabidopsis. *Plant Physiology*, 159(4), pp.1501–1510. https://doi.org/10.1104/pp.112.200402.

Guo, M., Thomas, J., Collins, G. and Timmermans, M.C.P., 2008. Direct Repression of KNOX Loci by the ASYMMETRIC LEAVES1 Complex of Arabidopsis. *The Plant Cell*, 20(1), pp.48–58. https://doi.org/10.1105/tpc.107.056127.

Ha, C.M., Jun, J.H., Nam, H.G. and Fletcher, J.C., 2007. BLADE-ON-PETIOLE1 and 2 Control Arabidopsis Lateral Organ Fate through Regulation of LOB Domain and Adaxial-Abaxial Polarity Genes. *The Plant Cell*, 19(6), pp.1809–1825. https://doi.org/10.1105/tpc.107.051938.

Hall, T.A., 1999. BioEdit: A User-Friendly Biological Sequence Alignment Editor and Analysis Program for Windows 95/98/NT. *Nucleic Acids Symposium Series,*. [online] Available at: <https://d1wqtxts1xzle7.cloudfront.net/29520866/1999hall1-libre.pdf?1390876715=&response-content-disposition=inline%3B+filename%3DBioEdit_a_user_friendly_biological_seque.pdf&Expires=1741299922&Signature=X7ZNl7nQPJ5onhq8uzl8GMWd0CTxxU2D0qzafMFboIstXOc4P6Zs~INf89SXpwa7c5OOXM8j~XkRLfZTEsJFWwDnSmHJjLhSalBCdDTuyzJgJkvxBdDmR0XczCsGbxEypG3P1ixMRQnqXdVViObfN3c6f1FK~gucd-Dr2euiAXnKowq-u-4YOr7tBJv1GM1eWUVJQkAamGojp-1u2AqUuVd2mdtPhIyIbe19kU~RTDINAikT3wNoiIqJr2dAF7GsF3997QKj05B8W9br29NfRC1d1qd0Zwu89~hbz7MB4TX3A9~sz1SI8evQe4yMdrsBrncGSHO1~5l5-L9u4VMqmw__&Key-Pair-Id=APKAJLOHF5GGSLRBV4ZA>.

Hay, A. and Tsiantis, M., 2006. The genetic basis for differences in leaf form between Arabidopsis thaliana and its wild relative Cardamine hirsuta. *Nature Genetics*, 38(8), pp.942–947. https://doi.org/10.1038/ng1835.

Hay, A. and Tsiantis, M., 2010. KNOX genes: versatile regulators of plant development and diversity. *Development*, 137(19), pp.3153–3165. https://doi.org/10.1242/dev.030049.

Heisler, M.G., 2021. Integration of Core Mechanisms Underlying Plant Aerial Architecture. *Frontiers in Plant Science*, 12, p.786338. https://doi.org/10.3389/fpls.2021.786338.

Heisler, M.G., Ohno, C., Das, P., Sieber, P., Reddy, G.V., Long, J.A. and Meyerowitz, E.M., 2005. Patterns of Auxin Transport and Gene Expression during Primordium Development Revealed by Live Imaging of the Arabidopsis Inflorescence Meristem. *Current Biology*, 15, pp.1899–1911. https://doi.org/10.1016/j.cub.2005.09.052.

Hibara, K., Karim, Md.R., Takada, S., Taoka, K., Furutani, M., Aida, M. and Tasaka, M., 2006. Arabidopsis CUP-SHAPED COTYLEDON3 Regulates Postembryonic Shoot Meristem and Organ Boundary Formation. *The Plant Cell*, 18(11), pp.2946–2957. https://doi.org/10.1105/tpc.106.045716.

Huang, T., Harrar, Y., Lin, C., Reinhart, B., Newell, N.R., Talavera-Rauh, F., Hokin, S.A., Barton, M.K. and Kerstetter, R.A., 2014. Arabidopsis KANADI1 acts as a transcriptional repressor by interacting with a specific cis-element and regulates auxin biosynthesis, transport, and signaling in opposition to HD-ZIPIII factors. *The Plant cell*, 26(1), pp.246–62. https://doi.org/10.1105/tpc.113.111526.

Husbands, A.Y., Feller, A., Aggarwal, V., Dresden, C.E., Holub, A.S., Ha, T. and Timmermans, M.C.P., 2023. The START domain potentiates HD-ZIPIII transcriptional activity. *The Plant Cell*, 35(6), pp.2332–2348. https://doi.org/10.1093/plcell/koad058.

Iwakawa, H., Iwasaki, M., Kojima, S., Ueno, Y., Soma, T., Tanaka, H., Semiarti, E., Machida, Y. and Machida, C., 2007. Expression of the ASYMMETRIC LEAVES2 gene in the adaxial domain of Arabidopsis leaves represses cell proliferation in this domain and is critical for the development

of properly expanded leaves. *The Plant Journal*, 51(2), pp.173–184. https://doi.org/10.1111/j.1365-313x.2007.03132.x.

Iwakawa, H., Ueno, Y., Semiarti, E., Onouchi, H., Kojima, S., Tsukaya, H., Hasebe, M., Soma, T., Ikezaki, M., Machida, C. and Machida, Y., 2002. The ASYMMETRIC LEAVES2 Gene of Arabidopsis thaliana, Required for Formation of a Symmetric Flat Leaf Lamina, Encodes a Member of a Novel Family of Proteins Characterized by Cysteine Repeats and a Leucine Zipper. *Plant and Cell Physiology*, 43(5), pp.467–478. https://doi.org/10.1093/pcp/pcf077.

Izhaki, A. and Bowman, J.L., 2007. KANADI and class III HD-Zip gene families regulate embryo patterning and modulate auxin flow during embryogenesis in Arabidopsis. *Plant Cell*, 19, pp.495–508. https://doi.org/10.1105/tpc.106.047472.

Jones, D.T., Taylor, W.R. and Thornton, J.M., 1992. The rapid generation of mutation data matrices from protein sequences. *Bioinformatics*, 8(3), pp.275–282. https://doi.org/10.1093/bioinformatics/8.3.275.

Jun, J.H., Ha, C.M. and Fletcher, J.C., 2010. BLADE-ON-PETIOLE1 Coordinates Organ Determinacy and Axial Polarity in Arabidopsis by Directly Activating ASYMMETRIC LEAVES2. *The Plant Cell*, 22(1), pp.62–76. https://doi.org/10.1105/tpc.109.070763.

Kaufmann, K., Muiño, J.M., Østerås, M., Farinelli, L., Krajewski, P. and Angenent, G.C., 2010. Chromatin immunoprecipitation (ChIP) of plant transcription factors followed by sequencing (ChIP-SEQ) or hybridization to whole genome arrays (ChIP-CHIP). *Nature Protocols*, 5(3), pp.457–472. https://doi.org/10.1038/nprot.2009.244.

Kayani, S.-I., Shen, Q., Ma, Y., Fu, X., Xie, L., Zhong, Y., Tiantian, C., Pan, Q., Li, L., Rahman, S., Sun, X. and Tang, K., 2019. The YABBY Family Transcription Factor AaYABBY5 Directly Targets Cytochrome P450 Monooxygenase (CYP71AV1) and Double-Bond Reductase 2 (DBR2) Involved in Artemisinin Biosynthesis in Artemisia Annua. *Frontiers in Plant Science*, 10, p.1084. https://doi.org/10.3389/fpls.2019.01084.

Khush, G.S. and Rick, C.M., 1967. Studies on the linkage map of chromosome 4 of the tomato and on the transmission of induced deficiencies. *Genetica*, 38(1), pp.74–94. https://doi.org/10.1007/bf01507450.

Kim, H., Kim, S.J., Abbasi, N., Bressan, R.A., Yun, D., Yoo, S., Kwon, S. and Choi, S., 2010. The DOF transcription factor Dof5.1 influences leaf axial patterning by promoting Revoluta transcription in Arabidopsis. *The Plant Journal*, 64(3), pp.524–535. https://doi.org/10.1111/j.1365-313x.2010.04346.x.

Kittiwongwattana, C., 2012. Leaf polarity establishment and the two sets of regulators. *Genomics and Genetics*, [online] 5, pp.21–33. https://doi.org/10.14456/tjg.2012.8.

Krizek, B.A., Blakley, I.C., Ho, Y.-Y., Freese, N. and Loraine, A.E., 2020. The Arabidopsis transcription factor AINTEGUMENTA orchestrates patterning genes and auxin signaling in the establishment of floral growth and form. [online] https://doi.org/10.1111/tpj.14769.

Kumar, S., Stecher, G., Suleski, M., Sanderford, M., Sharma, S. and Tamura, K., 2024. MEGA12: Molecular Evolutionary Genetic Analysis Version 12 for Adaptive and Green Computing. *Molecular Biology and Evolution*, 41(12), p.msae263. https://doi.org/10.1093/molbev/msae263.

Lincoln, C., Long, J., Yamaguchi, J., Serikawa, K. and Hake, S., 1994. A knotted1-like homeobox gene in Arabidopsis is expressed in the vegetative meristem and dramatically alters leaf morphology when overexpressed in transgenic plants. *The Plant cell*, 6(12), pp.1859–1876. https://doi.org/10.1105/tpc.6.12.1859.

Liu, L., Yahaya, B.S., Li, J. and Wu, F., 2024. Enigmatic role of auxin response factors in plant growth and stress tolerance. *Frontiers in Plant Science*, 15, p.1398818. https://doi.org/10.3389/fpls.2024.1398818.

Liu, Q., Huang, H., Chen, Y., Yue, Z., Wang, Z., Qu, T., Xu, D., Lü, S. and Hu, H., 2022. Two Arabidopsis MYB-SHAQKYF transcription repressors regulate leaf wax biosynthesis via transcriptional suppression on DEWAX. *New Phytologist*, 236(6), pp.2115–2130. https://doi.org/10.1111/nph.18498.

Liu, Z., Jia, L., Mao, Y. and He, Y., 2010. Classification and quantification of leaf curvature. *Journal of Experimental Botany*, 61(10), pp.2757–2767. https://doi.org/10.1093/jxb/erq111.

Livak, K.J. and Schmittgen, T.D., 2001. Analysis of Relative Gene Expression Data Using Real-Time Quantitative PCR and the 2−ΔΔC T Method. *Methods*, 25(4), pp.402–408. https://doi.org/10.1006/meth.2001.1262.

Long, J.A., Moan, E.I., Medford, J.I. and Barton, M.K., 1996. A member of the KNOTTED class of homeodomain proteins encoded by the STM gene of Arabidopsis. *Nature*, 379(6560), pp.66–69. https://doi.org/10.1038/379066a0.

Luo, X., Guo, L., Tagliere, E., Yang, Z. and Liu, Z., 2024. Leaf dissection and margin serration are independently regulated by two regulators converging on the CUC2-auxin module in strawberry. *Current Biology*, 34(4), pp.769-780.e5. https://doi.org/10.1016/j.cub.2024.01.010.

McConnell, J.R., Emery, J., Eshed, Y., Bao, N., Bowman, J. and Barton, M.K., 2001. Role of PHABULOSA and PHAVOLUTA in determining radial patterning in shoots. *Nature*, 411(6838), pp.709–713. https://doi.org/10.1038/35079635.

McHale, N.A. and Marcotrigiano, M., 1998. LAM1 is required for dorsoventrality and lateral growth of the leaf blade in Nicotiana. *Development*, 125(21), pp.4235–4243. https://doi.org/10.1242/dev.125.21.4235.

Merelo, P., Ram, H., Caggiano, M.P., Ohno, C., Ott, F., Straub, D., Graeff, M., Cho, S.K., Yang, S.W., Wenkel, S. and Heisler, M.G., 2016. Regulation of MIR165/166 by class II and class III homeodomain leucine zipper proteins establishes leaf polarity. *Proceedings of the National Academy of Sciences*, 113(42), pp.11973–11978. https://doi.org/10.1073/pnas.1516110113.

Merelo, P., Xie, Y., Brand, L., Ott, F., Weigel, D., Bowman, J.L., Heisler, M.G. and Wenkel, S., 2013. Genome-Wide Identification of KANADI1 Target Genes. *PLoS ONE*, 8(10), p.e77341. https://doi.org/10.1371/journal.pone.0077341.

Meyerowitz, E.M., 1997. Genetic Control of Cell Division Patterns in Developing Plants. *Cell*, 88(3), pp.299–308. https://doi.org/10.1016/s0092-8674(00)81868-1.

Meyerowitz, E.M., 2002. Plants Compared to Animals: The Broadest Comparative Study of Development. *Science*, 295(5559), pp.1482–1485. https://doi.org/10.1126/science.1066609.

Nakata, M., Matsumoto, N., Tsugeki, R., Rikirsch, E., Laux, T. and Okada, K., 2012a. Roles of the Middle Domain–Specific WUSCHEL-RELATED HOMEOBOX Genes in Early Development of Leaves in Arabidopsis. *The Plant Cell*, 24(2), pp.519–535. https://doi.org/10.1105/tpc.111.092858.

Nakata, M., Matsumoto, N., Tsugeki, R., Rikirsch, E., Laux, T. and Okada, K., 2012b. Roles of the middle domain-specific WUSCHEL-RELATED HOMEOBOX genes in early development of leaves in Arabidopsis. *Plant Cell*, 24, pp.519–535. https://doi.org/10.1105/tpc.111.092858.

Nakata, M. and Okada, K., 2012. The three-domain model. *Plant Signaling & Behavior*, [online] 7, pp.1423–1427. https://doi.org/10.4161/psb.21959.

Nakata, M. and Okada, K., 2013. The leaf adaxial-abaxial boundary and lamina growth. *Plants*, 2, pp.174–202. https://doi.org/10.3390/plants2020174.

Nardmann, J., Ji, J., Werr, W. and Scanlon, M.J., 2004. The maize duplicate genes narrow sheath1 and narrow sheath2 encode a conserved homeobox gene function in a lateral domain of shoot apical meristems. *Development*, 131(12), pp.2827–2839. https://doi.org/10.1242/dev.01164.

Ori, N., Eshed, Y., Chuck, G., Bowman, J.L. and Hake, S., 2000. Mechanisms that control knox gene expression in the Arabidopsis shoot. *Development*, 127(24), pp.5523–5532. https://doi.org/10.1242/dev.127.24.5523.

Pajoro, A., Madrigal, P., Muiño, J.M., Matus, J.T., Jin, J., Mecchia, M.A., Debernardi, J.M., Palatnik, J.F., Balazadeh, S., Arif, M., Ó'Maoiléidigh, D.S., Wellmer, F., Krajewski, P., Riechmann, J.-L., Angenent, G.C. and Kaufmann, K., 2014. Dynamics of chromatin accessibility and gene regulation by MADS-domain transcription factors in flower development. *Genome Biology*, 15(3), p.R41. https://doi.org/10.1186/gb-2014-15-3-r41.

Pekker, I., Alvarez, J.P. and Eshed, Y., 2005. Auxin Response Factors Mediate Arabidopsis Organ Asymmetry via Modulation of KANADI Activity. *The Plant Cell*, 17(11), pp.2899–2910. https://doi.org/10.1105/tpc.105.034876.

Prigge, M.J., Otsuga, D., Alonso, J.M., Ecker, J.R., Drews, G.N. and Clark, S.E., 2005. Class III Homeodomain-Leucine Zipper Gene Family Members Have Overlapping, Antagonistic, and Distinct Roles in Arabidopsis Development. *The Plant Cell*, 17(1), pp.61–76. https://doi.org/10.1105/tpc.104.026161.

Qi, J., Wang, Y., Yu, T., Cunha, A., Wu, B., Vernoux, T., Meyerowitz, E. and Jiao, Y., 2014. Auxin depletion from leaf primordia contributes to organ patterning. *Proceedings of the National Academy of Sciences of the United States of America*, 111, pp.18769–18774. https://doi.org/10.1073/pnas.1421878112.

Ram, H., Sahadevan, S., Gale, N., Caggiano, M.P., Yu, X., Ohno, C. and Heisler, M.G., 2020. An integrated analysis of cell-type specific gene expression reveals genes regulated by REVOLUTA and KANADI1 in the Arabidopsis shoot apical meristem. *PLOS Genetics*, [online] 16, pp.1–34. https://doi.org/10.1371/journal.pgen.1008661.

Reinhardt, D., Frenz, M., Mandel, T. and Kuhlemeier, C., 2005. Microsurgical and laser ablation analysis of leaf positioning and dorsoventral patterning in tomato. *Development*, [online] 132, pp.15–26. https://doi.org/10.1242/dev.01544.

Reinhart, B.J., Liu, T., Newell, N.R., Magnani, E., Huang, T., Kerstetter, R., Michaels, S. and Barton, M.K., 2013. Establishing a Framework for the Ad/Abaxial Regulatory Network of Arabidopsis: Ascertaining Targets of Class III HOMEODOMAIN LEUCINE ZIPPER and KANADI Regulation. *The Plant Cell*, 25(9), pp.3228–3249. https://doi.org/10.1105/tpc.113.111518.

Ren, W., Wang, H., Bai, J., Wu, F. and He, Y., 2018. Association of microRNAs with Types of Leaf Curvature in Brassica rapa. *Frontiers in Plant Science*, 9, p.73. https://doi.org/10.3389/fpls.2018.00073.

Runions, A., Tsiantis, M. and Prusinkiewicz, P., 2017. A common developmental program can produce diverse leaf shapes. *New Phytologist*, 216(2), pp.401–418. https://doi.org/10.1111/nph.14449.

Samalova, M., Brzobohaty, B. and Moore, I., 2005. pOp6/LhGR: a stringently regulated and highly responsive dexamethasone-inducible gene expression system for tobacco. *The Plant Journal*, 41(6), pp.919–935. https://doi.org/10.1111/j.1365-313x.2005.02341.x.

Satterlee, J.W. and Scanlon, M.J., 2019. Coordination of Leaf Development Across Developmental Axes. *Plants*, 8(10), p.433. https://doi.org/10.3390/plants8100433.

Scanlon, M.J., Schneeberger, R.G. and Freeling, M., 1996. The maize mutant narrow sheath fails to establish leaf margin identity in a meristematic domain. *Development*, 122(6), pp.1683–1691. https://doi.org/10.1242/dev.122.6.1683.

Schneider, C.A., Rasband, W.S. and Eliceiri, K.W., 2012. NIH Image to ImageJ: 25 years of image analysis. *Nature Methods*, 9(7), pp.671–675. https://doi.org/10.1038/nmeth.2089.

Schrick, K., Nguyen, D., Karlowski, W.M. and Mayer, K.F., 2004. START lipid/sterol-binding domains are amplified in plants and are predominantly associated with homeodomain transcription factors. *Genome Biology*, 5(6), p.R41. https://doi.org/10.1186/gb-2004-5-6-r41.

Scofield, S. and Murray, J.A.H., 2006. KNOX Gene Function in Plant Stem Cell Niches. *Plant Molecular Biology*, 60(6), pp.929–946. https://doi.org/10.1007/s11103-005-4478-y.

Semiarti, E., Ueno, Y., Tsukaya, H., Iwakawa, H., Machida, C. and Machida, Y., 2001. The ASYMMETRIC LEAVES2 gene of Arabidopsis thaliana regulates formation of a symmetric lamina, establishment of venation and repression of meristem-related homeobox genes in leaves. *Development*, 128(10), pp.1771–1783. https://doi.org/10.1242/dev.128.10.1771.

Shpak, E.D., Berthiaume, C.T., Hill, E.J. and Torii, K.U., 2004. Synergistic interaction of three ERECTA-family receptor-like kinases controls Arabidopsis organ growth and flower development by promoting cell proliferation. *Development*, 131(7), pp.1491–1501. https://doi.org/10.1242/dev.01028.

Siegfried, K.R., Eshed, Y., Baum, S.F., Otsuga, D., Drews, G.N. and Bowman, J.L., 1999. Members of the YABBY gene family specify abaxial cell fate in Arabidopsis. *Development*, 126(18), pp.4117–4128. https://doi.org/10.1242/dev.126.18.4117.

Sinha, S., Sahadevan, S., Ohno, C., Ram, H. and Heisler, M.G., 2023. Global gene regulatory network underlying miR165a in Arabidopsis shoot apical meristem. *Scientific Reports*, 13(1), p.22258. https://doi.org/10.1038/s41598-023-49093-2.

Somssich, M., Je, B.I., Simon, R. and Jackson, D., 2016. CLAVATA-WUSCHEL signaling in the shoot meristem. *Development*, 143(18), pp.3238–3248. https://doi.org/10.1242/dev.133645.

Steeves, T.A. and Sussex, I.M., 1989. Patterns in plant development. pp.333–347. https://doi.org/10.1017/cbo9780511626227.017.

Sussex, I.M., 1955. Morphogenesis in Solanum tuberosum L. : experimental investigation of leaf dorsiventrality and orientation in the juvenile shoot. *Phytomorphology*, [online] 5, pp.286–300. Available at: <https://cir.nii.ac.jp/crid/1572543025638675840>.

Tadege, M., Lin, H., Bedair, M., Berbel, A., Wen, J., Rojas, C.M., Niu, L., Tang, Y., Sumner, L., Ratet, P., McHale, N.A., Madueño, F. and Mysore, K.S., 2011. STENOFOLIA Regulates Blade Outgrowth and Leaf Vascular Patterning in Medicago truncatula and Nicotiana sylvestris . *The Plant Cell*, 23(6), pp.2125–2142. https://doi.org/10.1105/tpc.111.085340.

Talbert, P.B., Adler, H.T., Parks, D.W. and Comai, L., 1995. The REVOLUTA gene is necessary for apical meristem development and for limiting cell divisions in the leaves and stems of Arabidopsis thaliana. *Development*, 121(9), pp.2723–2735. https://doi.org/10.1242/dev.121.9.2723.

Tatematsu, K., Toyokura, K., Miyashima, S., Nakajima, K. and Okada, K., 2015. A molecular mechanism that confines the activity pattern of miR165 in Arabidopsis leaf primordia. *The Plant Journal*, 82(4), pp.596–608. https://doi.org/10.1111/tpj.12834.

Torii, K.U., Mitsukawa, N., Oosumi, T., Matsuura, Y., Yokoyama, R., Whittier, R.F. and Komeda, Y., 1996. The Arabidopsis ERECTA gene encodes a putative receptor protein kinase with extracellular leucine-rich repeats. *The Plant cell*, 8(4), pp.735–746. https://doi.org/10.1105/tpc.8.4.735.

Tsutsui, H. and Higashiyama, T., 2016. pKAMA-ITACHI Vectors for Highly Efficient CRISPR/Cas9-Mediated Gene Knockout in Arabidopsis thaliana. *Plant and Cell Physiology*, [online] 58, pp.46–56. https://doi.org/10.1093/pcp/pcw191.

Uzair, M., Camacho, R.A.U., Liu, Z., Overholt, A.M., DeGennaro, D., Zhang, L., Herron, B.S., Hong, T. and Shpak, E.D., 2024. An updated model of shoot apical meristem regulation by ERECTA family and CLAVATA3 signaling pathways in Arabidopsis. *Development*, 151(12). https://doi.org/10.1242/dev.202870.

Vandenbussche, M., Horstman, A., Zethof, J., Koes, R., Rijpkema, A.S. and Gerats, T., 2009. Differential Recruitment of WOX Transcription Factors for Lateral Development and Organ Fusion in Petunia and Arabidopsis. *The Plant Cell*, 21(8), pp.2269–2283. https://doi.org/10.1105/tpc.109.065862.

Vernoux, T., Besnard, F. and Traas, J., 2010. Auxin at the Shoot Apical Meristem. *Cold Spring Harbor Perspectives in Biology*, 2(4), p.a001487. https://doi.org/10.1101/cshperspect.a001487.

Vroemen, C.W., Mordhorst, A.P., Albrecht, C., Kwaaitaal, M.A.C.J. and Vries, S.C. de, 2003. The CUP-SHAPED COTYLEDON3 Gene Is Required for Boundary and Shoot Meristem Formation in Arabidopsis. *The Plant Cell*, 15(7), pp.1563–1577. https://doi.org/10.1105/tpc.012203.

Wang, H., Niu, H., Li, C., Shen, G., Liu, X., Weng, Y., Wu, T. and Li, Z., 2020. WUSCHEL-related homeobox1 (WOX1) regulates vein patterning and leaf size in Cucumis sativus. *Horticulture Research*, 7(1), p.182. https://doi.org/10.1038/s41438-020-00404-y.

Wang, Q., Marconi, M., Guan, C., Wabnik, K. and Jiao, Y., 2022. Polar auxin transport modulates early leaf flattening. *Proceedings of the National Academy of Sciences of the United States of America*, 119. https://doi.org/10.1073/pnas.2215569119.

William, D.A., Su, Y., Smith, M.R., Lu, M., Baldwin, D.A. and Wagner, D., 2004. Genomic identification of direct target genes of LEAFY. *Proceedings of the National Academy of Sciences*, 101(6), pp.1775–1780. https://doi.org/10.1073/pnas.0307842100.

Xu, P., Wan, Q., Shao, W., Wu, Y., Wu, F., Li, X., Ren, W., He, Y., Li, S. and Yu, X., 2025. Orchestration of leaf curvature by the SBP transcription factor SPL10–REVOLUTA module in Arabidopsis. *Journal of Integrative Plant Biology*. https://doi.org/10.1111/jipb.13893.

Yamaguchi, N., Winter, C.M., Wu, M.-F., Kwon, C.S., William, D.A. and Wagner, D., 2014. PROTOCOLS: Chromatin Immunoprecipitation from Arabidopsis Tissues. *The Arabidopsis Book / American Society of Plant Biologists*, [online] 12, p.e0170. https://doi.org/10.1199/tab.0170.

Yi, X., Yue, S., Wan-Qi, L. and Hai, H., 2002. The Arabidopsis AS2 Gene Encoding a Predicted Leucin zipper Protein Is Required for the Leaf Polarity Formation. *Acta Botanica Sinica*. [online] Available at: <https://www.jipb.net/CN/Y2002/V44/I10/1194>.

Yu, T., Guan, C., Wang, J., Sajjad, M., Ma, L. and Jiao, Y., 2017. Dynamic patterns of gene expression during leaf initiation. *Journal of Genetics and Genomics*, 44(12), pp.599–601. https://doi.org/10.1016/j.jgg.2017.11.001.

Zhang, J., Nieminen, K., Serra, J.A.A. and Helariutta, Y., 2014. The formation of wood and its control. *Current Opinion in Plant Biology*, 17, pp.56–63. https://doi.org/10.1016/j.pbi.2013.11.003.

Zhao, F. and Traas, J., 2021. Stable establishment of organ polarity several plastochrons before primordium outgrowth in Arabidopsis. *Development*, 148(18), p.dev198820. https://doi.org/10.1242/dev.198820.

Appendix

Trends in Developmental Biology

Review

Wounding and the establishment of leaf polarity: From historical perspectives to present controversies

Hiruni Fernando and Marcus G. Heisler*

School of Life and Environmental Sciences, University of Sydney, Camperdown, NSW 2006, Australia.

ABSTRACT

Leaves originate as primordia on the shoot apical meristem and undergo differentiation to become flat structures with distinct upper (adaxial) and lower (abaxial) tissue types. The establishment of adaxial and abaxial tissue types in leaves was investigated by Ian Sussex in 1955 through wounding experiments. Sussex proposed that a signal coming from the shoot apical meristem promotes the differentiation of adaxial leaf tissues and leaf flattening. Since then, many studies have followed up on Sussex's work to understand better how leaf polarity is first established using anatomical approaches, molecular genetics and live-imaging. While some studies have supported Sussex's findings, others have presented conflicting results. In this review, we focus on how recent evidence has shifted the debate.

KEYWORDS: Sussex signal, wounding, leaf polarity, dorsoventrality, adaxial, abaxial.

INTRODUCTION

During leaf development, three patterning axes can be distinguished: the adaxial-abaxial axis (also called dorsoventral), the proximal-distal axis, and the medial-lateral axis (Figure 1). Differential growth along these axes typically results in the formation of a flat or lamina-shaped organ that provides a large surface area to maximise photosynthesis [1]. Tissues of the leaf nearest, or adjacent, to the shoot are termed adaxial, while those farther away are referred to as abaxial. In terms of histology, adaxial and abaxial leaf tissues differ in a number of ways, reflecting their distinct roles in photosynthesis and gas exchange [2]. In *Arabidopsis*, the number of trichomes, or leaf hairs is higher on the early adaxial juvenile leaf surface compared to the respective abaxial side. The adaxial palisade mesophyll cells are elongated in shape and tightly packed to maximize light absorption. Conversely, the abaxial spongy mesophyll cells vary in shape and are loosely packed to better enable gas exchange. The central vasculature tissue is also different; the xylem is positioned towards the adaxial side, while the phloem is located towards the abaxial side.

How is the leaf adaxial-abaxial axis first established? The field has largely been split into two camps. In 1955, Sussex proposed, based on wounding experiments, that an inductive signal from the shoot apical meristem to the leaf primordium was required to specify adaxial identity and leaf flattening [3]. In contrast, others have proposed that adaxial and abaxial leaf tissues derive their character directly from the corresponding tissues of the shoot from which they originate [4]. More recently, due to the central role of auxin in organ initiation [5, 6], studies have investigated auxin in relation to leaf polarity, including the hypothesis that auxin corresponds to the inductive signal proposed by Sussex [7-9]. In this review, we discuss hypotheses on the origin of leaf adaxial-abaxial patterning with reference to recent data on the topic (see Table 1).

*Corresponding author: marcus.heisler@sydney.edu.au

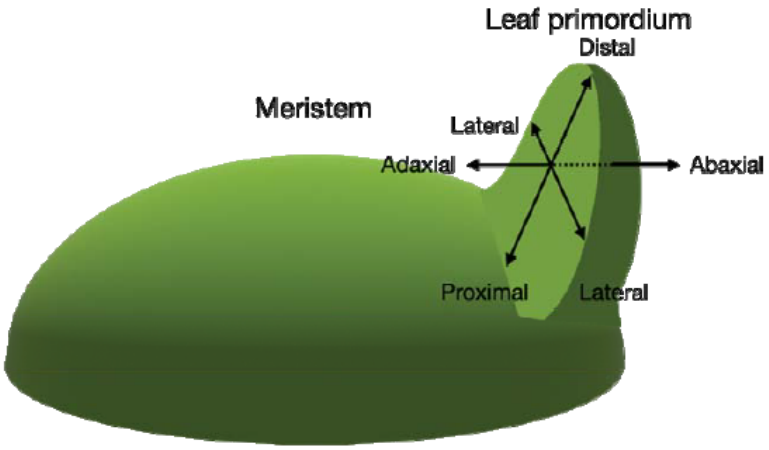

Figure 1. Major axes of a developing leaf with respect to the shoot meristem.

Table 1. Studies discussed in this review.

Research	Reference
Morphogenesis in Solanum tuberosum I: experimental investigation of leaf dorsiventrality and orientation in the juvenile shoot	[3]
Morphogenesis in plants; a contemporary study	[11]
Organogenetic capacity of leaves: The significance of marginal blastozones in angiosperms	[4]
Phantastica: a gene required for dorsoventrality of leaves in *Antirrhinum majus*	[14]
Microsurgical and laser ablation analysis of leaf positioning and dorsoventral patterning in tomato	[10]
Auxin depletion from leaf primordia contributes to organ patterning	[8]
Spatial Auxin Signalling Controls Leaf Flattening in *Arabidopsis*	[9]
Cell type boundaries organize plant development	[7]
Stable establishment of organ polarity occurs several plastochrons before primordium outgrowth in *Arabidopsis*	[33]
Specification of leaf dorsiventrality via a prepatterned binary readout of a uniform auxin input	[28]
Coactivation of antagonistic genes stabilizes polarity patterning during shoot organogenesis	[26]
Polar auxin transport modulates early leaf flattening	[29]

Pre-patterning or dependence on a 'Sussex' signal?

In 1955 Sussex reported that in potato, incisions separating the shoot apical meristem from young leaf primordia resulted in the formation of needle-like leaves without a blade. Further histological studies of these radially symmetric lateral organs demonstrated that they consisted entirely of abaxial cell types [3]. Sussex, therefore, concluded that a wound-sensitive inductive signal travelling from the shoot apical meristem to the primordium

was necessary for specifying adaxial identity (Figure 2A) on what would otherwise be a radially patterned, abaxialized primordium (Figure 2B). Fifty years later, the same experiment was repeated on tomato shoot tips. Instead of using a sharpened blade to make incisions, an infrared laser was used to ablate tissues. Experiments in which the laser was focused on regions separating young leaf primordia from the shoot apical meristem again resulted in abaxialization and organ radialization, recapitulating the early findings of Sussex based on potato [10]. Despite these results, other scientists in the field from the 1960's onwards, have argued against Sussex's interpretation. Alternatively, they have pointed out that leaf primordia must necessarily be patterned along their adaxial-abaxial axis from inception since the shoot tissue from which the organ is derived is already patterned along its radial axis, which at inception, corresponds to the leaf adaxial-abaxial axis (Figure 3).

For instance, citing the different growth and differentiation status of cells along the surface of the shoot between the centre and periphery, Wardlaw states that 'the growth relationships and rates of differentiation on the adaxial and abaxial sides of the primordium are different from the outset' [11]. Part of the confusion, it is argued, comes from the fact that in some species, including potato and tomato, leaf primordia start as roughly rod-shaped structures where lateral

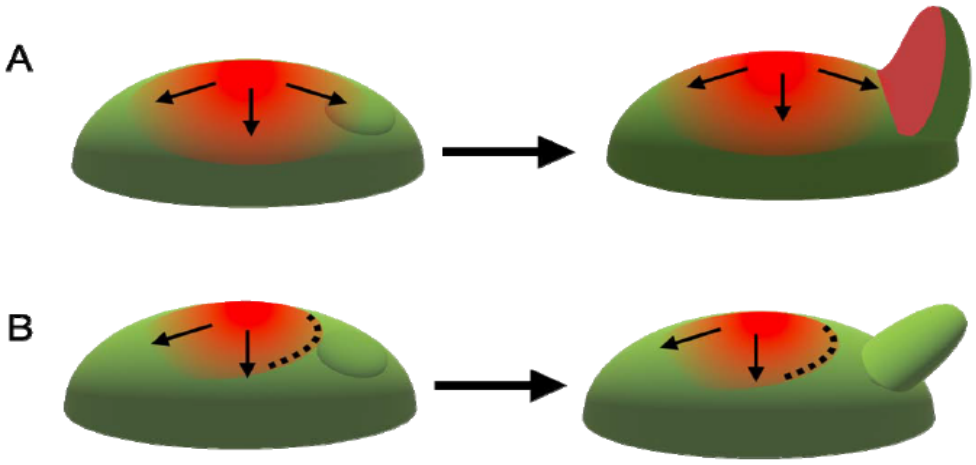

Figure 2. Sussex signal hypothesis for specification of adaxial identity **A.** Induction *via* mobile signal (red) leading to normal leaf development. **B.** Interruption of induction due to wound (dashed line) leading do abaxialized and radialized organ.

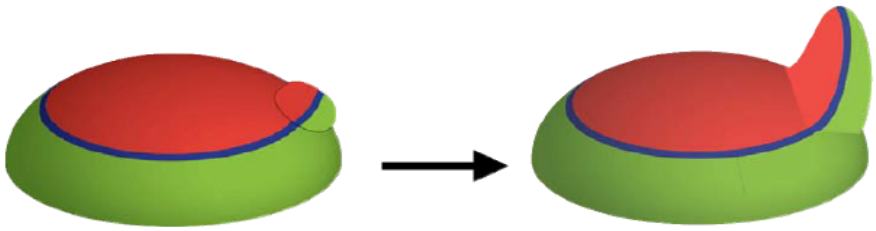

Figure 3. Leaf adaxial-abaxial patterning is derived directly from the radial pattern of the shoot.

growth occurs later, suggesting a radial rather than a flattened, adaxial/abaxial patterning at inception [4]. Weight given to Zimmerman's telome hypothesis, that leaves evolved from axial structures [12], may also promote such an interpretation [4]. In most other species however, leaves initiate as linear structures that extend around the circumference of the shoot. This is most obvious in grasses but also many other dicot species. Debate between these different views has been ongoing, until very recently.

A molecular understanding of adaxial-abaxial patterning

The first clues to understanding adaxial-abaxial patterning at a molecular level were gained by examining *Phantastica* (*phan)* mutants in *Antirrhinum* plants [13, 14] where it was reported that these mutants developed similar abaxialized needle-like leaves to those described by Sussex from wounding experiments, reinforcing the association between loss of adaxial/abaxial patterning and a radially symmetrical organ shape. Weaker phenotypes were also observed in which leaves appeared to develop patches of abaxial cells on the adaxial leaf surface. Along the boundaries of these patches, blade-like protuberances formed. To explain this phenomenon, the authors drew inspiration from wing development in Drosophila [15], suggesting that boundary cells act as 'organizers' to signal to neighbouring regions to promote the growth of laminal tissues. In their discussion, the authors suggest this process occurs downstream of adaxial-abaxial establishment, for which they invoke the Sussex signal hypothesis [14].

After discovering the role of *PHAN* in *Antirrhinum*, several genes involved in leaf morphogenesis and positioning were cloned and characterized in *Arabidopsis*. Members of the Class III HD-Zip gene family act redundantly and are expressed in the adaxial domain of *Arabidopsis* leaves. They include five members named *PHABULOSA* (*PHB*), *PHAVOLUTA* (*PHV*), *REVOLUTA* (*REV*), *ATHB8 and ATHB15* [16, 17]. Plants mutant for multiple members of this gene family exhibit a more dramatic phenotype compared to *phan* mutants – they lack an embryonic shoot meristem and in the most extreme cases, form a single radialized and abaxialized cotyledon in its place [17]. Gain of function mutants, in which suppression of HD-ZIPIII expression by miRNAs 165/166 is disrupted, develop leaf phenotypes similar to *phan* mutants in terms of radialized leaf shapes, but in this case, they consist only of adaxial cell types [16]. Plants mutant for multiple members of the abaxially expressed *KANADI (KAN)* genes on the other hand, develop leaves ectopically from the hypocotyl and abaxial side of the leaves [18]. Like gain of function HD-ZIPIII mutants, when KAN1 is expressed ectopically, leaves develop as rod-shaped structures [19]. To summarize, while many of the phenotypes associated with disruptions to adaxial-abaxial patterning result in a radially symmetrical leaf shapes, similar to wound-induced phenotypes, defects in leaf positioning are also apparent in loss of function mutants, hinting at a new connection between organ positioning and adaxial/abaxial patterning.

Is auxin Sussex's inductive signal?

Intriguingly, a phenotype similar to that caused by wounding has been reported to occur after applying auxin to the adaxial side of the leaf primordia in tomato [8] (Figure 4A). Using the DII auxin signalling sensor to monitor auxin levels [20], this study also reported that in *Arabidopsis*, adaxial leaf tissues exhibit lower levels of auxin compared to abaxial parts of the leaf. Linking these observations, the authors propose that low auxin levels in adaxial leaf tissues are critical for adaxial cell type specification (Figure 4B) and that wounding prevents depletion, thereby causing an abaxialized phenotype [8] (Figure 4C). The authors provide evidence that low auxin levels result from auxin movement from developing leaf primordia to the shoot apical meristem, as earlier reported for flowers [21]. Thus, they suggest a different model for the original Sussex signal; instead of a signal originating from the meristem and moving to the incipient leaf, they suggest a signalling molecule, in this case, auxin, is antagonistic to adaxial cell fate and moves from the adaxial side of the leaf primordium towards the shoot apical meristem. Further supporting the auxin depletion model, a subsequent study from the same research group

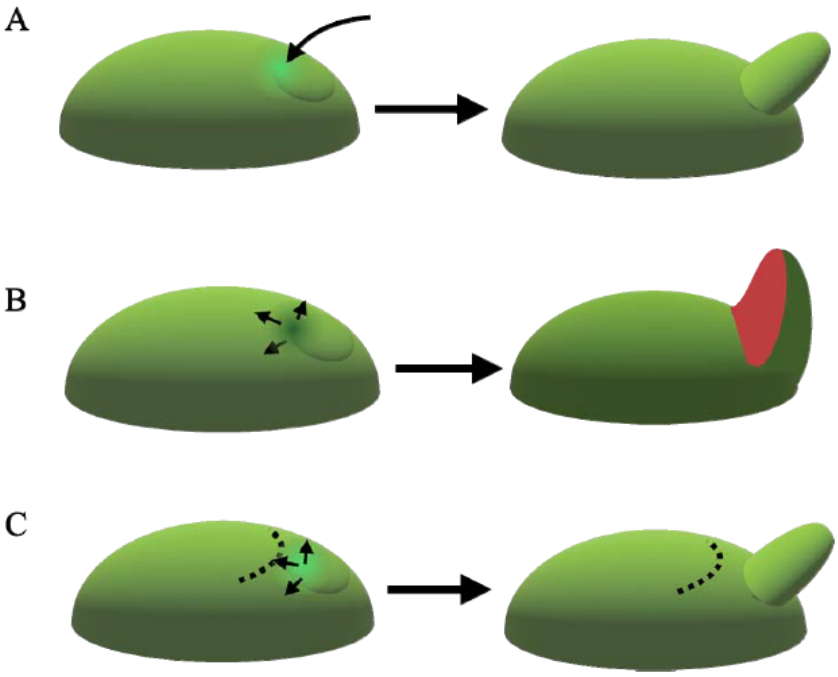

Figure 4. Reverse Sussex signal hypothesis [8]. A. Auxin application to the adaxial side of tomato leaf primordia causes an abaxialized phenotype. **B.** After an initial build-up of auxin that initiates organ formation, auxin is subsequently transported away from the primordium during normal development [21, 8]. **C.** Wounding is thought to prevent transport of auxin away, leading to abnormally high auxin levels in adaxial leaf tissues and subsequent abaxialization, as in (A).

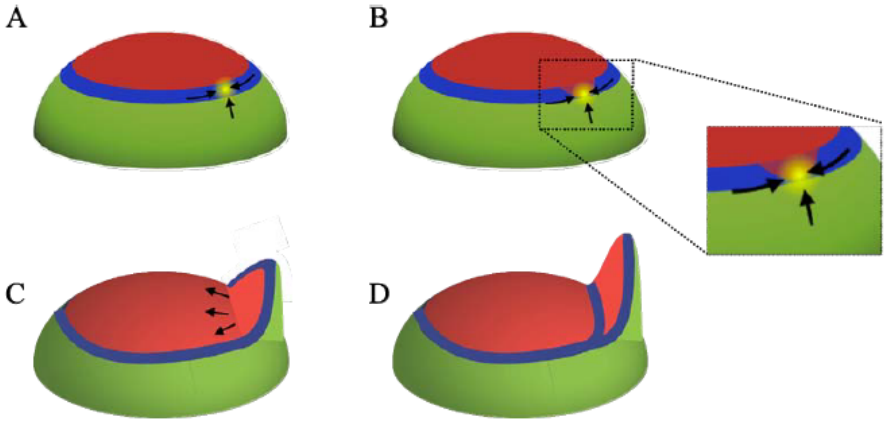

Figure 5. Patterns of REV (red), AS2 (blue) and KAN1 (green) as well as auxin (yellow) during organ inception [7]. Directions of auxin transport shown by black arrows. **A.** Initially, auxin is concentrated between the REV and KAN domains overlapping with AS2. **B.** REV expression extends peripherally towards the primordium. **C.** Auxin transport later directs auxin away from the primordium [21, 8]. **D.** REV expression reduces adjacent to the primordium.

concluded that maintaining low auxin levels in the adaxial leaf primordium restricts the expression of middle domain genes WOX1 and PRS, from adaxial leaf tissues while Auxin response Factors (ARFs) abaxially suppress WOX1 and PRS abaxially [9]. In contrast, it has separately been reported that auxin application to developing *Arabidopsis* leaves does not cause ectopic WOX1 or PRS expression [7]. Furthermore, the reported difference in auxin concentration between the two sides of the leaf has been disputed [22, 23] (see below for further discussion).

Pre-pattern or Sussex signal?

In addition to being expressed in leaves, KANADI and the Class III HD-ZIP transcription factors are expressed in the shoot meristem [16, 24]. Detailed examinations of their shoot expression domains reveal they form non-overlapping concentric patterns [7, 25] and that leaf initiation, as marked by high PIN1 expression, is centred on the boundary region between these domains (Figure 5A) [7]. During organ initiation, the pattern of KAN1 expression remains relatively stable with respect to the primordium progenitor cells while REV expression extended into these progenitors after inception (Figure 5B-D) [7, 25]. These findings reveal that KAN1 already marks the radial axis of the shoot in a way that closely corresponds to the adaxial-abaxial patterning of emerging leaves, supporting prior proposals that leaf tissue polarity is derived from radial patterning of the shoot [4]. By perturbing the expression of KAN1 specifically in shoot tissues, Caggiano *et al.* found that leaf polarity was subsequently changed accordingly, demonstrating a functional link between the two [7].

Given that loss of either KAN or HD-ZIPIII function leads to ectopic leaf formation [18], Caggiano *et al.* [7] also proposed that in the shoot apical meristem, the HD-ZIPIII and KAN genes act where they are expressed to suppress auxin-induced organ initiation. Thus, only at the boundary, where both sets of gene's expression levels are lower (although not completely absent [26]), can organs form (prior to the extension of HD-ZIPIII expression into the primordium). Supporting this proposal, when either REV and KAN1 are expressed ectopically throughout the shoot epidermis, organs fail to initiate [7]. According to this view then, adaxial-abaxial patterning arises in part, as a result of the broader role the KAN and HD-ZIPIII transcription factors have in helping position auxin-dependent cell proliferation, including the formation of new growth axes [7, 27].

More recently, another study also investigated adaxial-abaxial patterning in large vegetative *Arabidopsis* meristems [28]. Three conclusions from this study stand out. Firstly, by examining an auxin transcriptional reporter, the authors find that auxin response at primordium initiation sites is restricted to cells adaxial to the KAN1 expression domain and that in *kan1kan2* mutants, auxin transcriptional response expands abaxially, supporting the earlier proposal for KAN function in restricting auxin activity [7]. Secondly, AS2 was found to be expressed adaxially at the leaf initiation site prior to organ inception in a complementary pattern to KAN1. It was therefore found that AS2 and KAN1 pre-pattern leaf polarity [28]. Finally, after examining the DII auxin marker, the authors conclude that, consistent with Qi *et al.*, 2014 [8], an auxin minimum does exist specifically within the adaxial tissues of leaf primordia - but only transiently, before low auxin levels mark both adaxial and abaxial leaf tissues equally [28]. This observation helps to resolve earlier controversy over the auxin distribution in young leaf primordia [22, 23] but leaves open the question of whether low levels of auxin are necessary to restrict WOX and PRS expression to the middle domain of leaves in *Arabidopsis* [7, 9], although the data for tomato unambiguously support such a role [29] (see below).

Pre-pattern and Sussex signal?

If leaf adaxial-abaxial patterning is pre-patterned, what about the effects of wounding as revealed by Sussex? It turns out that one of the consequences of wounding is a change in auxin levels, due to the transport of auxin away from the wound [30, 31]. In addition, auxin regulates the expression of the HD-ZIPIII and KAN organ polarity genes. Caggiano *et al.*, 2017 for instance find that when auxin is applied exogenously to the inflorescence

meristem, it leads to a slight expansion of the REV expression domain out to the pre-existing boundary of KAN1 expression (mirror the dynamic changes in expression of these genes during organ initiation) [7]. In contrast, lower auxin levels lead to an expansion of KAN1 expression towards the meristem centre at the expense of REV expression [7]. As might be expected from these results, wounding also causes KAN1 expression (i.e. abaxial identity) to expand at the expense of REV expression (adaxial identity) around the wound and this response can be completely blocked by applying exogenous auxin [7]. Thus, auxin appears to be a signalling molecule that promotes adaxial identity, which wounding depletes – corresponding closely to what might be expected for a 'Sussex signal' [32]. Surprisingly however, while wounding was found to alter the expression of adaxial and abaxial genes in the shoot periphery, changes to the polarity of *Arabidopsis* leaf primordia were not detected and no radial leaf phenotype was observed [7], unlike the situation in tomato and potato [3, 10]. One possible reason for this was thought to be that the vegetative meristems used for the *Arabidopsis* experiments were very small. To address this issue, a separate study repeated the wounding experiments in *Arabidopsis* using older plants with larger vegetative meristems - but still the abaxialized leaf phenotype observed in the Solanaceae could not be reproduced [33]. Thus, while wounding's influence on auxin may still account for associated disruptions to leaf polarity, *Arabidopsis* leaves are somehow wound-insensitive.

Tomato revisited

As mentioned above, significant differences have been reported between *Arabidopsis* and tomato in the sensitivity of adaxial-abaxial patterning to both wounding and auxin. In both *Arabidopsis* and tomato, wounding promotes abaxial cell identity over adaxial. However, while this applies to developing leaves in tomato [10], in *Arabidopsis,* wounding only promotes abaxial tissue identity in meristem tissues [7, 33]. Regarding the role of auxin, different studies have reported conflicting results. For instance, Qi *et al*., 2014 [8] report that exogenously applied auxin *antagonises* adaxial identity and promotes a radialized leaf shape in tomato and *Arabidopsis*. Caggiano *et al*., 2017 [7] on the other hand report that exogenous auxin *promotes* adaxial identity (REV expression) in the *Arabidopsis* meristem but does not cause a change to leaf polarity. Indeed, more recent work provides evidence that REV is a direct target of the auxin responsive transcriptional regulator MONOPTEROS [26]. A recent study now investigates wounding and auxin in tomato in more detail [29]. Consistent with the situation in *Arabidopsis*, the authors find that auxin is depleted around tomato wounds and that wounds also lead to a loss of SIREV expression and an expansion of SIKAN2C expression (protein and mRNA) around the wound after 12 hrs and 2 days respectively. In contrast to wounding and consistent with auxin promoting **adaxial** identity, application of auxin and NPA to the tomato apex led to a small increase in REV expression and reduction in KAN expression 24 hrs after treatment. Seven days later however, the leaf developed a radialized shape and SIREV expression was not visible (SIKAN2C expression was not reported). Thus, in response to auxin, there is an initial slight strengthening of adaxial SIREV expression followed by a slower loss of expression - which is different to what is observed for wounding, indicating that the two perturbations are not as related as initially assumed [8]. In agreement, the authors suggest that in *Arabidopsis*, leaves are robust to wounding because they may synthesize their own auxin, while tomato leaves may not [29] - implying that auxin depletion [7] rather than accumulation [26] may be the root cause of wound-induced loss of leaf polarity. Finally, the authors show that by inhibiting the 26s Proteosome pathway, wound-induced reductions in the SIREV protein could be prevented. The authors conclude from this latter experiment that wound-induced SIREV depletion is independent of canonical auxin signalling. However, what happens at the protein level does not explain wound-induced reductions of SIREV mRNA [29]; hence the role of canonical auxin signalling in the transcriptional response of SIREV to wounding remains to be investigated. Overall then, what seems most striking from this recent tomato study is how similar, rather than different, the *Arabidopsis* and tomato wound

responses are in terms of auxin, HD-ZIPIII and KAN expression and that the radialization of tomato leaves in response to exogenous auxin, may be a distinct phenomenon.

CONCLUSION

The establishment of leaf adaxial-abaxial patterning has received significant attention from plant developmental biologists and several conflicting models have been proposed to explain this process. In this review, we have discussed and compared them in the context of the inductive signal original proposed by Sussex. While wounding experiments have suggested the existence of a shoot-derived signal necessary to promote adaxial leaf cell fate [3], it has also been argued that leaf primordia must be pre-patterned along their adaxial-abaxial axis at inception, due to the radial patterning of the shoot from which they develop [4]. How have more recent molecular studies influenced the debate? On the one hand, the analysis of molecular markers and experimental perturbations of gene expression demonstrate that radial patterning of the shoot does indeed pre-pattern leaf polarity from inception [7, 25, 28]. However, at the same time, the plant hormone auxin has been identified as a signalling molecule that also helps promote adaxial cell identity (via HD-ZIPIII expression) during organ initiation and that is depleted by wounds, not only in *Arabidopsis* but also in tomato, making auxin a very good candidate for the Sussex inductive signal as originally conceived [3]. Overall, the picture that is starting to emerge then is more nuanced. While a radial pre-pattern of transcription factors helps to establish leaf polarity, the wound-sensitive signalling molecule auxin also contributes, at least in part by promoting adaxial HD-ZIPIII expression over abaxial KAN expression, although the sensitivity of this pathway specifically for leaf development varies between species. We look forward to more updates on this fascinating story including on the role of auxin synthesis for the wound response and the characterization of wound responses in additional species including in monocots.

CONFLICT OF INTEREST STATEMENT

The authors declare no conflict of interest.

REFERENCES

1. Manuela, D. and Xu, M. 2020, Front. Plant Sci., 11, 568730.
2. Nakata, M. and Okada, K. 2013, Plants, 2, 174.
3. Sussex, I. M. 1955, Int. J. Plant Morphol., 5, 286.
4. Hagemann, W. and Gleissberg, S. 1996, Plant Syst. Evol., 199, 121.
5. Reinhardt, D., Pesce, E. R., Stieger, P., Mandel, T., Baltensperger, K., Bennett, M., Traas, J., Friml, J. and Kuhlemeier, C. 2003, Nature, 426, 255.
6. Reinhardt, D., Mandel, T. and Kuhlemeier, C. 2000, Plant Cell, 12, 507.
7. Caggiano, M. P., Yu, X., Bhatia, N., Larsson, A., Ram, H., Ohno, C. K., Sappl, P., Meyerowitz, E. M., Jönsson, H. and Heisler, M. G. 2017, eLife, 6, e27421.
8. Qi, J., Wang, Y., Yu, T., Cunha, A., Wu, B., Vernoux, T., Meyerowitz, E. and Jiao, Y. 2014, Proc. Natl. Acad. Sci. USA, 111, 18769.
9. Guan, C., Wu, B., Yu, T., Wang, Q., Krogan, N. T., Liu, X. and Jiao, Y. 2017, Curr. Biol., 27, 2940.
10. Reinhardt, D., Frenz, M., Mandel, T. and Kuhlemeier, C. 2005, Development, 132, 15.
11. Wardlaw, C. W. 1968, Morphogenesis in plants; a contemporary study, London, Methuen.
12. Zimmermann, W. 1965, Die Telomtheorie, Stuttgart: Fischer.
13. Waites, R., Selvadurai, H. R., Oliver, I. R. and Hudson, A. 1998, Cell, 93, 779.
14. Waites, R. and Hudson, A. 1995, Development, 121, 2143.
15. Diaz-Benjumea, F. J. and Cohen, S. M. 1993, Cell, 75, 741.
16. McConnell, J. R., Emery, J., Eshed, Y., Bao, N., Bowman, J. and Barton, M. K. 2001, Nature, 411, 709.
17. Emery, J. F., Floyd, S. K., Alvarez, J., Eshed, Y., Hawker, N. P., Izhaki, A., Baum, S. F. and Bowman, J. L. 2003, Curr. Biol., 13, 1768.
18. Izhaki, A. and Bowman, J. L. 2007, Plant Cell, 19, 495.

19. Bowman, J. L., Eshed, Y. and Baum, S. F. 2002, Trends Genet., 18, 134.
20. Vernoux, T., Brunoud, G., Farcot, E., Morin, V., Van den Daele, H., Legrand, J., Oliva, M., Das, P., Larrieu, A., Wells, D., Guedon, Y., Armitage, L., Picard, F., Guyomarc'h, S., Cellier, C., Parry, G., Koumproglou, R., Doonan, J. H., Estelle, M., Godin, C., Kepinski, S., Bennett, M., De Veylder, L. and Traas, J. 2011, Mol. Syst. Biol., 7, 508.
21. Heisler, M. G., Ohno, C., Das, P., Sieber, P., Reddy, G. V., Long, J. A. and Meyerowitz, E. M. 2005, Curr. Biol., 15, 1899.
22. Bhatia, N., Åhl, H., Jönsson, H. and Heisler, M. G. 2019, eLife, 8, e39298.
23. Guan, C., Du, F., Xiong, Y. and Jiao, Y. 2019, J. Integr. Plant Biol., 61, 1114.
24. Yadav, R. K., Perales, M., Gruel, J., Ohno, C., Heisler, M., Girke, T., Joensson, H. and Reddy, G. V. 2013, Mol. Sys. Biol., 9, 654.
25. Yu, T., Guan, C., Wang, J., Sajjad, M., Ma, L. and Jiao, Y. 2017, J. Genet. Genomics, 44, 599.
26. Guan, C., Qiao, L., Xiong, Y., Zhang, L. and Jiao, Y. 2022, Sci. Adv., 8, eabn0368.
27. Heisler, M. G. 2021, Front. Plant Sci., 12, 786338.
28. Burian, A., Paszkiewicz, G., Nguyen, K. T., Meda, S., Raczynska-Szajgin, M. and Timmermans, M. C. P. 2022, Nat. Plants, 8, 269.
29. Wang, Q., Marconi, M., Guan, C., Wabnik, K. and Jiao, Y. 2022, Proc. Natl. Acad. Sci. USA, 119, e2215569119.
30. Heisler, M. G., Hamant, O., Krupinski, P., Uyttewaal, M., Ohno, C., Jonsson, H., Traas, J. and Meyerowitz, E. M. 2010, PLoS Biol., 8, e1000516.
31. Landrein, B., Kiss, A., Sassi, M., Chauvet, A., Das, P., Cortizo, M., Laufs, P., Takeda, S., Aida, M., Traas, J., Vernoux, T., Boudaoud, A. and Hamant, O. 2015, elife, 4, e07811.
32. Kuhlemeier, C. and Timmermans, M. C. 2016, Development, 143, 3230.
33. Zhao, F. and Traas, J. 2021, Development, 148, dev198820.